Master Thesis

Dynamic Modeling of a Bridge Subjected to Seismic Waves

School of Engineering and Science
M.Sc. in Civil and Structural Engineering
Aalborg University

Jon André Adsersen

June 10, 2013

AALBORG UNIVERSITY
STUDENT REPORT

Faculty of Engineering and Science
School of Engineering and Science
Sohngaardsholmsvej 57, 9000 Aalborg
Telefon: 9940 8530
http://civil.aau.dk

Master Thesis

Title:
Dynamic Modeling of a Bridge Subjected to Seismic Waves

Written by:
Jon André Adsersen

Graduate Student
School of Engineering and Science
M.Sc. in Structural and Civil Engineering

Supervisors:
Associate Professor Lars Vabbersgaard Andersen

Project Period: 2013.02.02 - 2013.06.10 (Short Thesis)

Completed: 10$^{\text{th}}$ of June 2013

Copies printed: 3

Number of pages: 37

Number of Appendices: 10

Jon André Adsersen

Summary

In this thesis the propagation of seismic waves through a number of soft soil layers and up into a bridge with a total span of 2 km is investigated. Only horizontal shear waves (SH-waves) are modeled, as most buildings are often most vulnerable to excitations in the horizontal direction. In seismic design the local site effects of soft layers is often of big significance, as the amplification of seismic waves when they propagate through soft soil layers is often quite significant.

The wave propagation through the soft soil layers are modeled using both a dynamic linear viscoelastic semi-analytic Domain Transformation Method (DTM) and a dynamic linear viscoelastic Finite Element Method (FEM) model. The models are compared in order to validate the results, and the results fit quite nicely. The models are solved in the frequency domain in order to use hysteretic damping, which is recognized as a good damping model for soils. A partly linear model is introduced in the FEM soil model in order to take into account decrease of the small strain shear modulus and increase of the damping ratio as the shear strain amplitude increases.

Strong motion data for the 1995 Aqaba Earthquake, which had a moment magnitude of 7.3, is used. The soil response is determined and used as an input to the bridge model. It is found that the soft soil layers amplifies the seismic waves with several magnitudes. The wave propagation through the bridge is modeled using a dynamic linear viscoelastic three dimensional FEM beam model. Both compressional, torsional and shear wave propagation through the bridge can be modeled. The angle at which the the SH-waves hits the bridge can also be varied, which is used in a small parameter study.

Another parameter, which is investigated is the delay at which the seismic waves hits the different columns. The results of the parameter study show that the critical direction of the earthquake is parallel to the bridge due to the fact that high normal stresses and thus compressional waves occur in the bridge deck. The bridge is located in water and hydrodynamic mass is therefore applied in the bridge model. Soil structure interaction is also taken into account by using a lumped parameter model to model the rotational as well as the torsional stiffness of the foundations which are located on the soft soils. For the columns founded directly on bedrock, however, the rotational and torsional stiffness is assumed infinitely stiff.

Sammendrag

I denne kandidatopgave undersøges udbredelsen af seismiske bølger op gennem et givet antal jordlag og videre igennem en brokonstruktion med en total længde på 2 km. Det er kun horisontale forskydningsbølger der undersøges, da horisontale accelerationer er mest kritisk for de fleste konstruktioner i forhold til vertikale accelerationer. For seismisk design har lokale dæmpnings- og isærforstærknings effekter stor betydning mht. udbredelsen af seismiske bølger.

Bølgeudbredelsen gennem bløde jordlag er modeleret ved brug af en endimensional dynamisk lineær viskoelastisk semi-analytisk Domain Transformation Method (DTM) model, samt ved brug af en dynamisk viskoelastisk endimensional Finite Element Method (FEM) model. Resultaterne for de to modeller er sammenlignet for at evaluere modellerne, og de stemmer godt overens. Modellerne er løst i frekvensdomænet for at gøre det muligt at anvende hysteretisk dæmpning, som er anset for at være en udmærket dæmpningsmodel for jord. En delvis lineær model er introduceret i FEM modellen for at tage hensyn til reduktion af tangentforskydningsmodulet samt forøgelse af dæmpningsfaktoren ved stigende forskydningstøjninger.

Jordskælvsdata fra jordskælvet i Aqaba 1995 er anvendt. Responsen fra de anvendte jordlag er bestemt og derefter brugt som input til de bropiller, som står på de bløde jordlag. Der sker betydelig forstærkning, når jordskælvet udbredes op gennem de bløde jordlag. Bølgeudbredelsen for broen er bestemt ved anvendelse af en tredimensional dynamisk viskoelatisk FEM model. Både tryk, vridnings samt forskydningsbølger kan modelleres med modellen.

Et lille parameterstudie er udført, hvor den horisontale retning for de seismiske bølger varieres. En anden parameter som varieres er den tilsyneladende hastighed som de seismiske bølger udbreder sig med gennem klippen under de bløde jordlag. Variation af denne parameter medfører en forsinkelse af signalet fra bropille til bropille. Resultatet af parameter studiet viser, at en udbredelses retning langs med broen er mest kritisk. Nogle af bropillerne er placeret i vand, hvorfor hydrodynamisk masse er anvendt i modellen.

Preface

This thesis is submitted in the fulfillment of the requirements of the Master of Science degree in Structural and Civil Engineering at Aalborg University.

I would like to acknowledge my supervisor Associate Professor Lars Vabbersgaard Andersen for the work of this thesis.

The thesis consists of a main report and an appendix report, where derivations and other technical details can be found. An appendix CD is also enclosed and can be found at the inside of the back cover.

The Harvard reference system has been used and all references can be found in the bibliography located at the back of the main report.

Table of Contents

Part I

Main Report

1 Introduction

In this thesis the influence of seismic waves to a bridge located on top of a number of soft soil layers is investigated. The bridge which is investigated is a conceptual bridge and so is the soil stratigraphy beneath it. Consequently the dimensions of the bridge, material properties of both bridge and soil etc. are estimated based on typical values. The purpose of the thesis is not to carry out a seismic design of a bridge, but instead to clarify the influence of seismic waves to the stresses that occurs in bridge. A small parameter study is carried out as well to investigate the influence of some chosen parameters. As the focus of the thesis is the impact of seismic loads, no other loads will be considered, but it should be kept in mind that all loads need to be considered in a seismic design.

The total length of the bridge is 2 km, it has 9 columns along its span and one abutment in each end. In order to determine how the earthquake excitations affects the bridge, it is very important whether the location is close to a tectonic plate boundary (a typical fault line). One case, which is often very critical regarding seismic design is the case where the bridge crosses a tectonic plate boundary. In this case the two neighboring columns on each side of the plate boundary can move in opposite directions and the accelerations are generally very high compared to a location a couple of hundred kilometers away from the fault line. Another case is a location a couple of hundreds kilometers away from the plate boundary. Here the propagation direction of the seismic waves is often well defined. This is assumed to be the case for the considered bridge. Given the apparent velocity of the propagating waves, the time where the waves arrive at each bridge column can be determined. However, some of the bridge columns can be founded on soft soil layers, where amplification and damping effects are present (local site effects). Besides that the propagation velocity through soft soil layers is significantly lower than the propagation velocity through stiff soil.

In order to take into account both the wave propagation through the soft soil layers as well as the bridge itself, two models are made to investigated how the bridge reacts when it is subjected to earthquake excitations,

- A model to determine the wave propagation through the soft soil layers
- A model to determine the wave propagation through the bridge

1.1 The Considered Bridge

A sketch of the bridge can be seen in figure 1.1. The bridge crosses a valley with a lake, which has a maximum depth of 10 m. The bridge deck consist of 10 beams each with a span of 200 m, which gives the bridge a total length of 2000 m. The beams are supported on 9 columns with lengths from 20 m to 30 m and one abutment in each end of the bridge. As it can be seen in the figure the height of the bridge is scaled several magnitudes compared to its length. The beams are named 1 to 10 and the columns are named A to I from right to left. The abutments in each end are named Ab1 and Ab2.

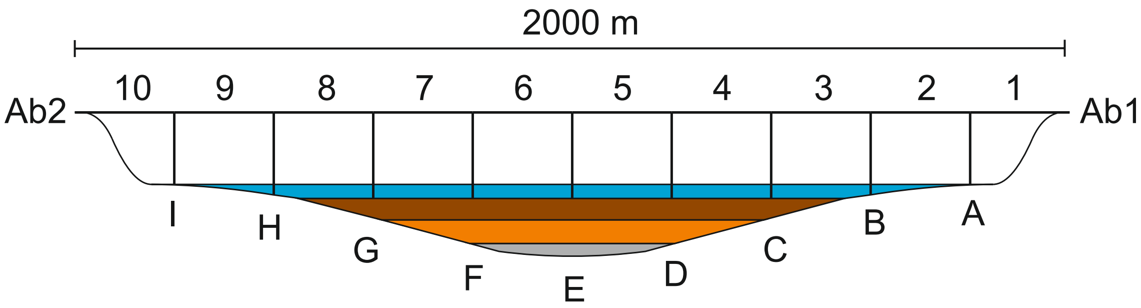

Figure 1.1. Sketch of the bridge.

Beneath the lake three soft soil layers are deposited: A soft clay layer (colored brown), a stiffer gravel layer (colored orange) and an even stiffer moraine layer, which is a mixture of rock and gravel (colored grey). The five bridge columns in water are all founded on the soft soil layers, some only on the clay layer and one on all three layers. All other columns as well as the two abutments are located directly on bedrock.

In chapter 2 the soil layers will described in more detail and the soil parameters will be determined as well. In chapter 3 the bridge dimensions and materials will be determined.

1.2 Wave propagation in soil

Three significant kind of waves traveling through elastic mediums are pressure waves (P-waves), shear waves (S-waves) and surface waves called Rayleigh waves (R-waves). The P-waves are compressional waves and they are the fastest existing wave. The S-waves travels slower than the P-wave and they are equivolumetrical shear waves. The R-waves travels a bit slower than S-waves and they are a combination of P-waves and S-waves and a result of the reflection of these two kind of waves.

write about only SV waves looked at...

Waves at sea refracts when they approach the coast due to the fact that the water depth decreases. This results in that the propagation direction of the waves is almost perpendicular to the coast. The same phenomena exists for waves traveling through elastic solids. The soil layers close to the surface of the earth are mostly horizontally stratified and the stiffness increases with the depth. This results in refraction of the waves and they will therefore encounter the surface of earth with an angle close to perpendicular, as illustrated in figure 1.2.

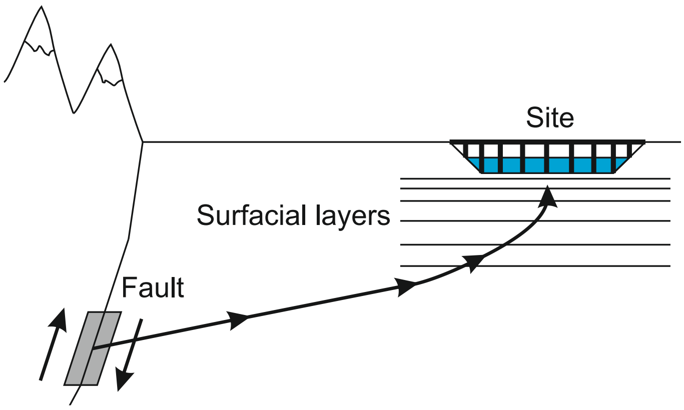

Figure 1.2. Refraction of seismic waves.

The seismic waves are assumed to emanate from a source located at the bedrock beneath the soft soil layers, and it is assumed that they are refracted traveling through the soft soil layers close to the soil surface and when the reach the bottom of the three soft soil layers they are assumed to have a propagation direction close to perpendicular to the soil surface. Consequently only horizontal S-waves (SH-waves) are looked at. Another reason for this is that most structures, including bridges, are much more vulnerable to horizontal excitations compared to vertical excitations.

Soil is a material that acts non-linear as the stiffness parameters vary with both depth due to an increasing stress state, and the amplitude of the strains within the soil. This implies that non-linear models need to be applied in order to describe the soil behavior properly. However, at low strain amplitudes the use of linear models can provide decent results. In figure 1.3 the applicability of linear viscoelatic models is given, and it can be seen that for strain amplitudes of a magnitude 10^{-5} and lower viscoelastic models can model the soil behavior accurately. The figure also shows that for shear train amplitudes higher than a magnitude 10^{-5}, viscoplastic models need to be applied and that for shear strains higher than a magnitude 10^{-3} the load history of the soil gets significant.

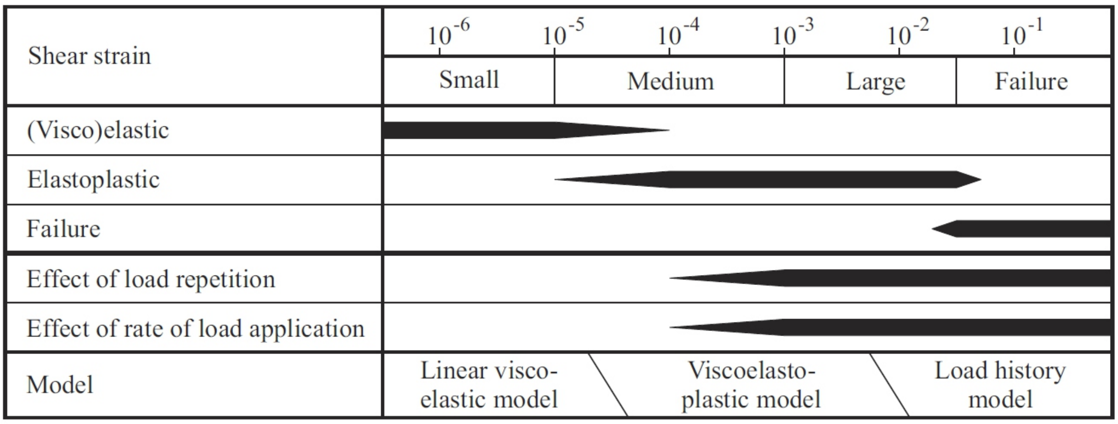

Figure 1.3. Suitability of different material models for soil for different shear strain amplitudes. [Andersen, December 2006]

Shear strains in soil due to seismic waves can be of a magnitude 10^{-3} or higher, which is far from the range of linear models. However, non-linear models are rather complicated to used and many soil parameters need to be determined in order to get accurate results.

The strong motion data used in the investigations are therefore scaled down so linear models can be applied.

Due to the fact that only SH-waves are considered, a 1D soil model is used to model the SH-waves propagation throught the soil layers. This model will be introduced in the next chapter.

1.3 Scope

Linear models will be applied for all the models in this thesis. The soil model will be one dimensional, as only SH-waves are considered. A three dimensional models of the bridge will be applied, as it makes it possible to model both compressional and shear waves in the bridge and vary the direction from which the SH-waves hits the bridge.

A hysteretic material damping model is applied for both soil and the bridge models, as it is recognized to estimate the damping quiet well. Geometrical damping will not be included in the model, as it is assumed that no geometrical damping is present.

In order to take into account the soil-foundation interaction, a lumped parameter model is used to model the stiffness of the foundations which are founded on the soft soil layers.

The following scope is formulated for the thesis,

1. Model of the soil layers
   - One dimensional dynamic linear viscoelastic domain transformation method (DTM) model of SH-waves propagating in the vertical direction through the soil layers.
   - One dimensional dynamic linear viscoelastic finite element (FEM) beam model of SH-waves propagating in the vertical direction through the soil layers.
     - Implementation of an iterative partly linear stiffness and damping model, where the small strain shear modulus is reduced as the shear strain amplitudes increase. The damping ratio will be increased as the shear strain amplitudes increase as well.
2. Model of the bridge
   - Three dimensional dynamic linear viscoelastic finite element beam model of the bridge.

2 Soil model

In this chapter a soil model will be introduced, which will be used to determine the soil response of the soft soil layers to seismic SH-waves.

The soft soil layers beneath the bridge are considered. In Figure 2.1 the bridge is sketched as well as the soft soil layers beneath it.

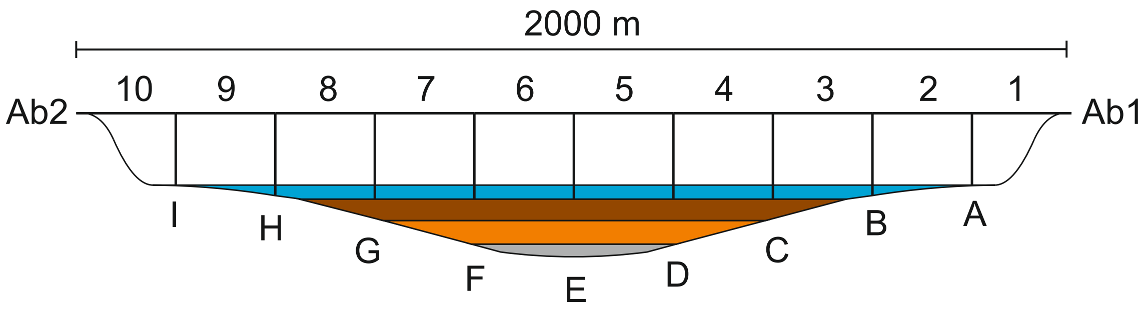

Figure 2.1. Sketch of the bridge and the soil beneath it

As mentioned in the introduction, the bridge has a total length of 2000 m and is build of 10 spans, each with a length of 200 m. The bridge columns are indexed A to I and the spans are indexed 1 to 10. Column A and I has a length of 20 m, column B and H has a length of 25 m and column C to G has a length of 30 m. In the figure three soil layers are sketched beneath the water. The top soil layer is a clay layer (colored brown), the mid soil layer is a gravel layer (colored orange), and the bottom soil layer is a stiff but still residual soil layer, which is a mixture of rock and gravel (colored grey). As it can be seen in the figure all three soil layers can be found beneath column E, only the clay and gravel layer can be found beneath D and F, and only the clay layer can be found under column C and G. The rest of the columns are supported directly on bedrock.

In the next section the material properties necessary to model wave propagation through the soft soil layers will be estimated.

2.1 Soil parameters

The three different soil profiles beneath column C, D and E respectively are illustrated in figure 2.2.

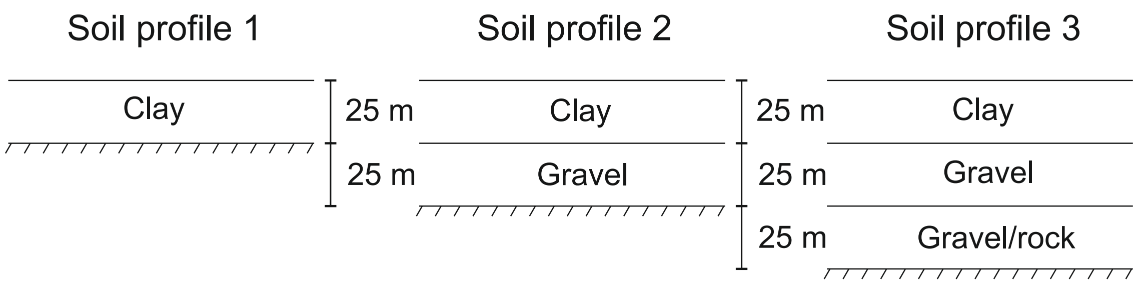

Figure 2.2. Soil stratigraphy for the three soil profiles.

The soil parameters of the three different layers are estimated and given in table 2.2. The estimated parameters are all for small strain amplitudes.

	Clay	Gravel	Gravel/rock mixture
Density, ρ [kg/m^3]	1900.0	2000.0	2500.0
Small strain modulus of elasticity, E_0 [MPa]	50.0	90.0	1000.0
Poisson's ratio, ν [-]	0.4	0.2	0.3
Small strain shear modulus, G_0 [MPa]	17.9	58.3	384.6
Small strain shear wave velocity, $v_{S,0}$ [m/s]	96.9	170.8	392.2

Table 2.1. Soil parameters at small strain amplitudes.

The zero index in the table means that it is the small strain amplitude values that are given. Young's modulus, the density and Poisson's ration are estimated from typical values for clay, gravel and gravel/rock mixture, respectively. The small strain shear modulus is determined as,

$$G_0 = \frac{E}{2\,(1+\nu)} \tag{2.1}$$

The small strain shear wave velocity is determined as,

$$v_{S,0} = \sqrt{\frac{G_0}{\rho}} \tag{2.2}$$

At small strain amplitudes material damping is small, i. e. the loss factor η is small as well. A loss factor of 0.05 is assumed as an initial estimate for all three layers, however, this will later be evaluated.

In figure 2.3 typical propagation velocities for S-waves as well as P-waves are given.

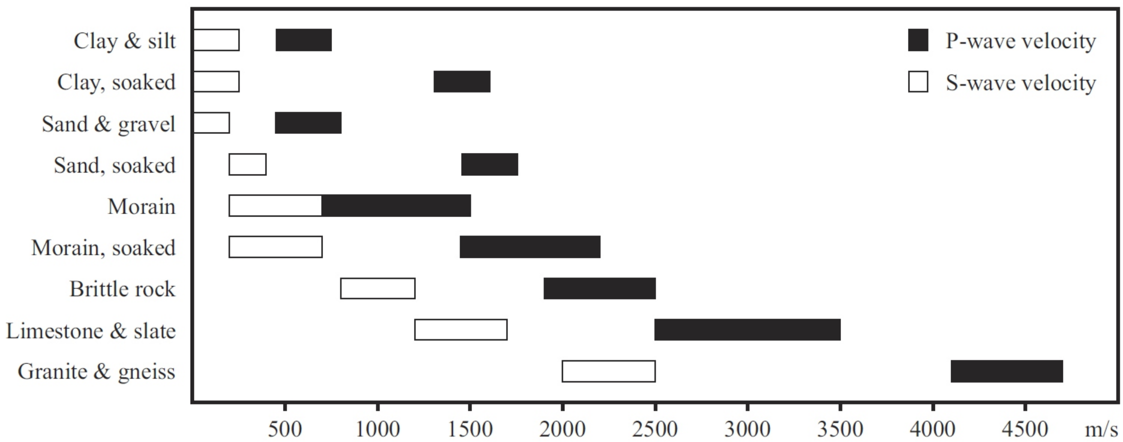

Figure 2.3. Typical propagation velocities for P- and S-waves in soils. [Andersen, December 2006]

The small strain shear wave velocity for the clay layer of 97 m/s fits soaked clay in the figure which has a shear wave in the range 0-250 m/s. The small strain shear wave velocity for gravel of 171 m/s fits somewhat in the transition between gravel and soaked sand, which is around 250 m/s. The small strain shear wave velocity for the gravel/rock mixture of 392 m/s fits soaked morain, which ranges from around 200-700 m/s. Consequently the soil parameters for the three layers coincides quiet well with the values of a soft clay layer, a more stiff gravel layer and an even stiffer residual morain layer.

2.1.1 Strain Dependent Shear Modulus and Loss Factor

With increasing shear strain the shear modulus decreases, and the damping ratio increases as well due to increasing material dissipation.

In Figure 2.4 a shear stress - shear strain backbone curve for soil is illustrated. The curve shows a typical variation of the secant shear modulus with shear strain.

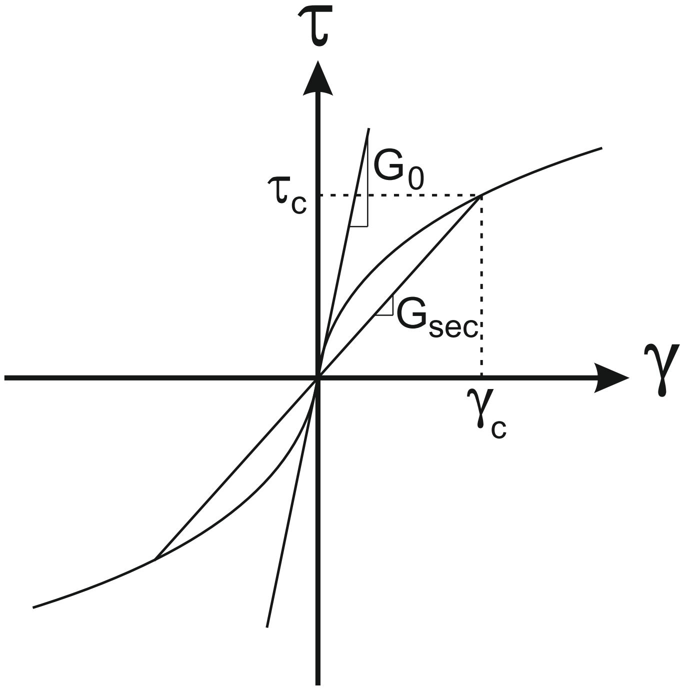

Figure 2.4. Backbone curve showing a typical variation of the secant shear modulus with shear strain.

The secant modulus is defined as,

$$G_{\mathrm{sec}} = \frac{\tau_{\mathrm{c}}}{\gamma_{\mathrm{c}}} \tag{2.3}$$

Where γ_{c} is the shear strain amplitude in the soil and τ_{c} is the shear stress.

The small strain shear modulus is the tangent modulus, which is equal to the secant shear modulus for a shear strain amplitude of zero. But as the shear strain amplitude increases, the secant shear strain modulus decreases as well, as it is illustrated in the figure.

In order to model the stiffness of the soil correctly, the secant shear strain modulus G_{sec} is applied. This can be modeled by the use of formulas given by Ishibashi and Zhang. These formulas account for both cohesive and non-cohesive soils and the fact the reduction of shear modulus as well as the increase of the damping ratio is less significant as the plasticity index increases. The ratio between the secant shear modulus G_{s} and the small strain shear modulus G_0 is given as,

$$\frac{G_{\mathrm{Sec}}}{G_0} = K(\gamma,PI)\ \sigma_{\mathrm{m}}'^{\,m(\gamma,PI)-m_0} \tag{2.4}$$

Where,

$$K(\gamma,PI) = 0.5\ \left(1+\tanh\left(\ln\left(\frac{0.000102+n(PI)}{\gamma}^{0.492}\right)\right)\right) \tag{2.5}$$

$$m(\gamma,PI) - m_0 = 0.272\ \left(1-\tanh\left(\ln\left(\frac{0.000556}{\gamma}^{0.4}\right)\right)\right)\ e^{-0.0145\ PI^{1.3}} \tag{2.6}$$

$$n(PI) = \begin{cases} 0.0 & \text{for} \quad PI = 0 \\ 3.37\ 10^{-6}\ PI^{1.404} & \text{for} \quad 0 < PI \leq 15 \\ 7.0\ 10^{-7}\ PI^{1.976} & \text{for} \quad 15 < PI \leq 70 \\ 2.7\ 10^{-5}\ PI^{1.115} & \text{for} \quad PI > 70 \end{cases} \tag{2.7}$$

Where γ is the shear strain, σ'_{m} is the effective confining pressure in kPa, and PI is the plasticity index.

The damping ratio ζ is given as,

$$\zeta = 0.333\ \frac{1+e^{-0.0145\ PI^{1.3}}}{2}\ \left(0.586\ \left(\frac{G_S}{G_0}\right)^2 - 1.547\ \frac{G_S}{G_0} + 1\right) \tag{2.8}$$

The loss factor is defined as,

$$\eta = 2\ \zeta \tag{2.9}$$

The clay is assumed to be a medium plastic soil with a plasticity index of 50. The other soil layers has a plasticity index of 0 as they are both non-cohesive soils. The effective confining pressure is found 1 m down in each soil layer to 9, 231 and 481 kPa for the clay, gravel and gravel/rock layers, respectively. The small strain shear modulus for the three layers are plotted in figure 2.5.

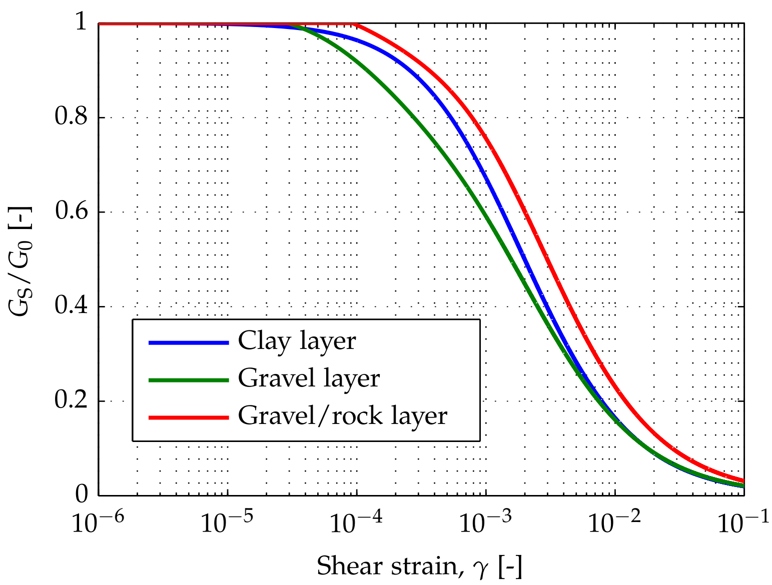

Figure 2.5. Small strain shear modulus as a function of the shear strain amplitude for the three layers.

The loss factor is plotted in figure 2.6.

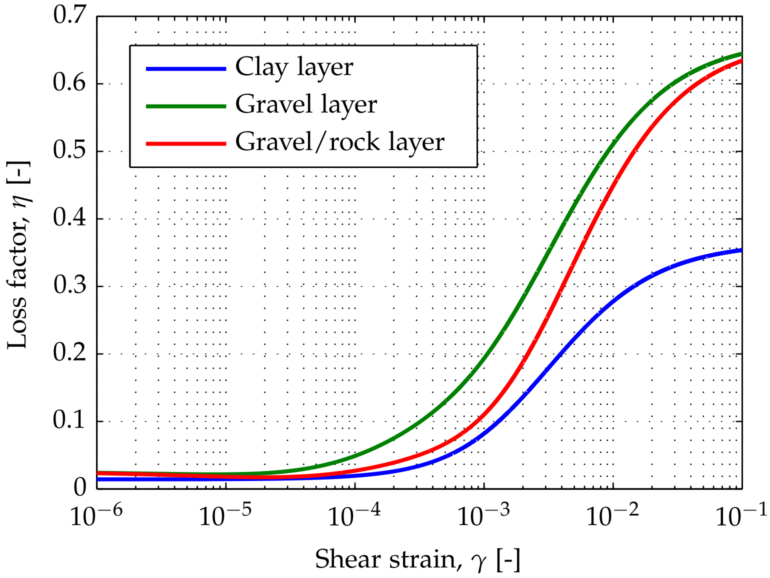

Figure 2.6. The loss factor as a function of the shear strain amplitude for the three layers.

In both the figures the effect of the plasticity index of the clay layer is significant. It can be seen that the reduction of the shear modulus for the clay layer is lower than for the gravel layer. The lowest increase of the loss factor is for the clay layer due to the plasticity index.

2.1.2 Increasing Stiffness with Depth

The stiffness of soils increases with depth as the effective confining pressure increases. Confer PLAXIS [2011] the small strain shear modulus throughout the soil column is assumed distributed as,

$$G_{0,\text{increasing}} = G_0^{\text{ref}} \left(\frac{c \ \cos\varphi + \sigma_3' \ \sin\varphi}{c \ \cos\varphi + \sigma_{3,\text{ref}}' \ \sin\varphi} \right)^m \tag{2.10}$$

where c is the cohesion, φ is the friction angle, m is a factor depending on the soil type and $\sigma_{3,\text{ref}}'$ is the reference stress at the depth where G_0^{ref} is given. The expression is simplified by assuming constant unit weight and zero cohesion for all the used soil layers, which reduces the expression to,

$$G_{0,\text{increasing}} = G_0^{\text{ref}} \left(\frac{K_0 \ \gamma \ z}{K_0 \ \gamma \ z^{\text{ref}}} \right)^m = G_0^{\text{ref}} \left(\frac{z}{z^{\text{ref}}} \right)^m \tag{2.11}$$

For sands m is typically 0.5, which will be used for all soil layers. The reference depth z_{ref} is assumed to be 10 m. The constant small strain and the increasing small strain shear modulus are plotted in figure 2.5.

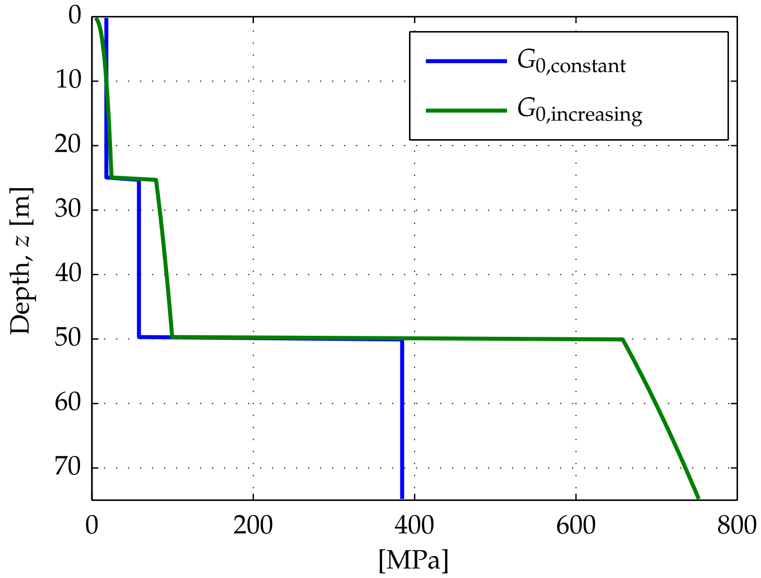

Figure 2.7. Constant and increasing small strain shear modulus plotted with depth.

The increasing small strain shear modulus can be decreased as a function of the shear strains in the soil.

2.2 Domain Transformation Model

The first model used to investigate horizontal shear wave (SH-wave) propagation through the soil is a one dimensional semi analytic Domain Transformation Method (DTM) model which can describe the response of one dimensional SH-waves propagating through a number of horizontally divided soil layers. The formulation of the method is given in appendix A.

The used coordinate system is given in Figure 2.8. The SH-waves propagate in the x_3-direction and the particle displacements is in the x_1-direction.

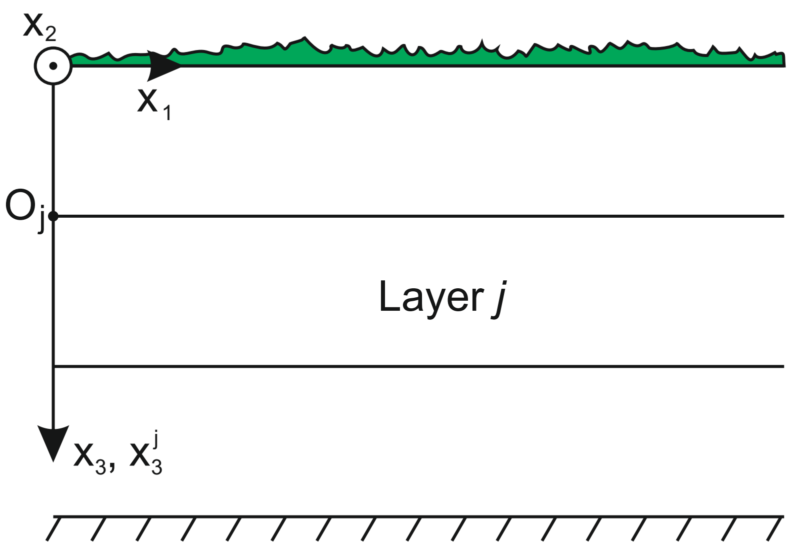

Figure 2.8. Orientation of the used coordinate system.

Inhomogeneities of the soil are only taken into account by dividing the soil into a number of soil layers. Local variations of the soil over a length much shorter than wave length are not of significance to the wave propagation. For a shear wave velocity of 100 m/s a wave a signal of 200 Hz has wave lengths of 0.5 m or more, which is much higher than the particle size for any of the soil layers. Earthquake motions have generally got a low frequency content well below 200 Hz, hence the propagation of SH-waves can be modeled correctly with the model. The behavior of soil can only be assumed to be linear for small strain amplitudes of a magnitude smaller $10^{-}5$ due to the fact that plastic strains start to occur as the strain amplitude gets higher [Andersen, December 2006].

The model is formulated in the frequency domain, which makes it possible to use hysteretic damping. This is done by the use of the complex shear modulus,

$$\mu^{\mathrm{j}} = G^{\mathrm{j}}\ (1 + i\ \eta^{\mathrm{j}}\ \mathrm{sign}(\omega)\ ), \quad \mathrm{sign}(\omega) = \begin{cases} 1 & \text{for } \omega > 0 \\ 0 & \text{for } \omega = 0 \\ -1 & \text{for } \omega < 0 \end{cases} \tag{2.12}$$

Where η is the loss factor, ω the circular frequency and sign is a sign function.

The response at the top of layer j to an excitation in the bottom of the bottom layer can be given as,

$$H^{j0}(\omega) = \left(T_{11}^{j0} - \frac{T_{12}^{j0}\ T_{21}^{10}}{T_{22}^{10}} \right) \tag{2.13}$$

Where $H^{j0}(\omega)$ is the relative response at the top the respective layer, the values of T can be found in Appendix A and they are a function of the wave number, the complex shear modulus and the height of the considered soil layers.

A MATLAB script is produced for the DTM method, where the output is the frequency response function $H^{j0}(\omega)$. The input to the program is the layer stratography, the shear modulus and the loss factor for each layer.

In Figure 2.9 the frequency response diagram at the soil surface for soil profile 3 is plotted for frequencies from 0 to 50 Hz. For seismic waves the highest energy content is found in frequencies from 0 to 20 Hz. Frequencies above this range has generally very low energy content.

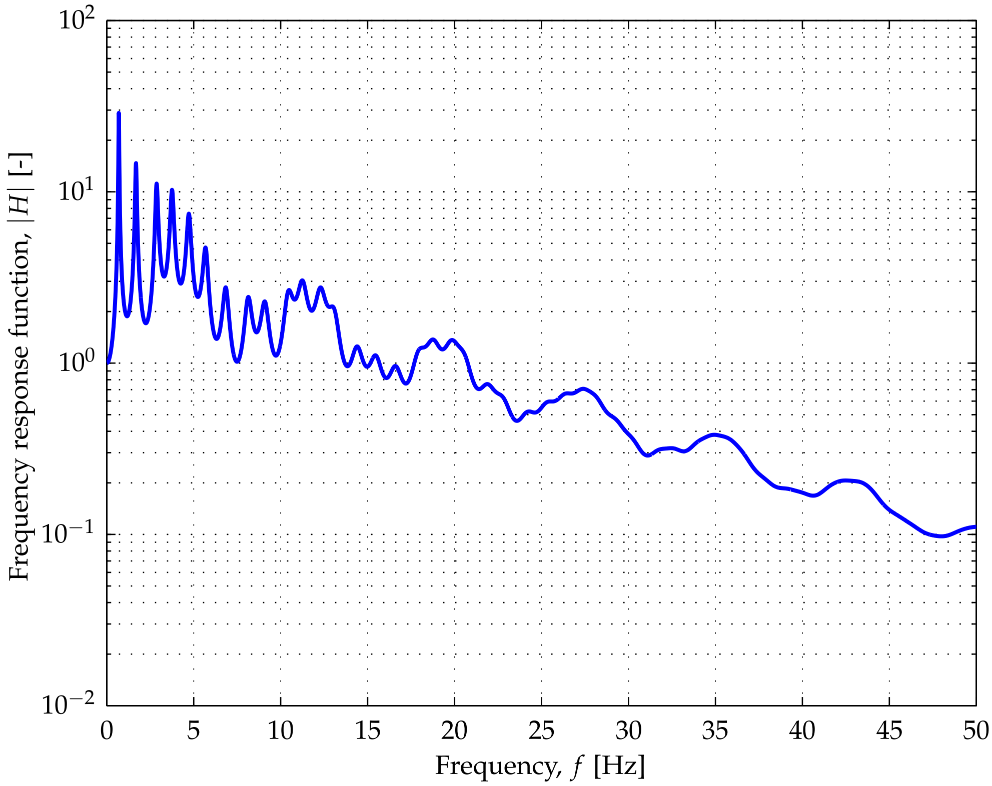

Figure 2.9.

It can be seen that some frequencies from 0 to 20 Hz will be amplified, which happens due to resonance in the soil column. The amplification of the low frequencies is critical as the energy of seismic waves are located in the low frequency content often below 20 Hz.

2.3 FEM model of the soil

A FEM model is also introduced to describe the wave propagation through the soil layers. The formulation of the FEM model is given in appendix B. The elements are located as illustrated in figure 2.10. One degree of freedom (DOF) is used for each node, which is translation in the x_1-direction. SH-waves propagating in the x_3-direction with particle displacement in the x_1-direction can therefore be modeled. The model is linear and viscoelastic and linear shape functions have been applied.

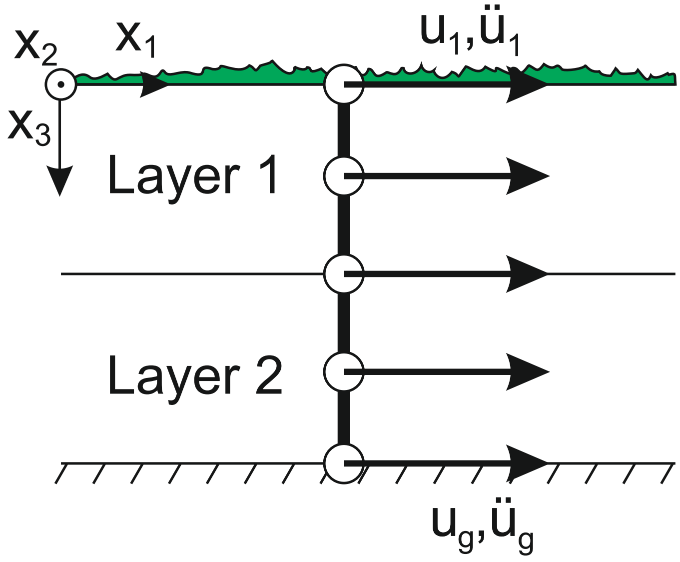

Figure 2.10. Elements in the FEM model

In the following three different approaches for solving the system equations in the frequency domain is described as well as one method for the time domain. By solving the problem in the frequency domain a direct time integration is avoided. In stead the FFT algorithm is used to convert from the frequency domain back into the time domain.

2.3.1 Solution in the frequency domain

Applying a hysteretic damping model, the system equations are given as,

$$\bar{\bar{M}}\,\ddot{\bar{u}} + \frac{1}{\omega}\,\bar{\bar{C}}\,\dot{\bar{u}} + \bar{\bar{K}}\,\bar{u} = \bar{f} \tag{2.14}$$

It can be seen that the circular frequency ω appears in the expression. This is problematic in order to solve the system in the time domain. However, this is not a problem, when a solution is found in the frequency domain, which is done in the following.

Using the Fourier series with exponential notation the displacement $u(t)$, velocity $\dot{u}(t)$ and acceleration $\ddot{u}(t)$ for a single harmonic wave are given by,

$$u(t) = U\,e^{i\,\omega\,t} \tag{2.15}$$

$$\dot{u}(t) = i\,\omega\,U\,e^{i\,\omega\,t} = i\,\omega\,u(t) \tag{2.16}$$

$$\ddot{u}(t) = -\omega^2\,U\,e^{i\,\omega\,t} = -\omega^2\,u(t) \tag{2.17}$$

(2.18)

where U is the amplitudes of the displacement, ω is the circular frequency and t is the time.

Analogously the external force applied to the system is given as,

$$f(t) = F\,e^{i\,\omega\,t} \tag{2.19}$$

where F is the amplitude of the applied force.

Using the given Fourier series formulations, equation 2.14 is formulated in the frequency domain,

$$-\omega^2\,\bar{\bar{M}}\,\bar{U} + i\,\bar{\bar{C}}\,\bar{U} + \bar{\bar{K}}\,\bar{U} = \bar{F} \quad \Leftrightarrow \tag{2.20}$$

$$\hat{\bar{\bar{K}}}\,\bar{U} = \bar{F}, \quad \hat{\bar{\bar{K}}} = -\omega^2\,\bar{\bar{M}} + i\,\bar{\bar{C}} + \bar{\bar{K}} \tag{2.21}$$

where $\hat{\bar{\bar{K}}}$ is named the dynamic stiffness.

Unit displacement approach

The dynamic stiffness is divided into four parts so the DOFS within the soil can be distinguished from the DOF at the bedrock. Thus the system equations are written as,

$$\begin{bmatrix} \hat{\bar{\bar{K}}}_{\mathrm{ss}} & \hat{\bar{\bar{K}}}_{\mathrm{sb}} \\ \hat{\bar{\bar{K}}}_{\mathrm{bs}} & \hat{K}_{\mathrm{bb}} \end{bmatrix} \begin{Bmatrix} \bar{U}_{\mathrm{s}} \\ U_{\mathrm{b}} \end{Bmatrix} = \begin{Bmatrix} \bar{F}_{\mathrm{s}} \\ F_{\mathrm{b}} \end{Bmatrix} \tag{2.22}$$

The system is subjected to base acceleration, which is done by subjecting it to a displacement amplitude of unity in the bottom node and calculating the response in every other nodes. This is done by dividing equation 2.22 with U_{bottom}. All nodes except the bottom node are free to move, hence no external forces are applied at them. This results in,

$$\begin{bmatrix} \hat{\bar{\bar{K}}}_{\mathrm{ss}} & \hat{\bar{K}}_{\mathrm{sb}} \\ \hat{\bar{K}}_{\mathrm{bs}} & \hat{K}_{\mathrm{bb}} \end{bmatrix} \begin{Bmatrix} \bar{U}'_{\mathrm{s}} \\ 1 \end{Bmatrix} = \begin{Bmatrix} \bar{0} \\ F'_{\mathrm{b}} \end{Bmatrix}, \quad \begin{cases} \bar{U}_{\mathrm{s}} = \bar{U}'_{\mathrm{s}}\,U_{\mathrm{b}} \\ F_{\mathrm{b}} = F'_{\mathrm{b}}\,U_{\mathrm{b}} \end{cases} \tag{2.23}$$

The relative displacements in all nodes can then be calculated as,

$$\hat{\bar{\bar{K}}}_{\mathrm{ss}}\,\bar{U}'_{\mathrm{s}} + \hat{\bar{K}}_{\mathrm{sb}} = 0 \quad \Leftrightarrow \quad \bar{U}'_{\mathrm{s}} = -\hat{\bar{\bar{K}}}{}_{\mathrm{ss}}^{-1}\,\hat{\bar{K}}_{\mathrm{sb}} \tag{2.24}$$

The total displacements are determined as,

$$\bar{U}_{\mathrm{s}} = \bar{U}'_{\mathrm{s}}\,U_{\mathrm{b}} \tag{2.25}$$

$$\tag{2.26}$$

Force approach

The displacements in the soil are formulated in relative coordinates as,

$$\bar{u}_{\mathrm{rel}} = \bar{u}_{\mathrm{tot}} - u_{\mathrm{g}}\,\bar{1} \tag{2.27}$$

Where $\bar{u}_{\mathrm{rel}}$ is the relative coordinates up through the soil column, $\bar{u}_{\mathrm{tot}}$ is the total displacements up through the soil column, u_{g} is the induced ground displacements at the bottom of the soil column and $\bar{1}$ is a unit vector with equal length as $\bar{u}_{\mathrm{rel}}$. This is illustrated in figure 2.11. Equation 2.27 is valid for velocity as well as acceleration.

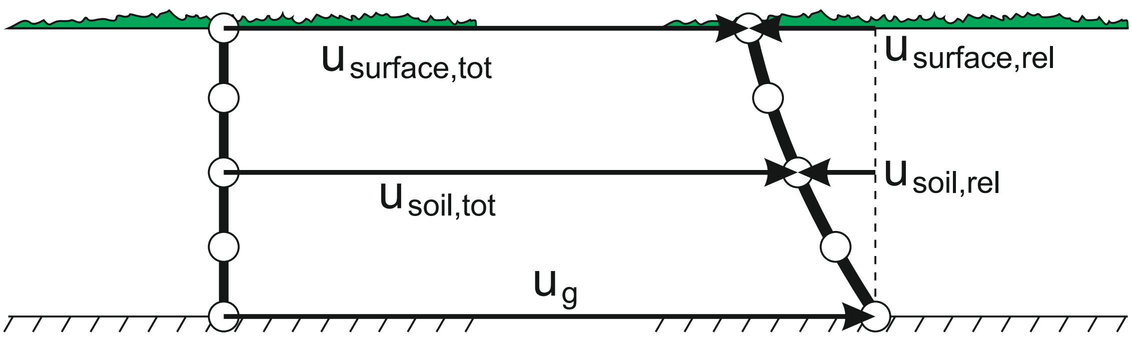

Figure 2.11. Relative coordinate system.

The system equations are given as,

$$\bar{\bar{M}}\ \ddot{\bar{u}}_{\text{tot}} + \frac{1}{\omega}\ \bar{\bar{C}}\ \bar{u}_{\text{rel}} + \bar{\bar{K}}\ \bar{u}_{\text{rel}} = \bar{f} = 0 \tag{2.28}$$

Using equation 2.27 the system of equations are reformulated as,

$$\bar{\bar{M}}\ \ddot{\bar{u}}_{\text{rel}} + \frac{1}{\omega}\ \bar{\bar{C}}\ \bar{u}_{\text{rel}} + \bar{\bar{K}}\ \bar{u}_{\text{rel}} = -\bar{\bar{M}}\ \bar{1}\ \ddot{u}_{\text{g}} \tag{2.29}$$

This means that a system subjected to base acceleration $\ddot{u}_{\text{g}}$ is equivalent to a system fixed at the base and subjected to the external forces $\bar{F} = -\bar{\bar{M}}\ \bar{1}\ \ddot{u}_{\text{g}}$.

Using the same approach as in the former section the system of equations can be written in the frequency domain as,

$$\begin{bmatrix} \hat{\bar{\bar{K}}}_{\text{soil,surface}} & \hat{\bar{K}}_{\text{soil,bottom}} \\ \hat{\bar{K}}_{\text{bottom,soil}} & \hat{K}_{\text{bottom,bottom}} \end{bmatrix} \begin{Bmatrix} \bar{U}_{\text{soil,rel}} \\ 0 \end{Bmatrix} = \begin{Bmatrix} -\bar{\bar{M}}\ \bar{1}\ \ddot{U}_{\text{g}} \\ F_{\text{bottom}} \end{Bmatrix} \tag{2.30}$$

Thus the relative displacement amplitudes can be determined as,

$$\bar{U}_{\text{soil,rel}} = -\hat{\bar{\bar{K}}}^{-1}_{\text{soil,surface}}\ \bar{\bar{M}}\ \bar{1}\ \ddot{U}_{\text{g}} \tag{2.31}$$

The total displacement amplitudes is determined as,

$$\bar{U}_{\text{soil,tot}} = \bar{U}_{\text{soil,rel}} + \bar{1}\ U_{\text{g}} \tag{2.32}$$

Application of the Fast Fourier Transform

In order to apply the models in the frequency domain, it is necessary to convert a displacement-time series to the frequency domain, calculate the response to a given excitation and transform the new displacement frequency spectrum back into the time domain. To do this the Fast Fourier Transform (FFT) in MATLAB is applied, which is an algorithm that by application of the Fourier Series numerically transforms a time data series into the frequency domain. One thing to note about the FFT is that it has a Nyquist frequency, which is the half of the sample frequency. The frequency spectrum is mirrored around the Nyquist frequency, but only frequencies below the Nyquist frequency provides physically meaningful results. This is shown in figure 2.12, where the time-displacement series for the 1995 Gulf of Aqaba Earthquake is plotted as well its frequency spectrum. The sample frequency for the earthquake record is 200 Hz, and it can be seen that the data is mirrored around 100 Hz.

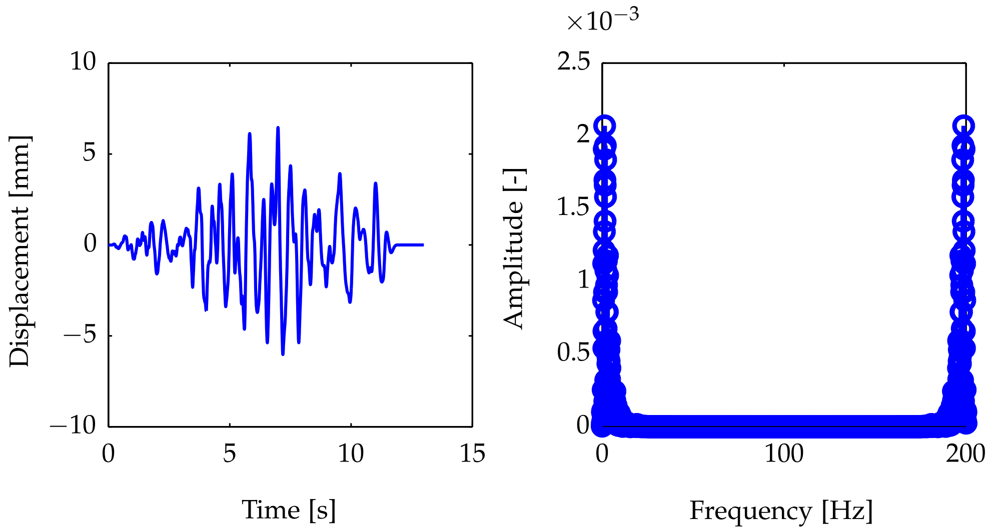

Figure 2.12. Displacement-time series and frequency spectrum for the 1995 Gulf Aqaba Earthquake.

Due to the fact that it is only the frequencies below the Nyquist frequency that make physical sense, the data above the Nyquist frequency are discarded. As a consequence the number of samples is reduced by half. Therefore a new time step is introduced as the double of the initial time step, when the data is transformed back into the time domain.

Another issue that needs to be addressed is processing of strong motion records. The strong motion records used in the project is downloaded from Pasific Earthquake Engineering Research Center [2013]. Both acceleration-time, velocity-time and displacement-time series are available for over 150 different earthquakes. The velocity and displacement data is determined using bandpass filters etc. to the acceleration-time series before performing a time integration. This can easily be seen performing a simple time integration on the acceleration-time data, which will not give close to the velocity-time series provided. To avoid inconsistencies only displacement-time series is used as input and output for the models.

2.3.2 Solution in the time domain

Viscous damping is applied, as hysteretic damping is not possible to implement in the time domain. The system equations for the time step $j+1$ is given as,

$$\bar{\bar{M}}\,\ddot{\bar{u}}_{\text{j+1}} + \bar{\bar{C}}\,\dot{\bar{u}}_{\text{j+1}} + \bar{\bar{K}}\,\bar{u}_{\text{j+1}} = \bar{f}_{\text{j+1}} \tag{2.33}$$

It is the relative system of equations that are considered again.

Using the Newmark Scheme the accelerations, velocities and displacements is determined as,

$$\ddot{\bar{u}}_{\text{j+1}} = \ddot{\bar{u}}_{\text{j}} + \hat{\bar{\bar{M}}}^{-1}\left(\bar{f}_{\text{j+1}} - \bar{\bar{M}}\,\ddot{\bar{u}}_{\text{j}} - \bar{\bar{C}}\,\dot{\bar{u}}^{*}_{\text{j+1}} - \bar{\bar{K}}\,\bar{u}^{*}_{\text{j+1}}\right) \tag{2.34}$$

$$\dot{\bar{u}}_{\text{j+1}} = \dot{\bar{u}}^{*}_{\text{j+1}} + \gamma\,(\ddot{\bar{u}}_{\text{j+1}} - \ddot{\bar{u}}_{\text{j}})\,\Delta t \tag{2.35}$$

$$\bar{u}_{\text{j+1}} = \bar{u}^{*}_{\text{j+1}} + \beta\,(\ddot{\bar{u}}_{\text{j+1}} - \ddot{\bar{u}}_{\text{j}})\,\Delta t^{2} \tag{2.36}$$

Where,

$$\hat{\bar{\bar{M}}} = \bar{\bar{M}} + \gamma\ \bar{\bar{C}}\ \Delta t + \beta\ \bar{\bar{K}}\ \Delta t^2 \tag{2.37}$$

$$\bar{\dot{u}}^*_{j+1} = \bar{\dot{u}}_j + \bar{\ddot{u}}_j\ \Delta t \tag{2.38}$$

$$\bar{u}^*_{j+1} = \bar{u}_j + \bar{\dot{u}}_j\ \Delta t + \frac{1}{2}\ \bar{\ddot{u}}_j\ \Delta t^2 \tag{2.39}$$

Where γ and β are integration constants. The values $\gamma = 1/2$ and $\beta = 1/4$ are used, which corresponds to constant acceleration within each time step. Thus the forces for every time step in the calculations need to be known, but the accelerations, velocities and displacements only need to be known for the initial time step.

2.3.3 Comparison of the different soil models

Until now one approach is described using the DTM model, three different approaches using the FEM soil model in the frequency domain and one in the time domain. In table 2.2 the different models are listed and it is compared which different applications they have.

	DTM	FEM force freq.	FEM disp. freq.	FEM force time
Excitation by equivalent force		X		X
Excitation by displacement	X		X	
Application of hysteretic damping	X	X	X	
Application of viscous damping	X	X	X	X
Frequency response diagram	X		X	

Table 2.2.

In order to verify the models they are compared two by two as following,

1. The DTM to the FEM frequency displacement model using hysteretic damping
2. The FEM frequency domain displacement model to the FEM frequency domain force model using hysteretic damping
3. The FEM frequency domain displacement model to the FEM time domain force model using viscous damping

This is done in the following sections.

Comparison of the DTM and FEM frequency displacement model

The frequency response of the FEM unit displacement model is compared to the frequency response of the semi analytic DTM model. The results are plotted in figure 2.13 for 400 elements applied in the FEM model.

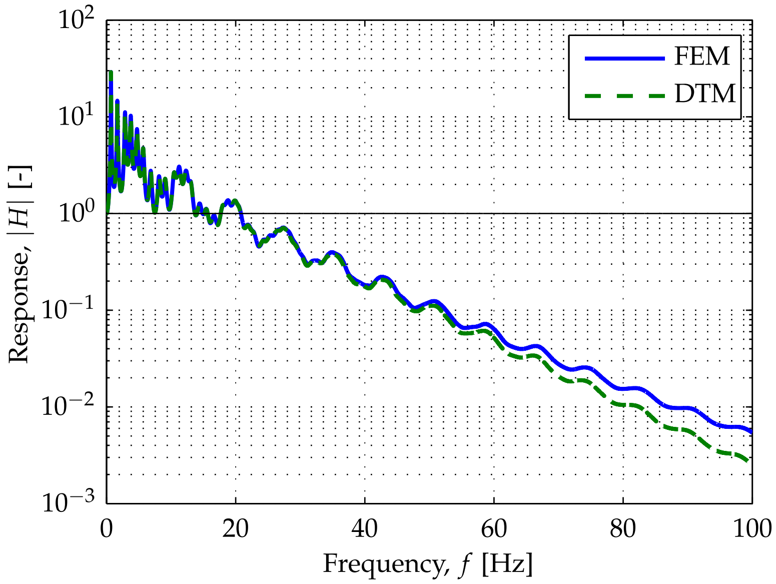

Figure 2.13. Comparison between the semi analytic DTM model and the FEM model with 400 elements.

It can be seen that the two models converge quiet nicely, even though the FEM model does not fit exactly at frequencies above 30 Hz. However, most earthquakes lies in the low frequency range between 0 and 20 Hz. Consequently the FEM soil model will describe the soil response quiet well. 400 Elements will there be used in FEM soil model.

Comparison of the FEM frequency displacement and force models

In figure 2.14 the FEM frequency domain displacement and force models are compared using hysteretic damping. They have exactly the same response, which is why it is concluded that the displacement approach and the force approach both can be used.

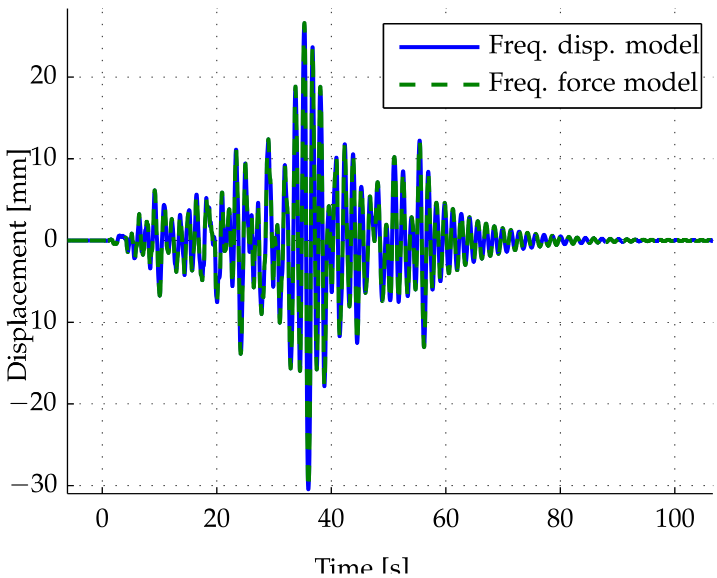

Figure 2.14.

Comparison of the FEM frequency domain displacement and time domain force models

In order to compare the FEM frequency domain displacement model to the FEM time domain force model viscous damping are used. The results of the two models are plotted in figure 2.15. The two models does not give exactly the same, but the results are close, which indicates that the models performs well.

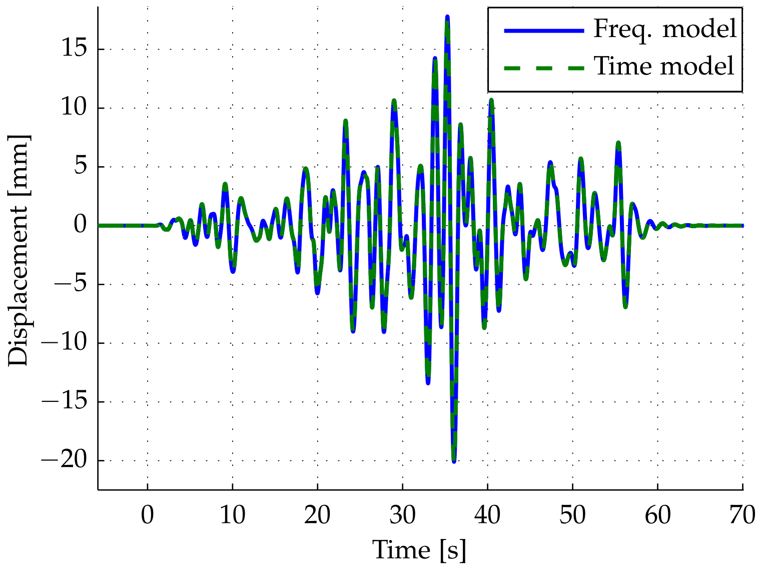

Figure 2.15.

Conclusion on the comparison

The comparison of the DTM and FEM frequency models indicates that the models calculates correctly, as the models are build differently, even though many of the assumptions they are build on are the same. The comparison of the FEM frequency domain model to the FEM time domain model indicates that the solution in the frequency domain is valid. The last comparison of the FEM frequency domain displacement model to the FEM frequency domain force model indicates that both the force approach and the displacement approach performs in the same manner, consequently both models can be used. All in all, the models seem to perform quite well.

The FEM model is used for the analysis of the soil response as the strains are easily determined, which can be used in a partly linear model, which is introduced in the next section.

2.3.4 Equivalent Linear Model

An equivalent linear model is developed, where the increase and decrease of the shear modulus and the loss factor, respectively, with increasing shear strain is taken into account, as given in figure 2.5 and 2.6. In order to do so the strains need to be determined, which is done as,

$$\gamma = \frac{\Delta u_1}{\Delta x_3} \tag{2.40}$$

This gives one shear strain value for each sublayer. An effective shear strains γ_{eff} is determined for each sublayer for the whole time series. Accounting to Kramer [1996] the effective shear strain for each layer is taken as 65 % of the peak shear strain in each layer, which is found to give decent results. This is close to the RMS value of a sine curve, which is around 70 % of the peak value. Due to the fact that only one value are used for the shear strains for the whole time series the equivalent linear model does not give accurate results for displacement-time series that varies much in magnitude. However, it gives a good estimate of the shear modulus and damping ratio for a signal that has a somewhat constant strain amplitude. The strains, shear modulus and loss factor are determined using the following iterative procedure,

1. Initial estimates of the shear modulus and the loss factor
2. The ground response is calculated using the initial estimates
3. The effective shear strain is determined for each sublayer
4. From the effective shear strain new estimates of the shear modulus and loss factor are determined
5. Steps 2 to 4 are repeated until differences between the strains, shear modulus and loss factor fall below an acceptable limit

The 1965 Gulf Aqaba Earthquake data is used, but the data are scaled with a factor 10^{-1} in order to reduce the maximum shear strain amplitude. In figure 2.16 three plots are given. The plotted values are from the first iteration. The old values refers to the initial estimates and the new values refers to the values from the first iteration. The plot to the left is the effective shear strains through the soil column, the plot in the middle is the corrected shear modulus through the soil column, and the plot to the right is the corrected loss factor through the soil column. It can be seen that the maximum shear strain amplitude is around $5 \cdot 10^{-4}$, which is a bit too high for the applied equivalent linear model. However, it is used anyway, since the accelerations and displacement of the strong motion data for the Aqaba 1995 Earthquake is somewhat constant over the time.

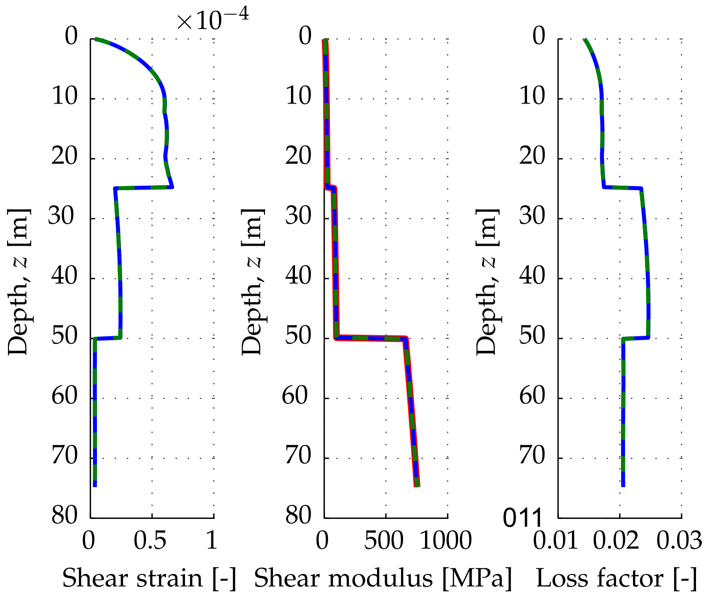

Figure 2.16. First iteration of correction of the shear modulus and loss factor and thereafter new determined shear strains.

In figure 2.17 the frequency response diagram at the soil surface is given. It can be seen that almost all frequencies from 0 to 40 Hz are amplified, which is very critical for earthquake excitations.

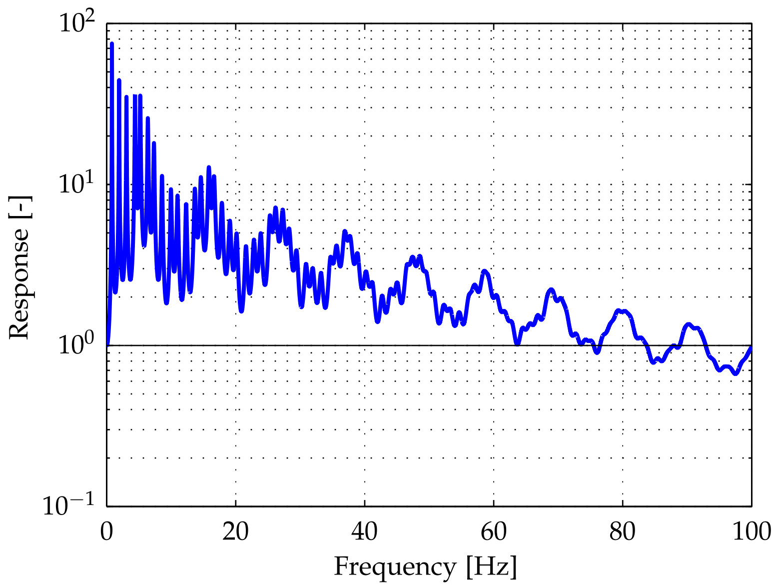

Figure 2.17.

In figure 2.18 the amplified time-displacement series at the soil surface is plotted with the original data at the bedrock. It can also be seen on this plot, that the signal is indeed amplified.

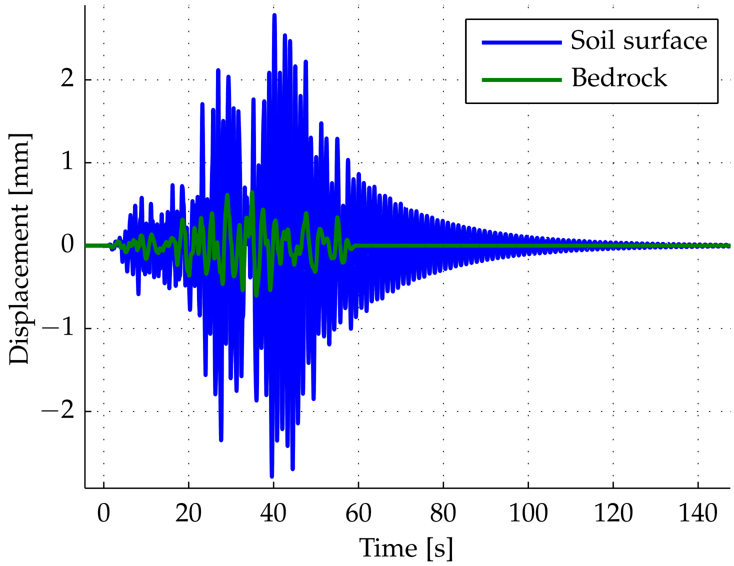

Figure 2.18.

A motion plot is made for the time series. In figure 2.19 a screen shot of the motion plot is given. It can be seen that the strains for the top layer are of a high amplitude, which can also be seen i figure 2.16.

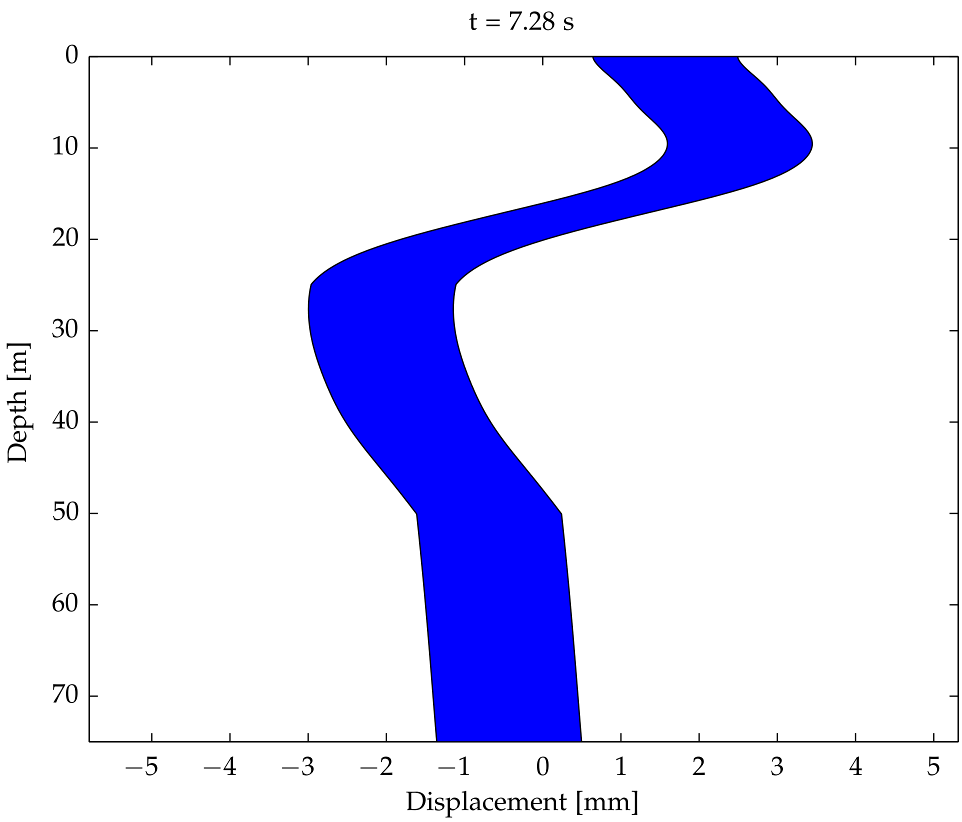

Figure 2.19.

3 Bridge Model

In this chapter a 3 dimensional FEM beam model is introduced in order to model the wave propagation through the bridge.

The bridge is constructed using hollow steel sections for the bridge deck, rectangular prestressed concrete sections for the columns and circular solid concrete foundations. In Figure 3.1 two spans of the bridge are illustrated and the used sections as well as the circular foundation are sketched.

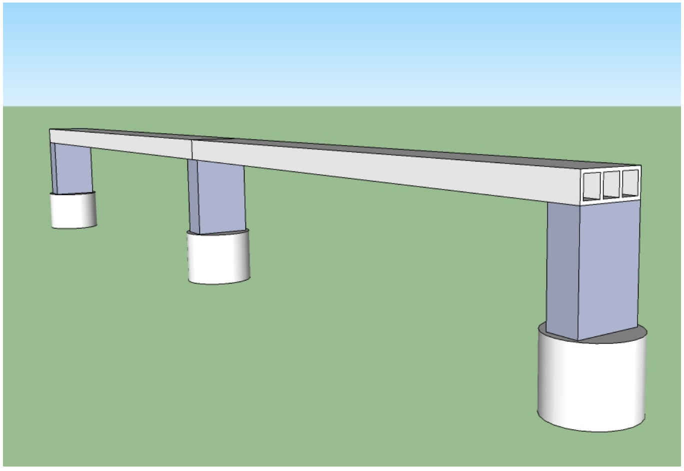

Figure 3.1. Sketch of the static system

The bridge deck will be analysed by calculation of the stresses that occurs due to the earthquake excitations. The bridge columns, however, will not be analysed, as design of prestressed concrete sections is not straight forward and besides that it is beyond the scope of this thesis. A small parameter study will be carried out for the stresses in the bridge deck and the two parameters which will be varied is the horizontal angle between the axis of the bridge deck and the propagation direction of the SH-waves and the propagation velocity in the bedrock.

In the next section the dimensions of the bridge are determined using rough estimates, and the material properties are determined.

The coordinate system used for the bridge is located on the bottom of the first column from the right hand side, and it is illustrated in figure 3.2.

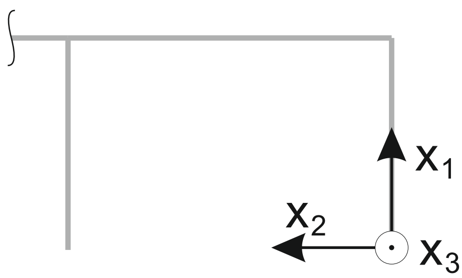

Figure 3.2. Coordinate system used for the bridge

3.1 Material Properties and Dimensions

In Appendix F the material properties for the steel deck and the concrete columns are found. In table 3.1 the results for both steel and concrete are given.

	Concrete	Steel
Tangent modulus of elasticity, E [MPa]	43550.0	210000.0
Poisson's ratio, ν [-]	0.2	0.3
Tangent shear modulus, G [MPa]	18146.0	80769.0
Density, ρ [kg/m^3]	2500.0	7850.0

Table 3.1. Material parameters for the concrete and steel sections.

For the foundations a unit weight of 2400 kg/m^3 is used.

For all elements in the bridge a loss factor η of 0.01 is used, as material damping is limited in the elastic domain.

In Appendix G the dimensions of the bridge deck, concrete columns and foundation beneath the columns are estimated. The results are given in table 3.2.

Width of the bridge deck [m]	20
Height of the bridge deck [m]	8
Material thickness of the bridge deck [m]	1
Free span of the bridge deck [m]	200
Width of the bridge column [m]	20
Depth of the bridge column [m]	10
Diameter of the foundation [m]	25
Depth of the foundation [m]	20

Table 3.2. Dimensions of the bridge.

3.2 FEM beam model of the bridge

A 3D FEM beam model is introduced for the bridge with six degrees of freedom (dofs) per node, as illustrated in figure 3.3. The sign convention for translation is positive in the respective coordinate directions. Rotations are positive counter clockwise the respective coordinate axis as illustrated in the figure.

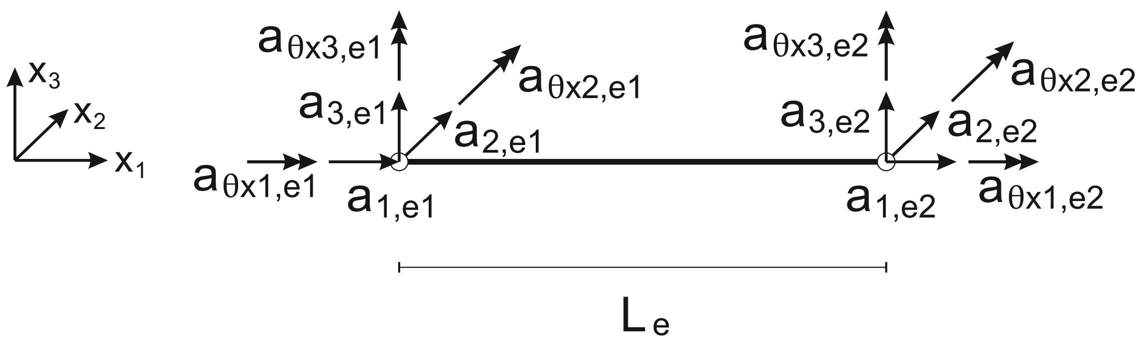

Figure 3.3. Degrees of freedom for the used beam elements.

Thus both compressional waves, torsional waves and shear waves can be modeled with the beam elements.

The beam elements used are Bernoulli Euler beam elements. In figure 3.4 the vibration of a beam element is sketched. In the top of the figure the case were the wave length is very high relative to the beam height is sketched. In this case the translational forces is by far the most significant and the Bernoulli Beam Theory can be used without problems. The other case sketched in the bottom of the figure is the case where the wave length is short relatively to the beam height. Here the rotational forces are significant and the Timoshenko Beam Theory need to be used to take account for the rotational forces on the beam mass. The Bernoulli Beam Theory is used for the FEM model, and it is later evaluated, whether this is acceptable.

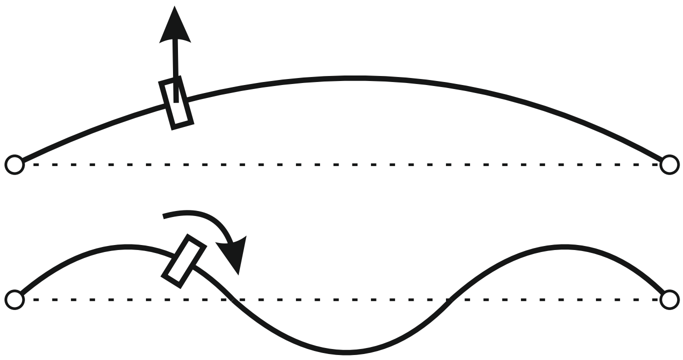

Figure 3.4. Vibration of beam elements.

In appendix C a FEM beam model is introduced for the two degrees of freedom: Rotation around the x_3-axis and translation in the x_2 direction using cubic shape functions. Thus the shear force in the x_2-direction is connected to bending around the x_3-axis confer the Bernoulli Beam Theory. Analogously the two dofs: Rotation around the x_2-axis and translation in the x_3-direction is introduced, however, the sign of the shape functions for the rotations are negative compared to the shape functions used for rotation around the x_3-axis and translation the the x_2 direction. In appendix D a torsional FEM model is introduced using linear shape functions. Analogously a FEM model is introduced for axial translation using linear shape functions as well. The stiffness and mass matrices for the introduced models are used to assemble the 12 dof stiffness and mass matrices given in appendix H. The resulting stiffness and mass matrix are validated by a comparison of the stiffness and mass matrices given for a 12 dof beam element [Cook *et al.*, 2002], and they are identical.

The global system matrices now need to be assembled. The elements are first divided into subelements. In figure 3.4 the bridge beams and columns are illustrated. The node numbers are given as well, and it can be seen that a total of 90 nodes have been used. The beams are divided into five elements each, the columns above water (A and I) are divided into three elements each, column B and H are divided into four elements each, three elements above water and one under water, columns C to G are divided into five elements each, three above water and two under water. This gives a total of 89 elements for the bridge.

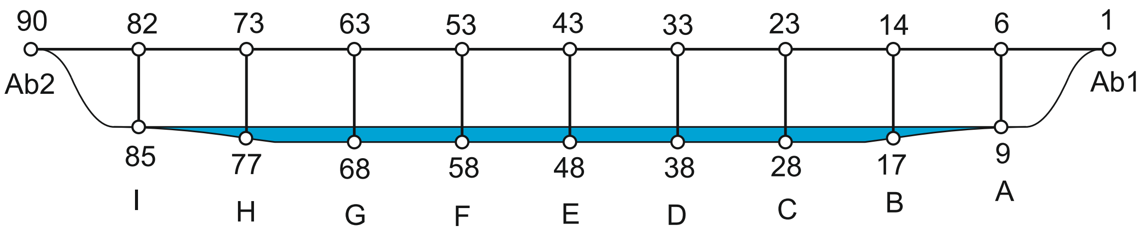

Figure 3.5.

3.2.1 Solving the System Equations

For the FEM bridge model hysteretic damping is used, which is the reason why the system equations are solved in the frequency domain. Analogously to the solution of the displacement induced soil model in the freqeuncy domain, the system equation are given as,

$$-\omega^2 \,\bar{\bar{M}}\, \bar{U} + i\, \bar{\bar{C}}\, \bar{U} + \bar{\bar{K}}\, \bar{U} = \bar{F} \quad \Leftrightarrow \tag{3.1}$$

$$\hat{\bar{\bar{K}}}\, \bar{U} = \bar{F}, \quad \hat{\bar{\bar{K}}} = -\omega^2 \,\bar{\bar{M}} + i\, \bar{\bar{C}} + \bar{\bar{K}} \tag{3.2}$$

The bridge is excited by induced displacements in the x_2- and x_3-direction direction only. It is excited at each end at Node 1 and 90 and at the end of each column in nodes 9, 17, 28, 38, 48, 58, 68, 77 and 85. This gives a total of 24 dofs which are excited, 12 in the x_2-direction and 12 in the x_3-direction. It is wished to be able to change the horizontal direction at which the bridge is excited. This can be done using a linear combination of excitations in the x_2- and x_3-direction. It is also wished to be able to delay the excitation at each column so the columns are excited one after another with a time interval depending on the propagation velocity of the seismic waves in the bedrock. Due to these two requirements the bridge columns are excited one by one in each horizontal coordinate direction. This gives a total of 24 solutions of the system equations. The system equations are solved using the same method that was used to solve the displacement induced soil model in the frequency domain. This is written as,

$$\begin{bmatrix} \underset{(N-24)\times(N-24)}{\hat{\bar{\bar{K}}}_{\mathrm{ii}}} & \underset{(N-24)\times 24}{\hat{\bar{\bar{K}}}_{\mathrm{ib}}} \\ \underset{(N-24)\times 24}{\hat{\bar{\bar{K}}}_{\mathrm{b}}} & \underset{24\times 24}{\hat{\bar{\bar{K}}}_{\mathrm{bb}}} \end{bmatrix} \begin{Bmatrix} \underset{(N-24)\times 1}{\bar{U}'_{\mathrm{i}}} \\ \underset{24\times 1}{\bar{U}'_{\mathrm{b}}} \end{Bmatrix} = \begin{Bmatrix} \underset{(N-24)\times 1}{\bar{0}} \\ \underset{24\times 1}{\bar{F}'_{\mathrm{b}}} \end{Bmatrix}, \quad \begin{cases} \bar{U}_{\mathrm{i}} = \bar{U}'_{\mathrm{i}}\, U_{\mathrm{b}} \\ \bar{F}_{\mathrm{b}} = \bar{F}'_{\mathrm{b}}\, U_{\mathrm{b}} \end{cases} \tag{3.3}$$

where the index i refers to the nodes that are not excited, the index b refers to the nodes which are excited, N is the number of dofs of the entire system, which is 540. The text below the matrices and vectors gives the size of them, row $\times$ columns. For example the matrix $\underset{(N-24)\times(N-24)}{\hat{\bar{\bar{K}}}_{\mathrm{ii}}}$ is a $(N-24)\times(N-24)$ matrix. As it can be seen all the dofs which are displacement induced are assembled down in the lower right corner of the stiffness matrix in $\underset{24\times 24}{\hat{\bar{\bar{K}}}_{\mathrm{bb}}}$ and lowest in the displacement vector in $\underset{24\times 1}{\bar{U}'_{\mathrm{b}}}$. All the dofs which are not displacement induced is free to move, hence the external force acting on them is equal to zero. However, all the dofs which are displacement induced has a equivalent force acting on them. The system is solved as,

$$\bar{U}'_{\mathrm{i}} = -\{\hat{\bar{\bar{K}}}_{\mathrm{ii}}\}^{-1}\, \hat{\bar{\bar{K}}}_{\mathrm{ib}}\, \bar{U}'_{\mathrm{b}} \tag{3.4}$$

Which is the response to unit displacement in only one of the 24 dofs which are to be excited. The response of the system can then be found as,

$$\bar{U}_{\mathrm{i}} = \bar{U}'_{\mathrm{i}}\ U_{\mathrm{b}} \tag{3.5}$$

Due to the fact that only one dof in $\bar{U}'_{\mathrm{b}}$ is different from zero, the system need to be solved 24 times. This is rather time consuming and the time used to solve the 24 systems of equations is around 2 hours.

Alternatively, the 24 systems of equations are written in one matrix equation as,

$$\begin{bmatrix} \underset{(N-24)\times(N-24)}{\hat{\hat{\bar{K}}}_{\mathrm{ii}}} & \underset{(N-24)\times 24}{\hat{\hat{\bar{K}}}_{\mathrm{ib}}} \\ \underset{(N-24)\times 24}{\hat{\hat{\bar{K}}}_{\mathrm{b}}} & \underset{24\times 24}{\hat{\hat{\bar{K}}}_{\mathrm{bb}}} \end{bmatrix} \left[\begin{Bmatrix} \underset{(N-24)\times 1}{\bar{U}'^{1}_{\mathrm{i}}} \\ \underset{24\times 1}{\bar{U}'^{1}_{\mathrm{b}}} \end{Bmatrix} \begin{Bmatrix} \underset{(N-24)\times 1}{\bar{U}'^{2}_{\mathrm{i}}} \\ \underset{24\times 1}{\bar{U}'^{2}_{\mathrm{b}}} \end{Bmatrix} \cdots \begin{Bmatrix} \underset{(N-24)\times 1}{\bar{U}'^{24}_{\mathrm{i}}} \\ \underset{24\times 1}{\bar{U}'^{24}_{\mathrm{b}}} \end{Bmatrix} \right] \tag{3.6}$$

$$= \left[\begin{Bmatrix} \underset{(N-24)\times 1}{\bar{0}} \\ \underset{24\times 1}{\bar{F}'^{1}_{\mathrm{b}}} \end{Bmatrix} \begin{Bmatrix} \underset{(N-24)\times 1}{\bar{0}} \\ \underset{24\times 1}{\bar{F}'^{2}_{\mathrm{b}}} \end{Bmatrix} \cdots \begin{Bmatrix} \underset{(N-24)\times 1}{\bar{0}} \\ \underset{24\times 1}{\bar{F}'^{24}_{\mathrm{b}}} \end{Bmatrix} \right] \tag{3.7}$$

where the matrix with displacement vectors as well as the matrix with the force vectors have the size $N \times 24$. The displacement of all the nodes that are free to move are found as,

$$\underset{(N-24)\times 24}{\left[\bar{U}'^{1}_{\mathrm{i}}\ \bar{U}'^{1}_{\mathrm{i}}\ ...\ \bar{U}'^{24}_{\mathrm{i}}\right]} = \underset{(N-24)\times(N-24)}{-\{\hat{\hat{\bar{K}}}_{\mathrm{ii}}\}^{-1}}\ \underset{(N-24)\times 24}{\hat{\hat{\bar{K}}}_{\mathrm{ib}}}\ \underset{24\times 24}{\left[\bar{U}'^{1}_{\mathrm{b}}\ \bar{U}'^{1}_{\mathrm{b}}\ ...\ \bar{U}'^{24}_{\mathrm{b}}\right]} \tag{3.8}$$

which is the relative displacements of the system. The $\left[\bar{U}'^{1}_{\mathrm{b}}\ \bar{U}'^{1}_{\mathrm{b}}\ ...\ \bar{U}'^{24}_{\mathrm{b}}\right]$ matrix is a 24×24 identity matrix, as the first dof in $\bar{U}'^{1}_{\mathrm{b}}$ is 1 and all other dofs zero, the second dof in $\bar{U}'^{2}_{\mathrm{b}}$ is one while all the other dofs are zero etc. The total displacements of the system are found as,

$$\underset{(N-24)\times 24}{\left[\bar{U}^{1}_{\mathrm{i}}\ \bar{U}^{1}_{\mathrm{i}}\ ...\ \bar{U}^{24}_{\mathrm{i}}\right]} = \underset{(N-24)\times 24}{\left[\bar{U}'^{1}_{\mathrm{i}}\ \bar{U}'^{1}_{\mathrm{i}}\ ...\ \bar{U}'^{24}_{\mathrm{i}}\right]}\ \underset{1\times 1}{U_{\mathrm{b}}} \tag{3.9}$$

The calculation time for the matrix equations is now around 12 minutes, which as an improvement by a factor 10. Consequently much time can be saved by solving the system of equations in one matrix equation.

3.2.2 Hydrodynamic and Additional Mass

For the elements that are under water hydrodynamic mass is added. Confer [Newman, 1977] the added mass per meter for a square cross section is,

$$\frac{M}{h} = 4.754\ \rho_{\mathrm{w}}\ a^2 \tag{3.10}$$

where ρ_{w} is the density for water and a is the width of the section. This gives an additional density of,

$$\rho_{\text{hydrodynamic mass}} = 4.754\ \rho_{\mathrm{w}} \tag{3.11}$$

Which is added to the density of the concrete columns for the elements which are under water. Even though the sections are rectangular the additional mass for a square section is used.

An additional weight for the beams per meter is calculated assuming that a one meter thick concrete deck is made on top of the beams. The additional mass per meter is,

$$\frac{M}{m} = 2400 \text{ kg/m}^3 \cdot 20 \text{ m} \cdot 1 \text{ m} = 48000 \text{ kg/m} \tag{3.12}$$

The equivalent additional mass that needs to be added to the beam elements is,

$$\rho_{\text{equivalent}} = \frac{48000 \text{ kg/m}}{A} = 750 \text{ kg/m}^3 \tag{3.13}$$

This is added to the density of all the beams when assembling the mass matrix.

3.2.3 Soil Foundation Interaction

The piles that are founded directly on bedrock are assumed to be infinitely stiff. The columns that are founded on the soft soil layers, however, are indeed not infinitely stiff. The rotational stiffness of the dofs founded in the soft soil layers are determined confer Andersen [December 2006].

3.2.4 Calculation of Displacements

The displacements along an elements is calculated using the shape functions. The shape functions are given as,

$$\Phi_1(x_\text{e}) = 1 - \frac{3\ x_\text{e}^2}{L_\text{e}^2} + \frac{2\ x_\text{e}^3}{L_\text{e}^3} \tag{3.14}$$

$$\Phi_2(x_\text{e}) = \frac{3\ x_\text{e}^2}{L_\text{e}^2} - \frac{2\ x_\text{e}^3}{L_\text{e}^3} \tag{3.15}$$

$$\Phi_3(x_\text{e}) = x_\text{e} + \frac{x_\text{e}^3}{L_\text{e}^2} - \frac{2\ x_\text{e}^2}{L_\text{e}} \tag{3.16}$$

$$\Phi_4(x_\text{e}) = -\frac{x_\text{e}^2}{L_\text{e}} + \frac{x_\text{e}^3}{L_\text{e}^2} \tag{3.17}$$

$$\Phi_5(x_\text{e}) = 1 - \frac{x_\text{e}}{L_\text{e}} \tag{3.18}$$

$$\Phi_6(x_\text{e}) = \frac{x_\text{e}}{L_\text{e}} \tag{3.19}$$

where x_e is the local x_1 coordinate of the element, which is equal zero at node 1 and equal the element length L_e at node 2. $\Phi_1(x_e)$ is the shape functions for a unit displacement at node 1 of the element in either the x_2 or x_3 direction, $\Phi_2(x_e)$ is the shape function for a unit displacement at node 2 in either the x_2 or x_3 direction, $\Phi_3(x_e)$ is the shape function for a unit rotation at node 1 around either the x_2- or x_3-axis, $\Phi_4(x_e)$ is the shape function for a unit rotation at node 2 around either the x_2- or x_3-axis, $\Phi_5(x_e)$ is the shape function for a unit axial displacement in the x_1 direction and also the shape function for unit axial rotation around the x_1-axis at node 1, and $\Phi_6(x_e)$ is the shape function for a unit axial displacement in the x_1 direction and also the shape function for a unit axial rotation around the x_1-axis at node 2.

The displacement in the x_2-direction along the element length can be determined as,

$$u_2(x_\text{e},t) = a_{2,\text{e}1}(t)\ \Phi_1(x_\text{e}) + a_{2,\text{e}2}(t)\ \Phi_2(x_\text{e}) + a_{\theta 3,\text{e}1}(t)\ \Phi_3(x_\text{e}) + a_{\theta 3,\text{e}2}(t)\ \Phi_4(x_\text{e}) \tag{3.20}$$

Analogously the displacement in the x_3-direction is determined, however a negative sign is applied to the rotations due to the applied sign convention,

$$u_3(x_\mathrm{e},t) = a_{3,\mathrm{e1}}(t)\ \Phi_1(x_\mathrm{e}) + a_{3,\mathrm{e2}}(t)\ \Phi_2(x_\mathrm{e}) - a_{\theta 2,\mathrm{e1}}(t)\ \Phi_3(x_\mathrm{e}) - a_{\theta 2,\mathrm{e2}}(t)\ \Phi_4(x_\mathrm{e}) \tag{3.21}$$

The axial displacement along the element is found as,

$$u_1(x_\mathrm{e},t) = a_{1,\mathrm{e1}}(t)\ \Phi_5(x_\mathrm{e}) + a_{1,\mathrm{e2}}(t)\ \Phi_6(x_\mathrm{e}) \tag{3.22}$$

The torsional rotation of can also be found along the element,

$$\theta_1(x_\mathrm{e},t) = a_{\theta 1,\mathrm{e1}}(t)\ \Phi_5(x_\mathrm{e}) + a_{\theta 1,\mathrm{e2}}(t)\ \Phi_6(x_\mathrm{e}) \tag{3.23}$$

3.2.5 Calculation of Forces

First the forces are calculated using the shape functions. Confer the Bernoulli Euler Beam Theory, the moment can be determined as,

$$M_\mathrm{x3} = E\ I_\mathrm{x3}\ \frac{\mathrm{d}^2 u_2(x_\mathrm{e},t)}{\mathrm{d}x_\mathrm{e}^2} \tag{3.24}$$

$$M_\mathrm{x2} = E\ I_\mathrm{x2}\ \frac{\mathrm{d}^2 u_3(x_\mathrm{e},t)}{\mathrm{d}x_\mathrm{e}^2} \tag{3.25}$$

And the shear force can be determined as,

$$V_2 = E\ I_\mathrm{x3}\ \frac{\mathrm{d}^3 u_2(x_\mathrm{e},t)}{\mathrm{d}x_\mathrm{e}^3} \tag{3.26}$$

$$V_3 = E\ I_\mathrm{x2}\ \frac{\mathrm{d}^3 u_3(x_\mathrm{e},t)}{\mathrm{d}x_\mathrm{e}^3} \tag{3.27}$$

The normal force is determined as,

$$N_1 = E\ A\ \frac{\mathrm{d}u_1(x_\mathrm{e},t)}{\mathrm{d}x_\mathrm{e}} \tag{3.28}$$

The torsional moment is determined as,

$$T_\mathrm{x1} = G\ K\ \frac{\mathrm{d}\theta_1(x_\mathrm{e},t)}{\mathrm{d}x_\mathrm{e}} \tag{3.29}$$

By insertion of equation 3.20 to 3.23 the equations are rewritten to,

$$M_{x3}(x_e,t) = E\ I_{x3}\ \left(a_{2,e1}(t)\ \frac{d^2\Phi_1(x_e)}{dx_e^2} + a_{2,e2}(t)\ \frac{d^2\Phi_2(x_e)}{dx_e^2} + a_{\theta3,e1}(t)\ \frac{d^2\Phi_3(x_e)}{dx_e^2} + a_{\theta3,e2}(t)\ \frac{d^2\Phi_4(x_e)}{dx_e^2} \right) \tag{3.30}$$

$$M_{x2}(x_e,t) = E\ I_{x2}\ \left(a_{3,e1}(t)\ \frac{d^2\Phi_1(x_e)}{dx_e^2} + a_{3,e2}(t)\ \frac{d^2\Phi_2(x_e)}{dx_e^2} - a_{\theta2,e1}(t)\ \frac{d^2\Phi_3(x_e)}{dx_e^2} - a_{\theta2,e2}(t)\ \frac{d^2\Phi_4(x_e)}{dx_e^2} \right) \tag{3.31}$$

$$V_2(x_e,t) = E\ I_{x3}\ \left(a_{2,e1}(t)\ \frac{d^3\Phi_1(x_e)}{dx_e^3} + a_{2,e2}(t)\ \frac{d^3\Phi_2(x_e)}{dx_e^3} + a_{\theta3,e1}(t)\ \frac{d^3\Phi_3(x_e)}{dx_e^3} + a_{\theta3,e2}(t)\ \frac{d^3\Phi_4(x_e)}{dx_e^3} \right) \tag{3.32}$$

$$V_3(x_e,t) = E\ I_{x2}\ \left(a_{3,e1}(t)\ \frac{d^3\Phi_1(x_e)}{dx_e^3} + a_{3,e2}(t)\ \frac{d^3\Phi_2(x_e)}{dx_e^3} - a_{\theta2,e1}(t)\ \frac{d^3\Phi_3(x_e)}{dx_e^3} - a_{\theta2,e2}(t)\ \frac{d^3\Phi_4(x_e)}{dx_e^3} \right) \tag{3.33}$$

$$N_1(x_e,t) = E\ A\ \left(a_{1,e1}(t)\ \frac{d\Phi_5(x_e)}{dx_e} + a_{1,e2}(t)\ \frac{d\Phi_6(x_e)}{dx_e} \right) \tag{3.34}$$

$$T_{x1}(x_e,t) = G\ K\ \left(a_{\theta1,e1}(t)\ \frac{d\Phi_5(x_e)}{dx_e} + a_{\theta1,e2}(t)\ \frac{d\Phi_6(x_e)}{dx_e} \right) \tag{3.35}$$

Differentiating the shape functions it can be seen that the moment varies linearly along the element, but the shear force, normal force and torsional moment has a constant value along the element.

3.2.6 Calculation of Stresses

In Figure 3.6 10 stress points are chosen, as they are assumed to be the most critical points of the cross section regarding combination of stresses from bending, shear and torsion. The chosen points are marked with circles and numbered.

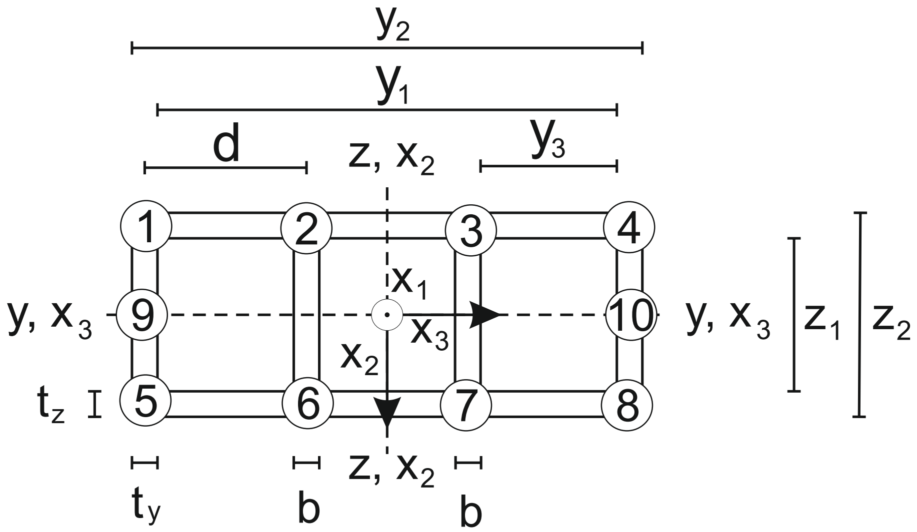

Figure 3.6. Cross section of the bridge deck and the ten chosen critical points.

The shear stresses from bending are determined using Grashof's formula. The shear stresses in stress points 1-8 in the top and bottom of the cross section is determined as,

$$\tau_3 = \frac{V_3\ S_{\mathrm{x2,top}}}{I_{\mathrm{x2}}\ y_2} \tag{3.36}$$

$$\tau_2 = \frac{V_2\ S_{\mathrm{x3,top}}}{I_{\mathrm{x3}}\ y_2} \tag{3.37}$$

The shear stresses from bending in stress points 9 and 10 in the middle of the cross section is determined as,

$$\tau_3 = \frac{V_3\ S_{\mathrm{x2,mid}}}{I_{\mathrm{x2}}\ 2\ t_{\mathrm{z}}} \tag{3.38}$$

$$\tau_2 = \frac{V_2\ S_{\mathrm{x3,mid}}}{I_{\mathrm{x3}}\ 2\ t_{\mathrm{y}}} \tag{3.39}$$

The first moment of area is determined in Appendix J.

The normal stresses are determined as,

$$\sigma_{\mathrm{N}} = \frac{N_{\mathrm{x1}}}{A} \tag{3.40}$$

The stresses from bending around the x_3-axis in stress points 1-8 are determined as,

$$\sigma_{\mathrm{M,x3,top}} = \frac{M_{\mathrm{x3}}\ \left(\frac{z_2}{2} - \frac{t_z}{2}\right)}{I_{\mathrm{x3}}} \tag{3.41}$$

The stresses from bending around the x_2-axis for stress points 1, 4, 5 and 8 are determined as,

$$\sigma_{\mathrm{M,x2,right}} = \frac{M_{\mathrm{x2}}\ \left(\frac{y_2}{2} - \frac{t_y}{2}\right)}{I_{\mathrm{x2}}} \tag{3.42}$$

The stresses from bending around the x_2-axis for stress points 2, 3, 6 and 8 is determined as,

$$\sigma_{\mathrm{M,x2,mid}} = \frac{M_{\mathrm{x2}}\ \frac{d}{2}}{I_{\mathrm{x2}}} \tag{3.43}$$

The normal stresses from the normal force and normal stresses from bending are combined using Naviers formula. For example the stress in stress point 5 is determined as,

$$\sigma_{\mathrm{Navier,5}} = \frac{N}{A} - \sigma_{\mathrm{M,x3,top}} - \sigma_{\mathrm{M,x2,right}} \tag{3.44}$$

The same procedure is followed for the rest of the stress points.

The shear stresses from torsion are determined in Appendix I. The results are given in figure 3.7.

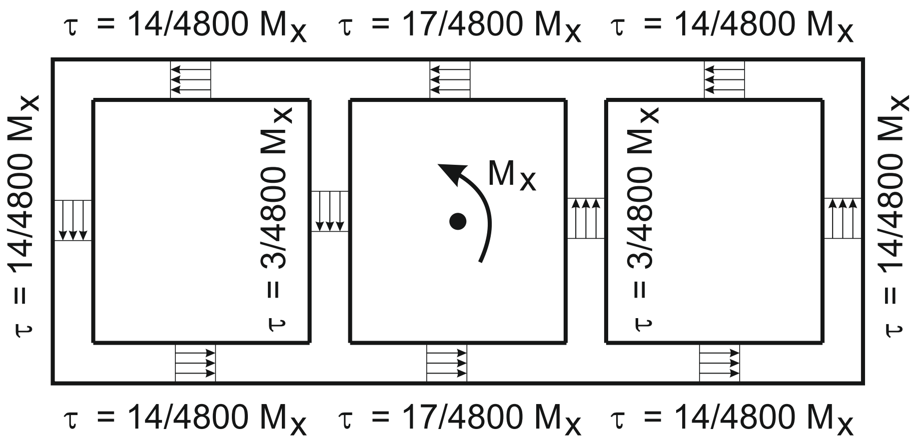

Figure 3.7. Shear stresses due to torsion in the steel section.

The total stress in the stress points is calculated adding the shear stress from torsion to the shear stress from bending. For example the total shear stress in the x_2-direction in stress point 10 is,

$$\tau_{3,10,\mathrm{tot}} = \frac{V_3\ S_{\mathrm{x2,mid}}}{I_{\mathrm{x2}}\ 2\ t_{\mathrm{z}}} - \frac{14}{4800}\ T_{\mathrm{x1}} \tag{3.45}$$

The same procedure is followed for the rest of the stress points.

In order to evaluate the combined effect of shear and normal stresses, Von Mises formula is used, which for the considered stress state reduces to,

$$\sigma_{\mathrm{v}} = \sqrt{\sigma^2_{\mathrm{Navier}} + 3\ (\tau^2_{2,\mathrm{tot}} + \tau^2_{3,\mathrm{tot}})} \tag{3.46}$$

The calculated Navier stresses and total shear stresses can be inserted directly into the equation. The results are evaluated in the next section.

3.3 Parameter Study

In figure 3.8 the apparent velocity is illustrated. The figure illustrates the distance that the SH-waves need to travel to hit the next pile in the moment they hit the first pile. It can be seen that as the angle θ goes towards 90 degrees the additional distance the SH-wave need to travel goes towards zero.

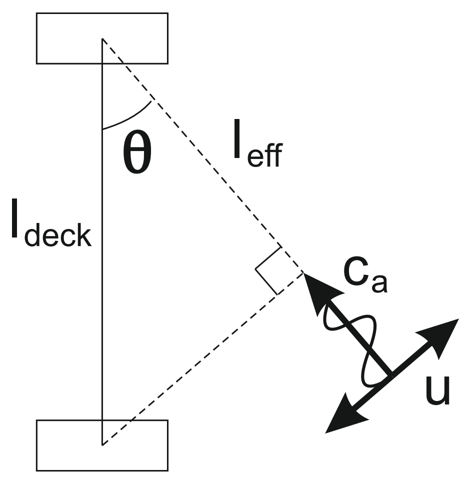

Figure 3.8. Shear stresses due to torsion in the steel section.

The resulting displacement for a given propagation direction for a pile is determined using a linear combination of the induced displacement in the x_3 and x_2 direction,

$$u_{\mathrm{res}} = \cos\theta \; u_{\mathrm{x2}} + \sin\theta \; u_{\mathrm{x3}} \tag{3.47}$$

The Von Mises stresses are used to perform a parameter study. Both the propagation angle θ and the apparent velocity of the SH-waves are varied. The results are shown in figure 3.9.

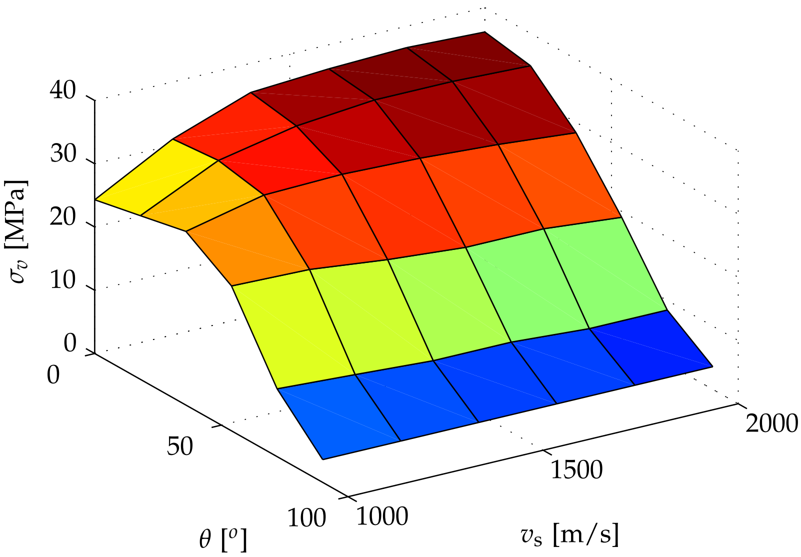

Figure 3.9.

It is found that the shear stresses for all combinations are under 1 MPa, consequently the shear stresses are insignificant and only the normal forces due to normal stress and bending are considered.

In figure 3.10 the stresses for a normal force only for $\theta = 0$ and c_a = 2000 m/s is plotted.

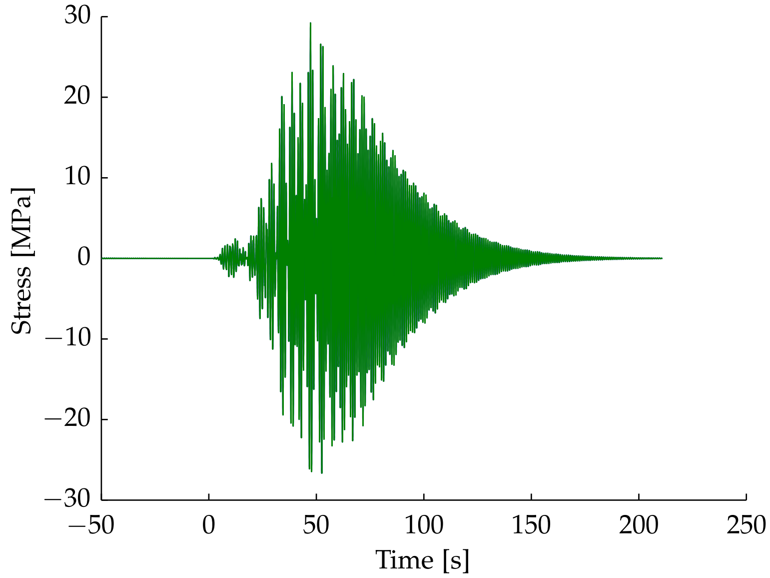

Figure 3.10. Critical normal stress for normal force $\theta = 0$ and c_a = 2000 m/s.

In figure 3.11 the normal stresses due to bending is plotted. Comparing the normal forces due to normal stress and bending it can be seen that the normal forces are the most significant. Thus compression waves in the beam elements are critical, which could indicate that the design of the bridge is not ideal. In order to eliminate the normal forces in the beam elements the bridge can be made free to move in the horizontal direction parallel to the beam at one of the abutments.

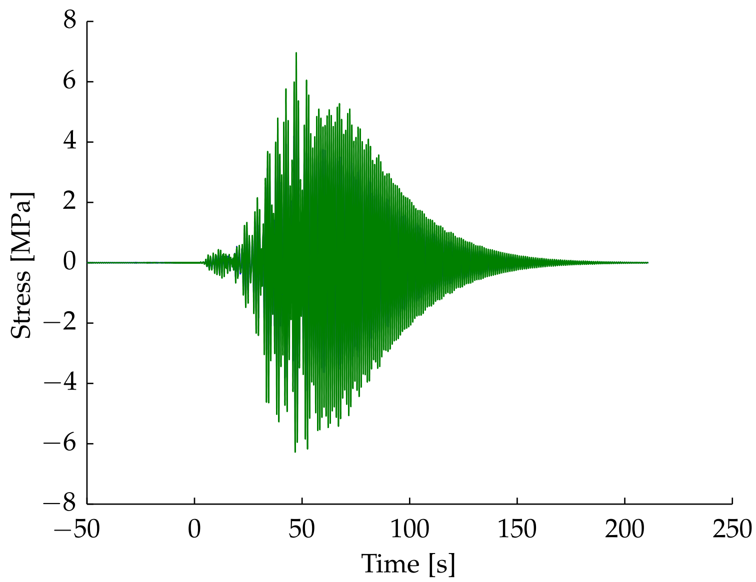

Figure 3.11. Critical normal stresses from bending for $\theta = 0$ and c_a = 2000 m/s.

Due to lack of time a further parameter study is not carried out.

4 Conclusion

From the investigation of the wave propagation in the soft soil layers it was found that the SH-waves were amplified by several magnitudes for the the clay layer profile, the clay and gravel layer profile and the clay, gravel and morain layer profile as well. Due to this high amplification of the seismic waves, the maximum stresses in the bridge deck occurred over the columns founded in the soft soil layers. As a result of the parameter study of the bridge, the critical stresses were found to occur due to compressional waves in the bridge. The most critical propagation direction is where the SH-waves hits the bridge parallel to its span direction. The critical compressional forces is a good indication that the bridge design could be done more optimal in order to eliminate the high compressional forces. This could be done by allowing the bridge to move horizontally in the direction parallel to its span direction at the one abutment. The apparent velocity of the SH-waves in the bedrock did also have a significance, and it was found that an apparent velocity of 2000 m/s was most critical. However, this can very much depending on the length between the piles, the soil properties, the stiffness and mass of the bridge elements etc. It is therefore not possible to predict a critical apparent propagation velocity of the SH-waves. The shear forces in the bridge deck were all insignificantly low, which could also be expected as the length/height ratio of the bridge deck is very high.

References

Lars Andersen, **December 2006**. Linear Elastodynamic Analysis. ISSN: 1901-7286. Aalborg University, Department of Civil Engineering.

Lars Vabbersgaard Andersen and Søren R.K. Nielsen, **2009**. Teknisk Ståbi. ISSN: 1901-7286. Aalborg University, Department of Civil Engineering.

Bent Bonnerup, Bjarne Chr. Jensen, and Carsten Munk Plum, **2009**. Stålkonstruktioner efter DS/EN 1993. ISBN: 978-87-571-2683-9. Nyt Teknisk Forlag.

Robert D. Cook, David S. Malkus, Michael E. Plesha, and Robert J. Witt, **2002**. Concepts and Application of Finite Element Analysis. ISBN: 978-0-471-35605-9. University of Wisconsin - Madison.

Isao Ishibashi and Xinjian Zhang. Unified Dynamic Shear Moduli and Damping Ratios of Sand and Clay. Soils and Foundations, Volume 33, Number 1.

Bjarne Chr. Jensen, **2008**. Betonkonstruktioner efter DS/EN 1992-1-1. ISBN: 978-87-571-2668-6. Nyt Teknisk Forlag.

Bjarne Chr. Jensen, **2009**. Teknisk Ståbi. ISBN: 978-87-571-2685-3. Nyt Teknisk Forlag.

Steven L. Kramer, **1996**. Geotechnical Earthquake Engineering. ISBN: 978-81-317-0718-0. Person.

J. N. Newman, **1977**. Marine Hydrodynamics. ISBN: 978-02-621-4026-3.

Pasific Earthquake Engineering Research Center, **2013**. Peer Ground Motion Database. URL: `http://peer.berkeley.edu/peer_ground_motion_database`. Downloadet: 15-02-2013.

PLAXIS, **2011**. Material Models Manual.

List of Corrections

Part II

Appendix Report

A Formulation of the DTM Soil Model

A.1 The Navier Equations

The forces on an infinitesimal cube in a $(x,y,z) = (x_1,x_2,x_3)$ coordinate system is given by the three equations,

$$\sum F_{\mathrm{i}} = \left(\frac{\partial \sigma_{\mathrm{ij}}}{\partial x_{\mathrm{j}}} + b_{\mathrm{i}}\, \rho \right)\, dx\, dy\, dz \tag{A.1}$$

Where the Taylor Series have been used to describe the stress increment, however, the terms of higher than first order have been neglected.

Applying Newton's Second Law the Cauchy Stress Equation is formulated,

$$\sum F_{\mathrm{i}} = m\, a_{\mathrm{i}} \quad \Leftrightarrow \tag{A.2}$$

$$\left(\frac{\partial \sigma_{\mathrm{ij}}}{\partial x_{\mathrm{j}}} + b_{\mathrm{i}}\, \rho \right)\, dx\, dy\, dz = \rho\, dx\, dy\, dz\, \frac{\partial^2 u_{\mathrm{i}}}{\partial t^2} \quad \Leftrightarrow \tag{A.3}$$

$$\frac{\partial \sigma_{\mathrm{ij}}}{\partial x_{\mathrm{j}}} + b_{\mathrm{i}}\, \rho = \rho\, \frac{\partial^2 u_{\mathrm{i}}}{\partial t^2} \tag{A.4}$$

Which is the dynamic condition of the problem.

The physical condition, ie. the stress-strain correlation, is described by Hooke's Law assuming linear elasticity,

$$\sigma_{\mathrm{ij}} = E_{\mathrm{ijkl}}\, \epsilon_{\mathrm{kl}} \tag{A.5}$$

Where the matrix E_{ijkl} has only got 27 independent variables due to symmetry of both the stress and strain tensor.

A geometrical condition is formulated by disregarding any higher order taylor expansions of the infenitesimal strain tensor,

$$\epsilon_{\mathrm{ij}} = \frac{1}{2} \left(\frac{\partial u_{\mathrm{i}}(\bar{x},t)}{\partial x_{\mathrm{j}}} + \frac{\partial u_{\mathrm{j}}(\bar{x},t)}{\partial x_{\mathrm{i}}} \right) \tag{A.6}$$

Homogeneity of the material is assumed, which implies that the elasticity matrix and the density is independent of $\bar{x}$, which is the notation used for (x_1,x_2,x_3). Isotropy is also assumed, which implies that Hooke's Law can be formulated as,

$$\sigma_{\mathrm{ij}} = \lambda\, \Delta \delta_{\mathrm{ij}} + 2\, \mu\, \epsilon_{\mathrm{ij}} \tag{A.7}$$

Where the dilation is given by,

$$\Delta = \frac{\partial u_{\mathrm{k}}(\bar{x},t)}{\partial x_{\mathrm{k}}} \tag{A.8}$$

And λ and μ are the Lamé constants, which will be given later.

Combining equation A.4, A.6 and A.7 results in the three Navier Equations,

$$(\lambda + \mu)\, \frac{\partial^2 u_{\mathrm{j}}(\bar{x},t)}{\partial x_{\mathrm{i}}\, \partial x_{\mathrm{j}}} + \mu\, \frac{\partial^2 u_{\mathrm{i}}(\bar{x},t)}{\partial x_{\mathrm{j}}\, \partial x_{\mathrm{j}}} + \rho\, b_{\mathrm{i}} = \frac{\partial^2 u_{\mathrm{i}}(\bar{x},t)}{\partial t^2} \tag{A.9}$$

A.2 The Governing Wave Equation

The problem is formulated in one dimension for SH-Waves only. The used coordinate system is illustrated in figure A.1.

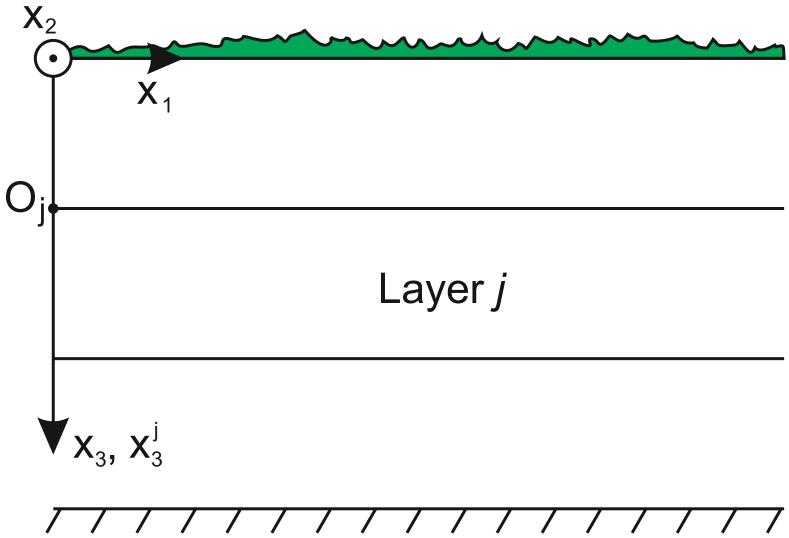

Figure A.1. Orientation of the used coordinate system.

The considered soil volume is divided into J layers. Counting from the surface and down, an index $j \in [1;J]$ is introduced indicating which soil layer that is being considered.

The problem will be formulated for SH-waves propagating in the x_3-direction vibrating in the x_1-direction. Therefore the Navier Equations reduce to,

$$\frac{\partial^2 u_1^{\mathrm{j}}(x_3,t)}{\partial x_3^2} = \frac{\rho^{\mathrm{j}}}{\mu^{\mathrm{j}}} \frac{\partial^2 u_1^{\mathrm{j}}(x_3,t)}{\partial t^2} \quad \Leftrightarrow \tag{A.10}$$

$$\frac{\partial^2 u_1^{\mathrm{j}}(x_3,t)}{\partial x_3^2} = \frac{1}{(c_{\mathrm{S}}^{\mathrm{j}})^2} \frac{\partial^2 u_1^{\mathrm{j}}(x_3,t)}{\partial t^2}, \quad c_{\mathrm{S}}^{\mathrm{j}} = \sqrt{\frac{\mu^{\mathrm{j}}}{\rho^{\mathrm{j}}}} \tag{A.11}$$

Which is the Wave Equation for one dimensional SH-waves. c_S in the equation is the S-wave propagation velocity. The layer index j has now been introduced in the equation. As it can be seen in the equation, the body forces are now disregarded, which is done because they are assumed constant over time. Therefore they do not contribute to the dynamic problem, which is considered.

A numerical Fourier transformation is used to describe the problem in the frequency domain,

$$u_{\mathrm{n}}^{\mathrm{j}}(x_3,t) \cong \sum_{\mathrm{n}=1}^{\mathrm{N}} \hat{u}_{\mathrm{n}}^{\mathrm{j}}(x_3)\, e^{i\,\omega\,t} \tag{A.12}$$

Where $\hat{u}_{\mathrm{n}}^{\mathrm{j}}(x_3)$ is the Fourier Transformation of $u_{\mathrm{n}}^{\mathrm{j}}(x_3,t)$ and N is the number of harmonic wave components.

Inserting equation A.12 into equation A.11 gives,

$$\frac{\mathrm{d}^2}{\mathrm{d}x_3^2}\left(\sum_{\mathrm{n}=1}^{\mathrm{N}} \hat{u}_\mathrm{n}^\mathrm{j}(x_3)\, e^{i\,\omega\,t}\right) = \frac{1}{c_\mathrm{S}^2}\,\frac{\mathrm{d}^2}{\mathrm{d}t^2}\left(\sum_{\mathrm{n}=1}^{\mathrm{N}} \hat{u}_\mathrm{n}^\mathrm{j}(x_3)\, e^{i\,\omega\,t}\right), \quad c_\mathrm{S}^\mathrm{j} = \sqrt{\frac{\mu}{\rho}} \quad \Leftrightarrow \tag{A.13}$$

$$e^{i\,\omega\,t}\,\frac{\mathrm{d}^2}{\mathrm{d}x_3^2}\left(\sum_{\mathrm{n}=1}^{\mathrm{N}} \hat{u}_\mathrm{n}^\mathrm{j}(x_3)\right) = \left(\frac{i\,\omega}{c_\mathrm{S}^\mathrm{j}}\right)^2 \sum_{\mathrm{n}=1}^{\mathrm{N}} \hat{u}_\mathrm{n}^\mathrm{j}(x_3)\, e^{i\,\omega\,t} \Leftrightarrow \tag{A.14}$$

$$\frac{\mathrm{d}^2}{\mathrm{d}x_3^2}\left(\sum_{\mathrm{n}=1}^{\mathrm{N}} \hat{u}_\mathrm{n}^\mathrm{j}(x_3)\right) = -\frac{1}{(k_\mathrm{n}^\mathrm{j})^2}\sum_{\mathrm{n}=1}^{\mathrm{N}} \hat{u}_\mathrm{n}^\mathrm{j}(x_3), \quad (k_\mathrm{n}^\mathrm{j})^2 = \left(\frac{\omega_\mathrm{n}}{c_\mathrm{S}^\mathrm{j}}\right)^2 \tag{A.15}$$

Which is the governing Wave Equation formulated in the frequency domain, and it has the particular solution,

$$\hat{u}_\mathrm{n}^\mathrm{j}(x_3) = B_\mathrm{n}^\mathrm{j}\, e^{i\,k_\mathrm{n}^\mathrm{j}\,x_3^\mathrm{j}} + D_\mathrm{n}^\mathrm{j}\, e^{-i\,k_\mathrm{n}^\mathrm{j}\,(x_3^\mathrm{j}-h^\mathrm{j})} \tag{A.16}$$

Where B_n^j and D_n^j are integration constants. The variable x_3^j is the local coordinate of the respective layers, which is equal to zero in the top of the layer and equal to h^j in the bottom of the layer. h^j is the height of the respective layer.

A.3 Matrix formulation

The physical and geometrical condition are in the frequency domain formulated as,

$$\hat{\sigma}_\mathrm{ik}^\mathrm{j} = \lambda^\mathrm{j}\,\hat{\Delta}^\mathrm{j}\,\delta_\mathrm{ik} + 2\,\mu^\mathrm{j}\,\hat{\epsilon}_\mathrm{ik}^\mathrm{j}, \quad \hat{\Delta}^\mathrm{j} = \hat{\epsilon}_\mathrm{ii}^\mathrm{j} \tag{A.17}$$

$$\hat{\epsilon}_\mathrm{ik}^\mathrm{j} = \frac{1}{2}\left(\frac{\partial \hat{u}_\mathrm{i}^\mathrm{j}}{\partial x_\mathrm{k}} + \frac{\partial \hat{u}_\mathrm{k}^\mathrm{j}}{\partial x_\mathrm{i}}\right) \tag{A.18}$$

The hat means that it is the Fourier Transformation of the respective parameter that is given.

The sum of the normal strains ϵ_ii is equal to zero, as only SH-Waves are present, hence $\hat{\epsilon}_\mathrm{ii}$ is zero as well. The only quantity different from zero in $\hat{\epsilon}_\mathrm{ik}$ is $\frac{\partial \hat{u}_1^\mathrm{j}}{\partial x_3} = \frac{\mathrm{d}\hat{u}_1^\mathrm{j}}{\mathrm{d}x_3}$. Consequently equation A.17 reduces to,

$$\hat{\sigma}_\mathrm{ik} = 2\,\mu^\mathrm{j}\,\hat{\epsilon}_\mathrm{ik} = \mu \begin{bmatrix} 0 & 0 & \frac{\mathrm{d}\hat{u}_1^\mathrm{j}}{\mathrm{d}x_3} \\ 0 & 0 & 0 \\ \frac{\mathrm{d}\hat{u}_1^\mathrm{j}}{\mathrm{d}x_3} & 0 & 0 \end{bmatrix} \tag{A.19}$$

The amplitude shear function in the layer is the defined as,

$$\hat{p}_\mathrm{n}^\mathrm{j} = \hat{\sigma}_{13} = \hat{\sigma}_{31} = \mu\,\frac{d\hat{u}_\mathrm{n}^\mathrm{j}(x_3)}{dx_3} = i\,k_\mathrm{n}^\mathrm{j}\,x_3^\mathrm{j}\,\mu\,\left(B_\mathrm{n}^\mathrm{j}\, e^{i\,k_\mathrm{n}^\mathrm{j}\,x_3^\mathrm{j}} - D_\mathrm{n}^\mathrm{j}\, e^{i\,k_\mathrm{n}^\mathrm{j}\,(x_3^\mathrm{j}-h^\mathrm{j})}\right) \tag{A.20}$$

As both the amplitude displacement function $\hat{u}_\mathrm{n}^\mathrm{j}$ and the shear amplitude function $\hat{p}_\mathrm{n}^\mathrm{j}$ are given, a matrix formulation is now performed,

$$\bar{S}_\mathrm{n}^\mathrm{j} = \begin{bmatrix} \hat{u}_\mathrm{n}^\mathrm{j}(x_3^\mathrm{j}) \\ \hat{p}_\mathrm{n}^\mathrm{j}(x_3^\mathrm{j}) \end{bmatrix} = \begin{bmatrix} e^{i\,k_\mathrm{n}^\mathrm{j}\,x_3^\mathrm{j}} & e^{-i\,k_\mathrm{n}^\mathrm{j}\,(x_3^\mathrm{j}-h^\mathrm{j})} \\ \mu^\mathrm{j}\,i\,k_\mathrm{n}^\mathrm{j}\,e^{i\,k_\mathrm{n}^\mathrm{j}\,x_3^\mathrm{j}} & -\mu\,i\,k_\mathrm{n}^\mathrm{j}\,e^{-i\,k_\mathrm{n}^\mathrm{j}\,(x_3^\mathrm{j}-h^\mathrm{j})} \end{bmatrix} \begin{bmatrix} B_\mathrm{n}^\mathrm{j} \\ D_\mathrm{n}^\mathrm{j} \end{bmatrix} \quad \Leftrightarrow \tag{A.21}$$

$$\bar{S}_\mathrm{n}^\mathrm{j} = \begin{bmatrix} \hat{u}_\mathrm{n}^\mathrm{j}(x_3^\mathrm{j}) \\ \hat{p}_\mathrm{n}^\mathrm{j}(x_3^\mathrm{j}) \end{bmatrix} = \bar{\bar{A}} \begin{bmatrix} B_\mathrm{n}^\mathrm{j} \\ D_\mathrm{n}^\mathrm{j} \end{bmatrix} \tag{A.22}$$

The $\bar{S}$ vector is now formulated in the top and bottom of a layer so that $\bar{S}_{\mathrm{n}}^{0\mathrm{j}}$ represents the top of layer j and $\bar{S_{\mathrm{n}}}^{\mathrm{j}1}$ represents the bottom. This is also illustrated in figure A.2.

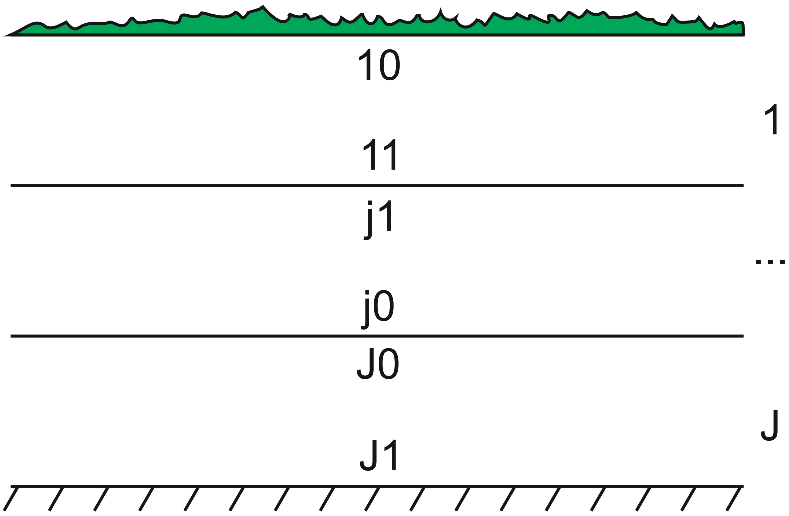

Figure A.2. Notation in the layers.

The $\bar{\bar{A}}$ matrix for the top and bottom of a layers is respectively,

$$\bar{\bar{A}}_{\mathrm{n}}^{\mathrm{j}}(x_3^{\mathrm{j}} = 0) = \bar{\bar{A}}_{\mathrm{n}}^{\mathrm{j}0} = \begin{bmatrix} 1 & e^{i\,k_{\mathrm{n}}^{\mathrm{j}}\,h^{\mathrm{j}}} \\ \mu^{\mathrm{j}}\,i\,k_{\mathrm{n}}^{\mathrm{j}} & -\mu^{\mathrm{j}}\,i\,k_{\mathrm{n}}^{\mathrm{j}}\,e^{i\,k_{\mathrm{n}}^{\mathrm{j}}\,h^{\mathrm{j}}} \end{bmatrix} \tag{A.23}$$

$$\bar{\bar{A}}_{\mathrm{n}}^{\mathrm{j}}(x_3^{\mathrm{j}} = h^{\mathrm{j}}) = \bar{\bar{A}}_{\mathrm{n}}^{\mathrm{j}1} = \begin{bmatrix} e^{i\,k_{\mathrm{n}}^{\mathrm{j}}\,h^{\mathrm{j}}} & 1 \\ \mu^{\mathrm{j}}\,i\,k_{\mathrm{n}}^{\mathrm{j}}\,e^{i\,k_{\mathrm{n}}^{\mathrm{j}}\,h^{\mathrm{j}}} & -\mu\,i\,k_{\mathrm{n}}^{\mathrm{j}} \end{bmatrix} \tag{A.24}$$

The displacement and traction at the bottom of layer j is given as,

$$\bar{S}_{\mathrm{n}}^{\mathrm{j}1} = \begin{bmatrix} \hat{u}_{\mathrm{n}}^{\mathrm{j}1}(x_3^{\mathrm{j}}) \\ \hat{p}_{\mathrm{n}}^{\mathrm{j}1}(x_3^{\mathrm{j}}) \end{bmatrix} = \bar{\bar{A}}_{\mathrm{n}}^{\mathrm{j}1} \begin{bmatrix} B_{\mathrm{n}}^{\mathrm{j}1} \\ D_{\mathrm{n}}^{\mathrm{j}1} \end{bmatrix} \tag{A.25}$$

The integration constants can then be determined as,

$$\begin{bmatrix} B_{\mathrm{n}}^{\mathrm{j}1} \\ D_{\mathrm{n}}^{\mathrm{j}1} \end{bmatrix} = (\bar{\bar{A}}_{\mathrm{n}}^{\mathrm{j}1})^{-1}\,\bar{S}_{\mathrm{n}}^{\mathrm{j}1} = \tag{A.26}$$

Consequently an equation of the bottom of layer j can be formulated as,

$$\bar{S}_{\mathrm{n}}^{\mathrm{j}0} = \bar{\bar{A}}_{\mathrm{n}}^{\mathrm{j}0} \begin{bmatrix} B_{\mathrm{n}}^{\mathrm{j}0} \\ D_{\mathrm{n}}^{\mathrm{j}0} \end{bmatrix} = \bar{\bar{A}}_{\mathrm{n}}^{\mathrm{j}0}\,(\bar{\bar{A}}_{\mathrm{n}}^{\mathrm{j}1})^{-1}\,\bar{S}_{\mathrm{n}}^{\mathrm{j}1} \tag{A.27}$$

The displacement as well as the traction between two adjacent layers have to be continuous, hence $S_{\mathrm{n}}^{\mathrm{j}1} = S_{\mathrm{n}}^{\mathrm{j}+1,0}$, which makes it possible to calculate the displacement in the top of layer 1 given the displacement and traction at the bottom layer,

$$\bar{S}_{\mathrm{n}}^{10} = \bar{\bar{A}}_{\mathrm{n}}^{10}\,(\bar{\bar{A}}_{\mathrm{n}}^{11})^{-1}\,\bar{S}_{\mathrm{n}}^{11} = \bar{\bar{A}}_{\mathrm{n}}^{10}\,(\bar{\bar{A}}_{\mathrm{n}}^{11})^{-1}\,\bar{S}_{\mathrm{n}}^{20} \tag{A.28}$$

$$\bar{S}_{\mathrm{n}}^{20} = \bar{\bar{A}}_{\mathrm{n}}^{20}\,(\bar{\bar{A}}_{\mathrm{n}}^{21})^{-1}\,\bar{S}_{\mathrm{n}}^{30} \tag{A.29}$$

$$\dots$$

$$\bar{S}_{\mathrm{n}}^{\mathrm{J}0} = \bar{\bar{A}}_{\mathrm{n}}^{\mathrm{J}0}\,(\bar{\bar{A}}_{\mathrm{n}}^{\mathrm{J}1})^{-1}\,\bar{S}_{\mathrm{n}}^{\mathrm{J}1} \tag{A.30}$$

Now a $\bar{\bar{T}}$ matrix is formulated,

$$\bar{\bar{T}}^{j0} = \bar{\bar{A}}_{\mathrm{n}}^{j0}\ (\bar{\bar{A}}_{\mathrm{n}}^{j1})^{-1}\ \bar{\bar{A}}_{\mathrm{n}}^{j+1,0}\ (\bar{\bar{A}}_{\mathrm{n}}^{j+1,1})^{-1}\ ...\ \bar{\bar{A}}_{\mathrm{n}}^{\mathrm{J}0}\ (\bar{\bar{A}}_{\mathrm{n}}^{\mathrm{J}1})^{-1} \tag{A.31}$$

So that,

$$\bar{S}_{\mathrm{n}}^{10} = \bar{\bar{T}}^{10}\ \bar{S}_{\mathrm{n}}^{\mathrm{J}1} \tag{A.32}$$

A.4 Amplitude response matrix

The $\bar{S}$ vector for the surface is given as,

$$\bar{S}_{\mathrm{n}}^{10} = \begin{bmatrix} \hat{u}_{\mathrm{n}}^{j0} \\ \hat{p}_{\mathrm{n}}^{j0} \end{bmatrix} = \begin{bmatrix} T_{11}^{10} & T_{12}^{10} \\ T_{21}^{10} & T_{22}^{10} \end{bmatrix} \begin{bmatrix} \hat{u}_{\mathrm{n}}^{\mathrm{J}1} \\ \hat{p}_{\mathrm{n}}^{\mathrm{J}1} \end{bmatrix} \tag{A.33}$$

It is used that the traction amplitude at the surface $\hat{p}_{\mathrm{n}}^{10}$ is equal to zero. The traction amplitude at the bottom of the bottom layer can therefore be given as,

$$\hat{p}_{\mathrm{n}}^{10} = 0 = T_{21}^{10}\ \hat{u}_{\mathrm{n}}^{\mathrm{J}1} + T_{22}^{10}\ \hat{p}_{\mathrm{n}}^{\mathrm{J}1} \Leftrightarrow \hat{p}_{\mathrm{n}}^{\mathrm{J}1} = -\frac{T_{21}^{10}\ \hat{u}_{\mathrm{n}}^{\mathrm{J}1}}{T_{22}^{10}} \tag{A.34}$$

Using this the displacement amplitude at the j'th layer can be given as,

$$\hat{u}_{\mathrm{n}}^{j0} = \hat{u}_{\mathrm{n}}^{\mathrm{J}1}\ T_{11}^{j0} + \hat{p}_{\mathrm{n}}^{\mathrm{J}1}\ T_{11}^{j0} = \hat{u}_{\mathrm{n}}^{\mathrm{J}1}\ \left(T_{11}^{j0} - \frac{T_{12}^{j0}\ T_{21}^{10}}{T_{22}^{10}} \right) \tag{A.35}$$

A frequency response function is now defined as,

$$H^{j0}(\omega) = \left(T_{11}^{j0} - \frac{T_{12}^{j0}\ T_{21}^{10}}{T_{22}^{10}} \right) \tag{A.36}$$

A.5 Damping model

The Lamé constant μ is given as,

$$\mu^{\mathrm{j}} = \frac{E^{\mathrm{j}}}{2\ (1+\nu^{\mathrm{j}})} = G^{\mathrm{j}} \tag{A.37}$$

A hysteretic material damping model is introduced,

$$G(\omega) = G_0\ (1 + i\ \eta\ \mathrm{sign}(\omega)), \quad \mathrm{sign}(\omega) = \begin{cases} 1 & \text{for } \omega > 0 \\ 0 & \text{for } \omega = 0 \\ -1 & \text{for } \omega < 0 \end{cases} \tag{A.38}$$

Which gives a complex Lamé constant,

$$\mu^{\mathrm{j}} = G^{\mathrm{j}}\ (1 + i\ \eta^{\mathrm{j}}\ \mathrm{sign}(\omega)\ ) \tag{A.39}$$

B Formulation of the FEM Soil Model

B.1 Strong formulation

Using index notation the Cauchy Stress Equations are formulated as,

$$\frac{\partial \sigma_{\mathrm{ij}}}{\partial x_{\mathrm{j}}} + \rho\, b_{\mathrm{i}} = \rho\, \frac{\partial^2 u_{\mathrm{i}}}{\partial t^2} \tag{B.1}$$

Where $\rho\, b_{\mathrm{i}}$ is body forces per unit volume. They equation can be written out as,

$$\begin{bmatrix} \frac{\partial \sigma_{11}}{\partial x_1} + \frac{\partial \sigma_{12}}{\partial x_2} + \frac{\partial \sigma_{13}}{\partial x_3} \\ \frac{\partial \sigma_{21}}{\partial x_1} + \frac{\partial \sigma_{22}}{\partial x_2} + \frac{\partial \sigma_{23}}{\partial x_3} \\ \frac{\partial \sigma_{31}}{\partial x_1} + \frac{\partial \sigma_{32}}{\partial x_2} + \frac{\partial \sigma_{33}}{\partial x_3} \end{bmatrix} + \rho \begin{bmatrix} b_1 \\ b_2 \\ b_3 \end{bmatrix} = \rho\, \frac{\partial^2}{\partial t^2} \begin{bmatrix} u_1 \\ u_2 \\ u_3 \end{bmatrix} \tag{B.2}$$

In figure B.1 the used coordinate system is illustrated.

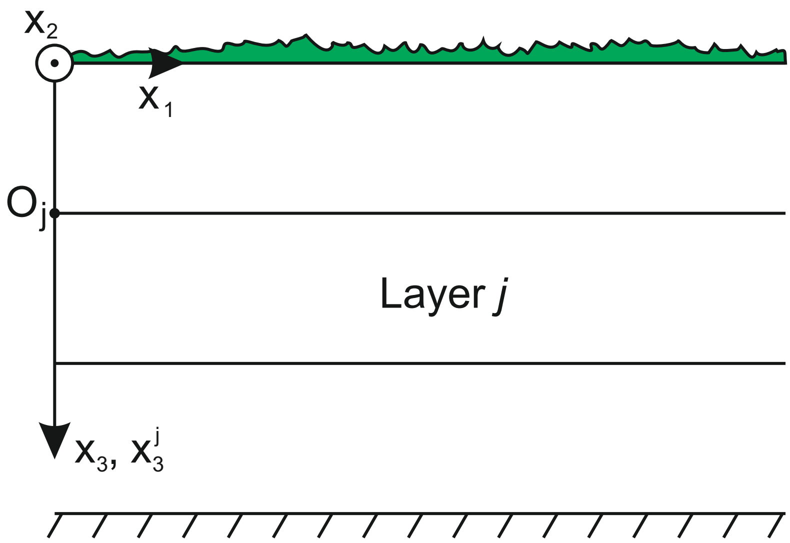

Figure B.1. Orientation of the used coordinate system.

It is only one dimensional SH-waves propagating in the x_3-direction with particle displacements in the x_1-direction, which are considered. Hence the only quantity different from zero in the first vector on the left hand side of equation B.2 is $\frac{\partial \sigma_{13}}{\partial x_3} = \frac{\partial \sigma_{31}}{\partial x_3}$. In the body force vector and the displacement vector the non-zero quantities are b_1 and u_1, respectively.

Assuming linear elastic material, Hooke's law is applied in one direction,

$$\sigma_{13} = G\, \gamma_{13} \tag{B.3}$$

Where the angular shear strain is defined as,

$$\gamma_{13} = \frac{\partial u_1}{\partial x_3} + \frac{\partial u_3}{\partial x_1} \tag{B.4}$$

Where $\dfrac{\partial u_3}{\partial x_1}$ is zero for the considered problem.

Using equation B.3 and B.4 equation B.2 is reformulated,

$$G \, \frac{\partial^2 u_1(x_3,t)}{\partial x_3^2} + \rho \, b_1(x_3,t) = \rho \, \frac{\partial^2 u_1(x_3,t)}{\partial t^2} \tag{B.5}$$

A soil column with unit cross section area is considered, as illustrated in figure B.2. Each term in equation B.5 is therefore multiplied with unit area, which gives units of force per unit length in the x_3-direction for the terms on the left hand side of the equation and units of mass per unit length multiplied with acceleration for the term on the right hand side.

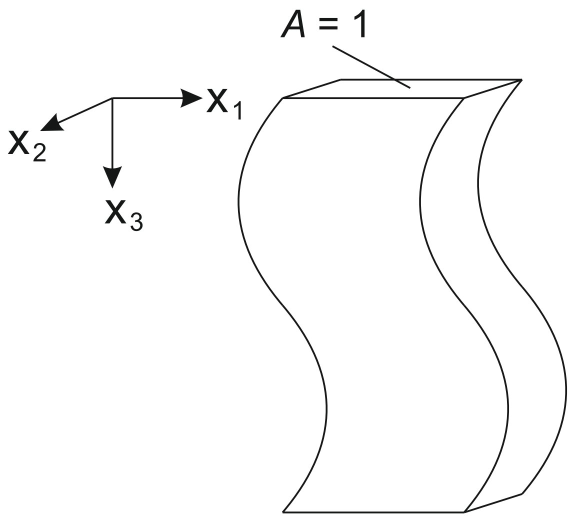

Figure B.2. The considered soil column.

By introduction of the applied traction per unit length $p(x_3,t)$, equation B.5 is rewritten as,

$$G \, \frac{\partial^2 u_1(x_3,t)}{\partial x_3^2} + p(x_3,t) = \rho \, \frac{\partial^2 u_1(x_3,t)}{\partial t^2}, \quad p(x_3,t) = \rho \, b_1(x_3,t) \tag{B.6}$$

Which is the strong formulation of the considered problem.

B.2 Weak formulation

The soil column illustrated in figure B.2 is discretized into a finite number of elements. This is done as the change in displacement, velocity and accelerations over an element will decrease as the element length decreases. By choosing a sufficiently small element length the change of the physical quantities can be approximated quiet well by the use of simple shape functions.

A single element is illustrated in figure B.3.

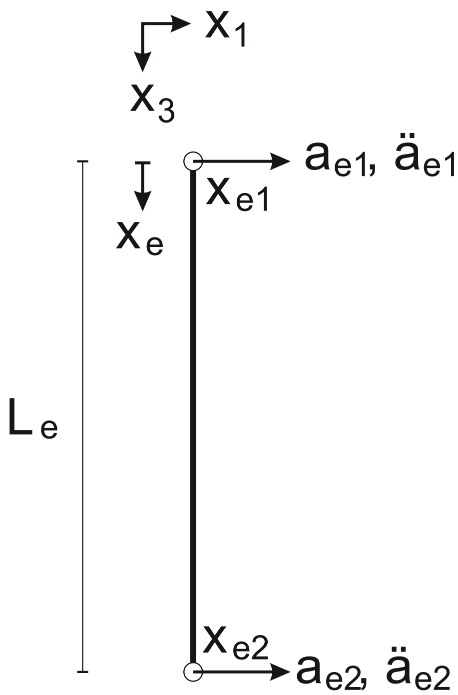

Figure B.3. The considered element.

In the figure a is the nodal displacements and $\ddot{a}$ is the nodal accelerations.

The strong formulation given in equation B.6 is now considered for a single element. The x_3 coordinate is replaced by the local coordinate x_e. The equation is multiplied with a virtual displacement $\delta u(x_e,t)$ and integrated over the element length,

$$\int_{x_{\mathrm{e}1}}^{x_{\mathrm{e}2}} \delta u(x_\mathrm{e},t)\; G\, \frac{\partial^2 u_1(x_\mathrm{e},t)}{\partial x_\mathrm{e}^2}\; \mathrm{d}x_\mathrm{e} + \int_{x_{\mathrm{e}1}}^{x_{\mathrm{e}2}} \delta u(x_e,t)\; p(x_\mathrm{e},t)\; \mathrm{d}x_\mathrm{e} = \int_{x_{\mathrm{e}1}}^{x_{\mathrm{e}2}} \delta u(x_e,t)\; \rho\, \frac{\partial^2 u_1(x_\mathrm{e},t)}{\partial t^2}\; \mathrm{d}x_\mathrm{e} \tag{B.7}$$

The rule of integration by parts is given as,

$$\int_{x_1}^{x_2} u(x)\; v'(x)\; \mathrm{d}x = [u(x)\; v(x)]_{x_1}^{x_2} - \int_{x_1}^{x_2} u'(x)\; v(x)\; \mathrm{d}x \tag{B.8}$$

Applying that equation B.7 is rewritten,

$$\begin{aligned} &[\delta u(x_\mathrm{e},t)\; V(x_\mathrm{e},t)]_{x_{\mathrm{e}1}}^{x_{\mathrm{e}1}} + \int_{x_{\mathrm{e}1}}^{x_{\mathrm{e}2}} \delta u(x_e,t)\; p(x_\mathrm{e},t)\; \mathrm{d}x_\mathrm{e} \\ &= \int_{x_{\mathrm{e}1}}^{x_{\mathrm{e}2}} \frac{\partial \delta u(x_e,t)}{\partial x_\mathrm{e}}\; G\, \frac{\partial u_1(x_\mathrm{e},t)}{\partial x_\mathrm{e}}\; \mathrm{d}x_\mathrm{e} + \int_{x_{\mathrm{e}1}}^{x_{\mathrm{e}2}} \delta u(x_e,t)\; \rho\, \frac{\partial^2 u_1(x_\mathrm{e},t)}{\partial t^2}\; \mathrm{d}x_\mathrm{e} \end{aligned} \tag{B.9}$$

Where the shear force per unit area is defined as,

$$V(x_\mathrm{e},t) = G\, \frac{\partial u_1(x_\mathrm{e},t)}{\partial x_\mathrm{e}} \tag{B.10}$$

Equation B.9 is the weak formulation of the considered problem, which will be evaluated in the next section.

B.3 Matrix Formulation

The weak formulation for a single element will now, by evaluation of the integrals, be formulated in a matrix equation given as,

$$\bar{\bar{K}}_e\ \bar{a}_e + \bar{\bar{M}}_e\ \ddot{\bar{a}}_e = \bar{b}_e + \bar{f}_e \tag{B.11}$$

In equation B.9 the first term on the left hand side of the equation is identified as the body forces, noted $\bar{b}_e$. The second term is the traction forces, noted $\bar{f}_e$. On the right hand side of the equation the first term is the stiffness multiplied with the displacements, noted $\bar{\bar{K}}_e$ and $\bar{a}_e$, respectively. The second term on the right hand side of the equation is the mass of the element multiplied with the acceleration, noted $\bar{\bar{M}}_e$ and $\ddot{\bar{a}}_e$, respectively.

In order to evaluate the integrals, shape and weight functions are defined,

$$u_1(x_e,t) = \bar{\Phi}(x_e)\ \bar{a}(t) \tag{B.12}$$

$$\delta u_1(x_e,t) = \bar{\Psi}(x_e)\ \delta\bar{a}(t) \tag{B.13}$$

Where $\bar{\Phi}(x_e)$ is the shape function and $\bar{\Psi}(x_e)$ is the weight function. Using Galerkin's method, the weight function is assumed equal to the shape function, hence,

$$u_1(x_e,t) = \bar{\Phi}(x_e)\ \bar{a}(t) \tag{B.14}$$

$$\delta u_1(x_e,t) = \bar{\Phi}(x_e)\ \delta\bar{a}(t) \tag{B.15}$$

Where,

$$\bar{a}_e(t) = \begin{bmatrix} a_{e1}(t) & a_{e2}(t) \end{bmatrix}^T \tag{B.16}$$

$$\delta\bar{a}_e(t) = \begin{bmatrix} \delta a_{e1}(t) & \delta a_{e2}(t) \end{bmatrix}^T \tag{B.17}$$

A linear shape function is applied, which is equal to 1 in the respective node and equal to 0 at the other node. Hence the shape function is given as,

$$\bar{\Phi}(x_e) = \begin{bmatrix} 1 - \frac{x_e}{L_e} & \frac{x_e}{L_e} \end{bmatrix} \tag{B.18}$$

Using the given shape function and defining that $x_{e1} = 0$ and $x_{e2} = L_e$, the stiffness integral is evaluated,

$$\int_0^{L_e} \frac{\partial\bar{\Phi}(x_e)}{\partial x_e}\ \delta\bar{a}_e(t)\ G\ \frac{\partial\bar{\Phi}(x_e)}{\partial x_e}\ \bar{a}_e(t)\ \mathrm{d}x_e \tag{B.19}$$

The following is used,

$$\bar{\Phi}(x_e)\ \delta\bar{a}(t) = \delta\bar{a}^T(t)\ \bar{\Phi}^T(x_e) \tag{B.20}$$

Due to the fact that $\delta\bar{a}(t)$ is unknown, the equation can be solved as,

$$\delta\bar{a}(t)\ (X_1 + X_2) = 0 \tag{B.21}$$

$$\Leftrightarrow \quad X_1 + X_2 = 0 \quad \vee \quad \delta\bar{a}(t)\ = 0 \tag{B.22}$$

The non trivial solution $X_1 + X_2 = 0$ is chosen, which reduces the system of equations to,

$$G \int_0^{L_e} \frac{\partial \bar{\Phi}^T(x_e)}{\partial x_e} \; \frac{\partial \bar{\Phi}(x_e)}{\partial x_e} \; dx_e \; \bar{a}_e(t) \tag{B.23}$$

$$= G \int_0^{L_e} \begin{bmatrix} \frac{-1}{L_e} \\ \frac{1}{L_e} \end{bmatrix} \begin{bmatrix} \frac{-1}{L_e} & \frac{1}{L_e} \end{bmatrix} dx_e \; \bar{a}_e(t) \tag{B.24}$$

$$= G \left[\begin{bmatrix} \frac{x_e}{L_e^2} & -\frac{x_e}{L_e^2} \\ -\frac{x_e}{L_e^2} & \frac{x_e}{L_e^2} \end{bmatrix} \right]_0^{L_e} \bar{a}_e(t) \tag{B.25}$$

$$= \frac{G}{L_e} \begin{bmatrix} 1 & -1 \\ -1 & 1 \end{bmatrix} \bar{a}_e(t) = \bar{\bar{K}}_e \; \bar{a}_e(t) \tag{B.26}$$

Considering the units it can be seen that the stiffness matrix represents the stiffness per unit area of the soil column.

The mass matrix integral is evaluated,

$$\int_0^{L_e} \bar{\Phi}^T(x_e) \; \rho \; \bar{\Phi}(x_e) \; \frac{\partial^2 \bar{a}(t)}{\partial t^2} \; dx_e \tag{B.27}$$

$$= \rho \int_0^{L_e} \begin{bmatrix} 1 - \frac{x_e}{L_e} \\ \frac{x_e}{L_e} \end{bmatrix} \begin{bmatrix} 1 - \frac{x_e}{L_e} & \frac{x_e}{L_e} \end{bmatrix} dx_e \; \frac{\partial^2 \bar{a}(t)}{\partial t^2} \tag{B.28}$$

$$= \frac{\rho \; L_e}{6} \begin{bmatrix} 2 & 1 \\ 1 & 2 \end{bmatrix} \ddot{\bar{a}}_e(t) = \bar{\bar{M}}_e \; \ddot{\bar{a}}_e(t) \tag{B.29}$$

Considering the units it can be seen that the mass matrix represents the mass per unit area of the soil column.

The body force vector is evaluated,

$$\left[\bar{\Phi}^T(x_e) \; V(x_e,t) \right]_0^{L_e} = \left[\begin{bmatrix} 1 - \frac{x_e}{L_e} \\ \frac{x_e}{L_e} \end{bmatrix} V(x_e,t) \right]_0^{L_e} = \begin{bmatrix} -V_{e1}(t) \\ V_{e2}(t) \end{bmatrix} = \begin{bmatrix} F_{e1}(t) \\ F_{e2}(t) \end{bmatrix} = \bar{F}(t) \tag{B.30}$$

The last reformulation has been performed considering the force diagram illustrated in figure B.4. $\bar{V}(t)$ is the internal shear forces within the element acting at each node and $\bar{F}(t)$ is the external forces applied in the nodes. The sign convention of the shear forces is due to the sign convention of the shear strain, which is defined positive counter clockwise, as given in the figure.

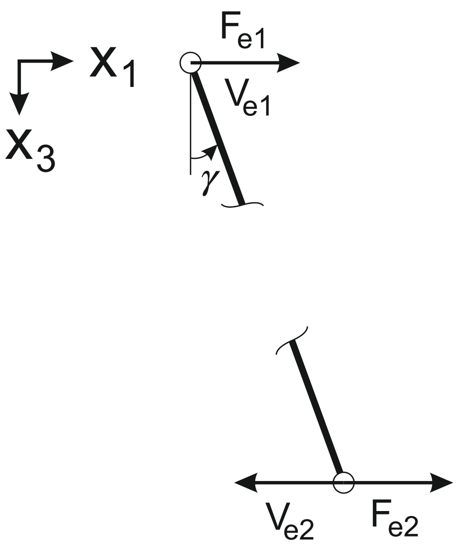

Figure B.4. Force diagram at the two nodes.

The traction force vector can be evaluated as well, however no traction forces are applied in the model, but only nodal forces.

It should be noted that the force vector represents the forces applied in the nodes per unit area of the soil column.

The final matrix equation can the be formulated as,

$$\bar{\bar{K}}_e \; \bar{a}_e + \bar{\bar{M}}_e \; \ddot{\bar{a}}_e = \bar{F}_e \tag{B.31}$$

C Formulation of the FEM Beam Model

A FEM beam model for a beam element is introduced. A Bernoulli Euler beam element with two degrees of freedom (DOF) per node is considered, as illustrated in figure C.1.

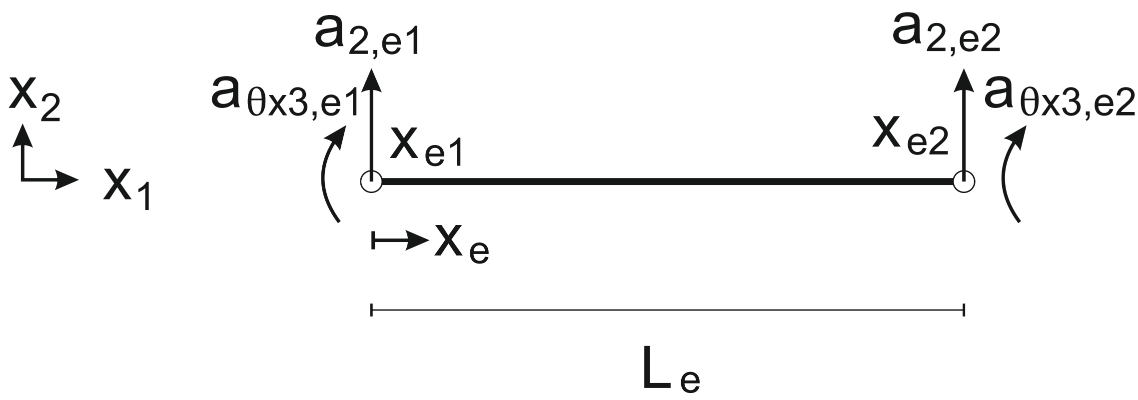

Figure C.1. Beam element with two DOF per node.

C.1 Strong formulation

The cauchy stress equation in the x_2-direction is considered (see equation B.2),

$$\frac{\partial \sigma_{12}}{\partial x_1} + \rho\ b_2 = \rho\ \frac{\partial^2 u_2}{\partial t^2} \tag{C.1}$$

The equation is integrated over the cross section area $A = \mathrm{d}x_2\ \mathrm{d}x_3$ and it is used that,

$$V_{12} = \int \int \sigma_{12}\ \mathrm{d}x_2\ \mathrm{d}x_3 \tag{C.2}$$

Which gives,

$$\frac{\partial V_{12}}{\partial x_1} + p_2 = A\ \rho\ \frac{\partial^2 u_2}{\partial t^2}, \quad p_2 = A\ \rho\ b_2 \tag{C.3}$$

Confer the Bernoulli Euler beam theory the bending moment are defined as,

$$M_{1,x3} = E\ I_{x3}\ \kappa_{x3} = E\ I_{x3}\ \frac{\partial^2 u_2}{\partial x_1^2} \tag{C.4}$$

The shear force is defined as,

$$V_{12} = G\ A\ \frac{\partial u_2}{\partial x_1} \tag{C.5}$$

$$\tag{C.6}$$

Consequently the sign convention is as illustrated in figure C.2.

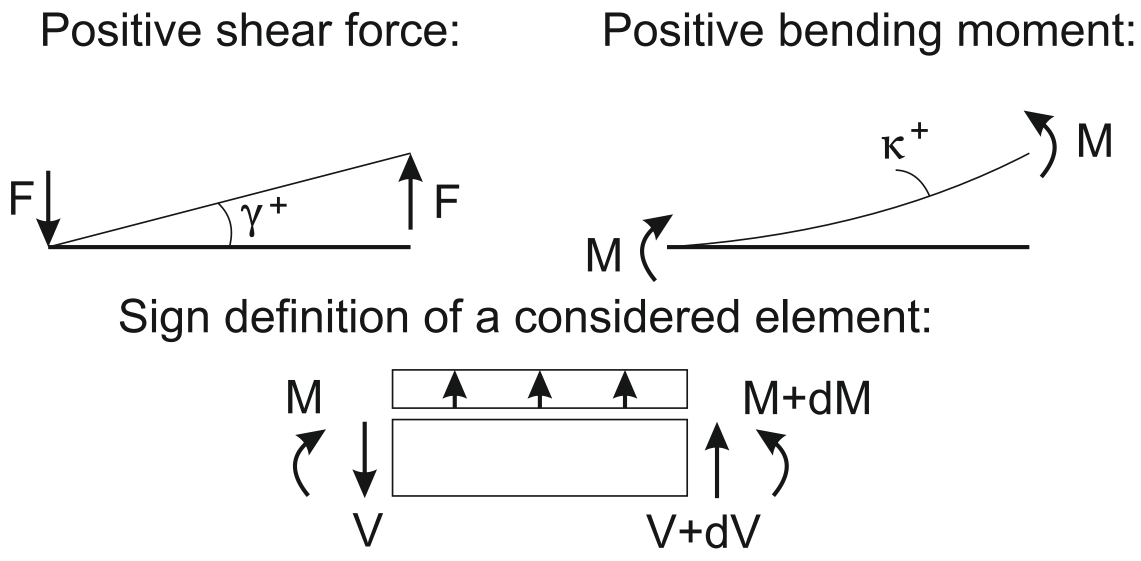

Figure C.2. Sign convention for bending moment and shear force.

Moment equilibrium around the right end of the element illustrated in figure C.2 gives,

$$\frac{\partial M_{1,\text{x3}}}{\partial x_1} = -V_{12} \tag{C.7}$$

Which is introduced into equation C.3,

$$-\frac{\partial^2 M_{1,\text{x3}}}{\partial x_1^2} + p_2 = A\,\rho\,\frac{\partial^2 u_2}{\partial t^2} \tag{C.8}$$

The principle of virtual displacement is applied by multiplying the equation with an arbitrary virtual displacement δu_2 and integrating over the element length,

$$-\int_0^{L_\text{e}} \delta u_2\,\frac{\partial^2 M_{1,\text{x3}}}{\partial x_1^2}\,\mathrm{d}x_1 + \int_0^{L_\text{e}} \delta u_2\;p_2\,\mathrm{d}x_1 = \int_0^{L_\text{e}} \delta u_2\;A\,\rho\,\frac{\partial^2 u_2}{\partial t^2}\,\mathrm{d}x_1 \tag{C.9}$$

Integrating the first term in equation C.9 twice by parts gives,

$$-\int_0^{L_\text{e}} \frac{\partial^2 \delta u_2}{\partial x_1^2}\,M_{1,\text{x3}}\,\mathrm{d}x_1 - \left[\delta u_2\,\frac{\partial M_{1,\text{x3}}}{\partial x_1}\right]_0^{L_\text{e}} + \left[\frac{\partial \delta u_2}{\partial x_1}\,M_{1,\text{x3}}\right]_0^{L_\text{e}} \tag{C.10}$$

Using equation C.7 and the definition of the rotation,

$$\theta_{\text{x3}} = \frac{\partial u_2}{\partial x_1} \tag{C.11}$$

Equation C.10 is reformulated as,

$$-\int_0^{L_\text{e}} \frac{\partial^2 \delta u_2}{\partial x_1^2}\,M_{1,\text{x3}}\,\mathrm{d}x_1 + [\delta u_2\;V_{12}]_0^{L_\text{e}} + [\delta\theta_{\text{x3}}\;M_{1,\text{x3}}]_0^{L_\text{e}} \tag{C.12}$$

The curvature is given as,

$$\kappa_{\text{x3}} = \frac{\partial^2 u_2}{\partial x_1^2} \tag{C.13}$$

Assuming linear elasticy the normal stress is expressed as,

$$\sigma_{11} = \epsilon_{11}\;E \tag{C.14}$$

The moment of inertia is defined as,

$$I_{x3} = \int\int x_3^2 \, \mathrm{d}x_2 \, \mathrm{d}x_3 \tag{C.15}$$

Using C.13, C.14 and C.15 the definition of the moment is rewritten to,

$$M_{1,x3} = \int\int \sigma_{11} \, x_3 \, \mathrm{d}x_2 \, \mathrm{d}x_3 = \int\int \kappa_{x3} \, x_3^2 \, E \, \mathrm{d}x_2 \, \mathrm{d}x_3 = \kappa_{x3} \, E \, I_{x3} \tag{C.16}$$

Using this equation C.10 is rewritten as,

$$-\int_0^{L_e} \frac{\delta M_{1,x3}}{EI} \, M_{1,x3} \, \mathrm{d}x_1 + [\delta u_2 \, V_{12}]_0^{L_e} + [\delta\theta_{x3} \, M_{1,x3}]_0^{L_e} \tag{C.17}$$

The first term in equation C.9 is replaced with equation C.17,

$$[\delta u_2 \, V_{12}]_0^{L_e} + [\delta\theta_{x3} \, M_{1,x3}]_0^{L_e} + \int_0^{L_e} \delta u_2 \, p_2 \, \mathrm{d}x_1 = \int_0^{L_e} \frac{\delta M_{1,x3}}{EI} \, M_{1,x3} \, \mathrm{d}x_1 + \int_0^{L_e} \delta u_2 \, A \, \rho \, \frac{\partial^2 u_2}{\partial t^2} \, \mathrm{d}x_1 \tag{C.18}$$

By neglecting the dynamic part at the right hand side of the equation, this is the virtual displacement equation for the Bernoulli Euler beam.

C.2 Weak formulation

Using the difinition of the curvature equation C.18 is rewritten,

$$[\delta u_2 \, V_{12}]_0^{L_e} + [\delta\theta_{x3} \, M_{1,x3}]_0^{L_e} + \int_0^{L_e} \delta u_2 \, p_2 \, \mathrm{d}x_1 = \int_0^{L_e} \frac{\partial^2 \delta u_2}{\partial x_1^2} \, E \, I_{x3} \, \frac{\partial^2 u_2}{\partial x_1^2} \, \mathrm{d}x_1 + \int_0^{L_e} \delta u_2 \, A \, \rho \, \frac{\partial^2 u_2}{\partial t^2} \, \mathrm{d}x_1 \tag{C.19}$$

This is the strong formulation of the Bernoulli Euler beam element. In the following the strong formulation is reformulated to a weak formulation of the form,

$$\bar{\bar{K}}_e \, \bar{a}_{2,e} + \bar{\bar{M}}_e \, \ddot{\bar{a}}_{2,e} = \bar{b}_e + \bar{f}_e \tag{C.20}$$

The first and second term on the left hand side of equation C.19 is recognized as the body moments and body forces, respectively. The third term on the left hand side is recognized as the traction forces applied over the surface of the beam. The first term on the right hand side of the equation is recoqnized as the stiffness multiplied with the displacements. The second term on the right hand side is recognized as the mass matrix multiplied with the accelerations. As indicated by the ∂ symbol the displacement u_2 is dependent on both x_1 and t. In order to seperate these two variables shape functions are introduced,

$$u_2(x_1,t) = \bar{\Phi}(x_1) \, \bar{a}_{2,e}(t) \tag{C.21}$$

$$\delta u_2(x_1,t) = \bar{\Phi}(x_1) \, \delta\bar{a}_{2,e}(t) \tag{C.22}$$

It is used that,

$$\bar{\Phi}(x_1) \, \delta\bar{a}_{2,e}(t) = \delta\bar{a}_{2,e}^{\mathrm{T}}(t) \, \bar{\Phi}^{\mathrm{T}}(x_1) \tag{C.23}$$

The shape functions can then be introduced into equation C.19,

$$
\begin{aligned}
&\left[\delta\bar{a}^{\mathrm{T}}_{2,\mathrm{e}}(t)\ \bar{\Phi}^{\mathrm{T}}(x_1)\ V_{12}\right]_0^{L_\mathrm{e}} + \left[\delta\bar{a}^{\mathrm{T}}_{2,\mathrm{e}}(t)\ \frac{\partial\bar{\Phi}^{\mathrm{T}}(x_1)}{\partial x_1}\ M_{1,\mathrm{x}3}\right]_0^{L_\mathrm{e}} + \int_0^{L_\mathrm{e}} \delta\bar{a}^{\mathrm{T}}_{2,\mathrm{e}}(t)\ \bar{\Phi}^{\mathrm{T}}(x_1)\ p_2\ \mathrm{d}x_1 \\
= &\int_0^{L_\mathrm{e}} \delta\bar{a}^{\mathrm{T}}_{2,\mathrm{e}}(t)\ \frac{\partial^2\bar{\Phi}^{\mathrm{T}}(x_1)}{\partial x_1^2}\ E\ I_{\mathrm{x}3}\ \frac{\partial^2\bar{\Phi}(x_1)}{\partial x_1^2}\ \bar{a}_{2,\mathrm{e}}(t)\ \mathrm{d}x_1 + \int_0^{L_\mathrm{e}} \delta\bar{a}^{\mathrm{T}}_{2,\mathrm{e}}(t)\ \bar{\Phi}^{\mathrm{T}}(x_1)\ A\ \rho\ \bar{\Phi}(x_1)\ \frac{\partial^2\bar{a}_{2,\mathrm{e}}(t)}{\partial t^2}\ \mathrm{d}x_1
\end{aligned}
\tag{C.24}
$$

Due to the fact that $\delta\bar{a}_{2,\mathrm{e}}(t)$ is unknown, the equation can be solved as,

$$\delta\bar{a}_{2,\mathrm{e}}\ (X_1 + X_2) = 0 \tag{C.25}$$

$$\Leftrightarrow \quad X_1 + X_2 = 0 \quad \vee \quad \delta\bar{a}_{2,\mathrm{e}}\ = 0 \tag{C.26}$$

The non trivial solution $X_1 + X_2 = 0$ is chosen, which reduces the system of equations to,

$$
\begin{aligned}
&\left[\bar{\Phi}^{\mathrm{T}}(x_1)\ V_{12}\right]_0^{L_\mathrm{e}} + \left[\frac{\partial\bar{\Phi}^{\mathrm{T}}(x_1)}{\partial x_1}\ M_{1,\mathrm{x}3}\right]_0^{L_\mathrm{e}} + \int_0^{L_\mathrm{e}} \bar{\Phi}^{\mathrm{T}}(x_1)\ p_2\ \mathrm{d}x_1 \\
= &\int_0^{L_\mathrm{e}} \frac{\partial^2\bar{\Phi}^{\mathrm{T}}(x_1)}{\partial x_1^2}\ E\ I_{\mathrm{x}3}\ \frac{\partial^2\bar{\Phi}(x_1)}{\partial x_1^2}\ \mathrm{d}x_1\ \bar{a}_{2,\mathrm{e}}(t)\ + \int_0^{L_\mathrm{e}} \bar{\Phi}^{\mathrm{T}}(x_1)\ A\ \rho\ \bar{\Phi}(x_1)\ \mathrm{d}x_1\ \frac{\partial^2\bar{a}_{\mathrm{e}}(t)}{\partial t^2}
\end{aligned}
\tag{C.27}
$$

Shape functions

To determine the shape functions the principle of virtual work is used, which is given as,

$$\int_0^{L_\mathrm{e}} M\ \frac{\delta M}{E\ I_{\mathrm{x}3}}\ \mathrm{d}x_1 = \int_0^{L_\mathrm{e}} u_2\ \delta p_2\ \mathrm{d}x_1 \tag{C.28}$$

In order to derive the shape functions it is necessary to activate one DOF at the time, which is done considering four different cases of a cantilever beam which are,

1. Displacement from a point load
2. Displacement from an end moment
3. Rotation from a point load
4. Rotation from an end moment

The four cases are illustrated in figure C.3.

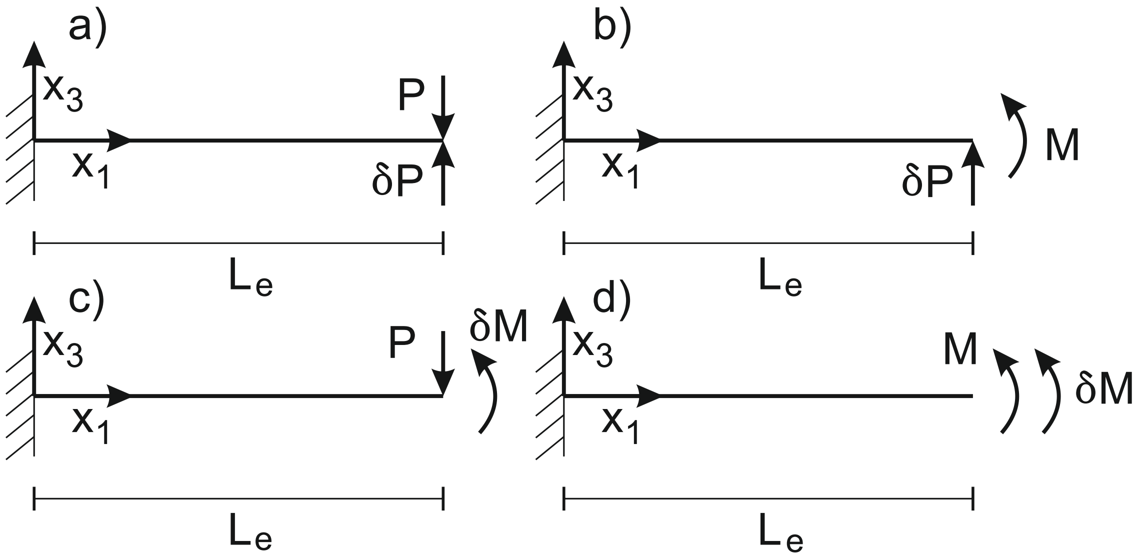

Figure C.3. The four considered cases for a cantilever beam.

The virtual work equation is used for case a),

$$u_{3,\mathrm{a}}(x_1) = \int_0^{L_\mathrm{e}} M_{1,\mathrm{x3}} \frac{\delta M}{E\ I_{\mathrm{x3}}}\ \mathrm{d}x_1 = -\frac{1}{6}\ \frac{P\ x^2\ (3\ l - x)}{E\ I_{\mathrm{x3}}} \tag{C.29}$$

For case b),

$$u_{3,\mathrm{b}}(x_1) = \int_0^{L_\mathrm{e}} M_{1,\mathrm{x3}} \frac{\delta M}{E\ I_{\mathrm{x3}}}\ \mathrm{d}x_1 = \frac{1}{2}\ \frac{M\ x^2}{E\ I_{\mathrm{x3}}} \tag{C.30}$$

For case c),

$$\theta_\mathrm{c}(x_1) = \int_0^{L_\mathrm{e}} M_{1,\mathrm{x3}} \frac{\delta M}{E\ I_{\mathrm{x3}}}\ \mathrm{d}x_1 = -\frac{1}{2}\ \frac{P\ x\ (2\ l - x)}{E\ I_{\mathrm{x3}}} \tag{C.31}$$

And for case d),

$$\theta_\mathrm{d}(x_1) = \int_0^{L_\mathrm{e}} M_{1,\mathrm{x3}} \frac{\delta M}{E\ I_{\mathrm{x3}}}\ \mathrm{d}x_1 = \frac{M\ x}{E\ I_{\mathrm{x3}}} \tag{C.32}$$

First displacement is considered and it should be satisfied that $w(l) = 1$,

$$u_{3,\mathrm{a}}(l) + u_{3,\mathrm{b}}(l) = 1\ \Leftrightarrow\ -\frac{1}{3}\ \frac{P\ l^3}{E\ I_{\mathrm{x3}}} + \frac{1}{2}\ \frac{M\ l^2}{E\ I_{\mathrm{x3}}} = 1 \tag{C.33}$$

and $\theta(l) = 0$,

$$\theta_\mathrm{c}(l) + \theta_\mathrm{d}(l) = 0\ \Leftrightarrow\ -\frac{1}{2}\ \frac{P\ l^2}{E\ I_{\mathrm{x3}}} + \frac{M\ l}{E\ I_{\mathrm{x3}}} = 0 \tag{C.34}$$

Solving these two equations, the two unknowns P and M can be found, and the shape functions for unit displacement can be given as,

$$\Phi_2(x_1) = u_{3,\mathrm{P}}(x) + u_{3,\mathrm{M}}(x) = \frac{3\ x^2}{L_\mathrm{e}^2} - \frac{2\ x^3}{L_\mathrm{e}^3} \tag{C.35}$$

$$\Phi_1(x_1) = 1 - u_{3,\mathrm{P}}(x) = 1 - \frac{3\ x^2}{L_\mathrm{e}^2} + \frac{2\ x^3}{L_\mathrm{e}^3} \tag{C.36}$$

Analogously the rotation is considered and it should be satisfied that $\theta(l) = 1$,

$$\theta_{\mathrm{c}}(l) + \theta_{\mathrm{d}}(l) = 1 \;\Leftrightarrow\; -\frac{1}{2}\,\frac{P\,l^2}{E\,I_{\mathrm{x3}}} + \frac{M\,l}{E\,I_{\mathrm{x3}}} = 1 \tag{C.37}$$

and $w(l) = 0$,

$$u_{3,\mathrm{a}}(l) + u_{3,\mathrm{b}}(l) = 0 \;\Leftrightarrow\; -\frac{1}{3}\,\frac{P\,l^3}{E\,I_{\mathrm{x3}}} + \frac{1}{2}\,\frac{M\,l^2}{E\,I_{\mathrm{x3}}} = 0 \tag{C.38}$$

P and M are found an the shape functions for unit rotation can be given as,

$$\Phi_4(x_1) = u_{3,\mathrm{P}}(x) + u_{3,\mathrm{M}}(x) = -\frac{x^2}{L_{\mathrm{e}}} + \frac{x^3}{L_{\mathrm{e}}^2} \tag{C.39}$$

$$\Phi_3(x_1) = -1\;(u_{3,\mathrm{P}}(l-x) + u_{3,\mathrm{M}}(l-x)) = x + \frac{x^3}{L_{\mathrm{e}}^2} - \frac{2\,x^2}{L_{\mathrm{e}}} \tag{C.40}$$

For the axial displacements as well as torsional moments the shape functions are assumed to be linear,

$$\Phi_5(x_1) = 1 - \frac{x}{L_{\mathrm{e}}} \tag{C.41}$$

$$\Phi_6(x_1) = \frac{x}{L_{\mathrm{e}}} \tag{C.42}$$

The shape functions are plotted in figure C.4.

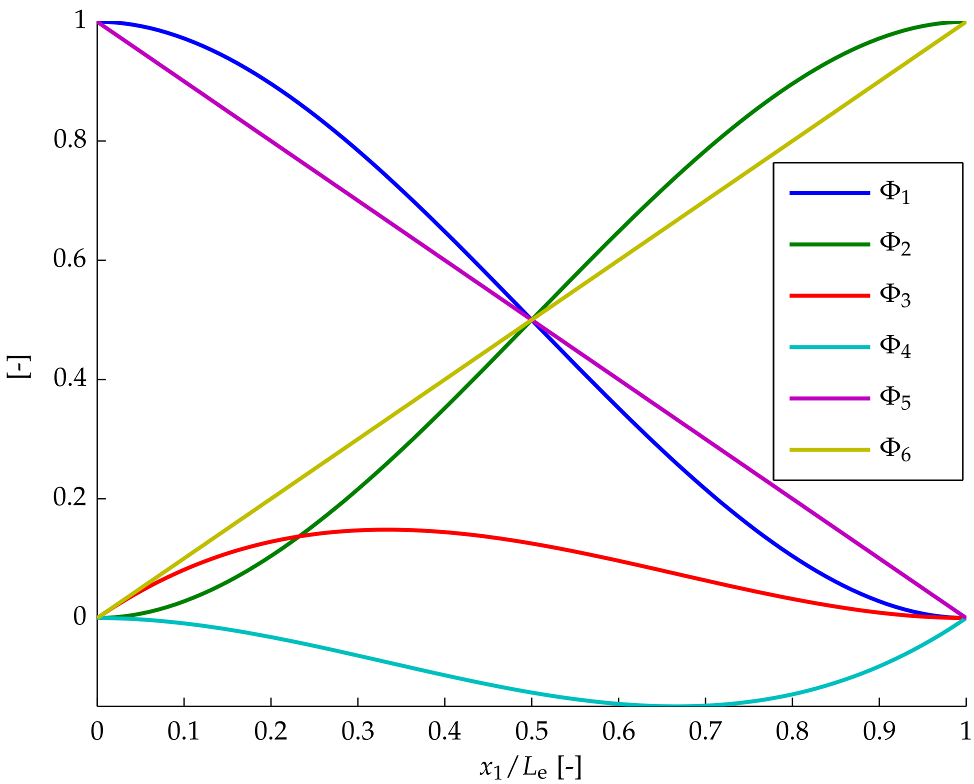

Figure C.4.

The displacement can now be given as a functions of the shape functions multiplied by the nodal displacements,

$$u_2(x_1,t) = \bar{\Phi}(x_1)\ \bar{a}_{2,\mathrm{e}}(t) = \begin{Bmatrix} \Phi_1(x_1) & \Phi_2(x_1) & \Phi_3(x_1) & \Phi_4(x_1) \end{Bmatrix} \begin{Bmatrix} u_{3,\mathrm{e1}}(t) \\ \theta_{\mathrm{e1}}(t) \\ u_{3,\mathrm{e2}}(t) \\ \theta_{\mathrm{e2}}(t) \end{Bmatrix} \tag{C.43}$$

$$u_1(x_1,t) = \bar{\Phi}(x_1)\ \bar{a}_{2,\mathrm{e}}(t) = \begin{Bmatrix} \Phi_5(x_1) & \Phi_6(x_1) \end{Bmatrix} \begin{Bmatrix} u_{1,\mathrm{e1}}(t) \\ u_{1,\mathrm{e2}}(t) \end{Bmatrix} \tag{C.44}$$

$$\tag{C.45}$$

C.3 Matrix formulation

The stiffness integral is evaluated

$$\int_0^{L_\mathrm{e}} \frac{\partial^2 \bar{\Phi}^\mathrm{T}(x_1)}{\partial x_1^2}\ E\ I_{\mathrm{x3}}\ \frac{\partial^2 \bar{\Phi}(x_1)}{\partial x_1^2}\ \mathrm{d}x_1\ \bar{a}_{2,\mathrm{e}}(t) \tag{C.46}$$

$$= E\ I_{\mathrm{x3}} \int_0^{L_\mathrm{e}} \frac{\partial^2 \bar{\Phi}^\mathrm{T}(x_1)}{\partial x_1^2}\ \frac{\partial^2 \bar{\Phi}(x_1)}{\partial x_1^2}\ \mathrm{d}x_1\ \bar{a}_{2,\mathrm{e}}(t) \tag{C.47}$$

$$= \frac{E\ I_{\mathrm{x3}}}{L_\mathrm{e}} \begin{bmatrix} \frac{12}{L_\mathrm{e}^2} & \frac{6}{L_\mathrm{e}} & -\frac{12}{L_\mathrm{e}^2} & \frac{6}{L_\mathrm{e}} \\ \frac{6}{L_\mathrm{e}} & 4 & -\frac{6}{L_\mathrm{e}} & 2 \\ -\frac{12}{L_\mathrm{e}^2} & -\frac{6}{L_\mathrm{e}} & \frac{12}{L_\mathrm{e}^2} & -\frac{6}{L_\mathrm{e}} \\ \frac{6}{L_\mathrm{e}} & 2 & -\frac{6}{L_\mathrm{e}} & 4 \end{bmatrix} \bar{a}_{2,\mathrm{e}}(t) \tag{C.48}$$

$$\tag{C.49}$$

The mass integral is evaluated,

$$\int_0^{L_\mathrm{e}} \bar{\Phi}^\mathrm{T}(x_1)\ A\ \rho\ \bar{\Phi}(x_1)\ \mathrm{d}x_1\ \frac{\partial^2 \bar{a}_{2,\mathrm{e}}(t)}{\partial t^2} \tag{C.50}$$

$$= A\ \rho \int_0^{L_\mathrm{e}} \bar{\Phi}^\mathrm{T}(x_1)\ \bar{\Phi}(x_1)\ \mathrm{d}x_1\ \frac{\partial^2 \bar{a}_{2,\mathrm{e}}(t)}{\partial t^2} \tag{C.51}$$

$$= A\ \rho\ L_\mathrm{e} \begin{bmatrix} \frac{13}{35} & \frac{11\ L_\mathrm{e}}{210} & \frac{9}{70} & -\frac{13\ L_\mathrm{e}}{420} \\ \frac{11\ L_\mathrm{e}}{210} & \frac{L_\mathrm{e}^2}{105} & \frac{13\ L_\mathrm{e}}{420} & -\frac{L_\mathrm{e}^2}{140} \\ \frac{9}{70} & \frac{13\ L_\mathrm{e}}{420} & \frac{13}{35} & -\frac{11\ L_\mathrm{e}}{210} \\ -\frac{13\ L_\mathrm{e}}{420} & -\frac{L_\mathrm{e}^2}{140} & -\frac{11\ L_\mathrm{e}}{210} & \frac{L_\mathrm{e}^2}{105} \end{bmatrix} \ddot{\bar{a}}_{2,\mathrm{e}}(t) \tag{C.52}$$

The body force integral is evaluated,

$$\left[\bar{\Phi}^\mathrm{T}(x_1)\ V_{12}\right]_0^{L_\mathrm{e}} = \begin{Bmatrix} -V_{12,\mathrm{e1}} \\ V_{12,\mathrm{e2}} \end{Bmatrix} = \begin{Bmatrix} F_{2,\mathrm{e1}} \\ F_{2,\mathrm{e2}} \end{Bmatrix} \tag{C.53}$$

The body moment integral is evaluated,

$$\left[\frac{\partial\bar{\Phi}^{\mathrm{T}}(x_1)}{\partial x_1}\ M_{1,\mathrm{x3}}\right]_0^{L_\mathrm{e}} = \begin{Bmatrix} -M_{1,\mathrm{Internal,x3,e1}} \\ M_{1,\mathrm{Internal,x3,e2}} \end{Bmatrix} = \begin{Bmatrix} M_{1,\mathrm{x3,e1}} \\ M_{1,\mathrm{x3,e2}} \end{Bmatrix} \tag{C.54}$$

D Formulation of The Torsional FEM Beam Model

A torsional model is introduced in order to take into account torsion around the beam axis for the applied beams. One DOF per node is used, as illustrated in figure D.1

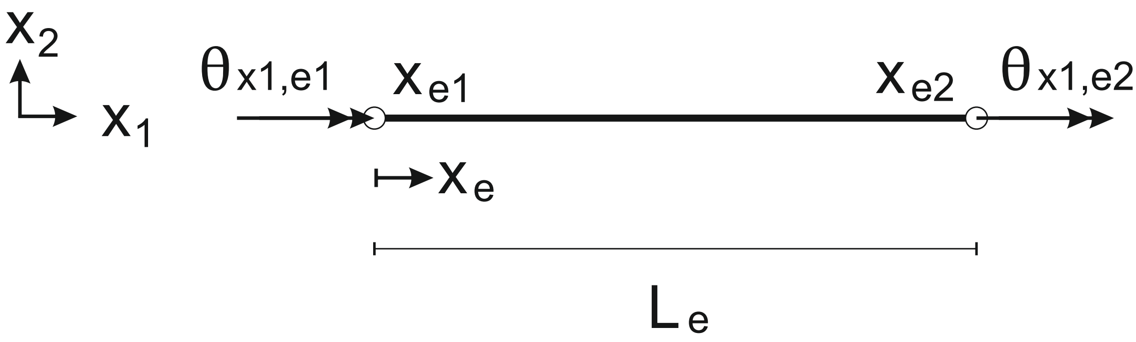

Figure D.1. Torsional element element with one DOF per node.

Dynamic equilibrium of an infinitesimal element subjected to torsion gives,

$$T_{x1} + \frac{\partial T_{x1}}{\partial x_1}\,\mathrm{d}x - T_{x1} = \rho\,J\,\mathrm{d}x\,\frac{\partial^2 \theta_{x1}}{\partial t^2}$$
$$\Leftrightarrow \quad \frac{\partial T_{x1}}{\partial x_1} = \rho\,J\,\frac{\partial^2 \theta_{x1}}{\partial t^2} \tag{D.1}$$

Where T_{x1} is the torsional moment around the x_1-axis, J is the polar moment of inertia and θ_{x1} is the rotation around the x_1-axis.

The torsional moment is defined as,

$$T_{x1} = G\,J\,\frac{\partial \theta_{x1}}{\partial x_1} \tag{D.2}$$

This is introduced into equation D.1,

$$G\,J\,\frac{\partial^2 \theta_{x1}}{\partial x_1^2} = \rho\,J\,\frac{\partial^2 \theta_{x1}}{\partial t^2} \tag{D.3}$$

The equation is multiplied by an arbitrary torsional rotation $\delta\theta_{x1}$ and integrated over the element length,

$$\int_0^{L_e} \delta\theta_{x1}\,G\,J\,\frac{\partial^2 \theta_{x1}}{\partial x_1^2}\,\mathrm{d}x_1 = \int_0^{L_e} \delta\theta_{x1}\,\rho\,J\,\frac{\partial^2 \theta_{x1}}{\partial t^2}\,\mathrm{d}x_1 \tag{D.4}$$

Integrating the first term by parts gives,

$$\left[\delta\theta_{x1}\,G\,J\,\frac{\partial \theta_{x1}}{\partial x_1}\right]_0^{L_e} = \int_0^{L_e} \frac{\partial \delta\theta_{x1}}{\partial x_1}\,G\,J\,\frac{\partial \theta_{x1}}{\partial x_1}\,\mathrm{d}x_1 + \int_0^{L_e} \delta\theta_{x1}\,\rho\,J\,\frac{\partial^2 \theta_{x1}}{\partial t^2}\,\mathrm{d}x_1 \tag{D.5}$$

The left side can be reformulated to,

$$[\delta\theta_{x1}\,T_{x1}]_0^{L_e} = \int_0^{L_e} \frac{\partial \delta\theta_{x1}}{\partial x_1}\,G\,J\,\frac{\partial \theta_{x1}}{\partial x_1}\,\mathrm{d}x_1 + \int_0^{L_e} \delta\theta_{x1}\,\rho\,J\,\frac{\partial^2 \theta_{x1}}{\partial t^2}\,\mathrm{d}x_1 \tag{D.6}$$

Linear shape functions are applied,

$$\theta_{\mathrm{x1}}(x_1,t) = \bar{\Phi}(x_1)\ \bar{a}_{\theta\mathrm{x1,e}}(t) = \begin{Bmatrix} 1-\dfrac{x_1}{L_\mathrm{e}} & \dfrac{x_1}{L_\mathrm{e}} \end{Bmatrix} \begin{Bmatrix} a_{\theta\mathrm{x1,e1}}(t) \\ a_{\theta\mathrm{x1,e2}}(t) \end{Bmatrix} \tag{D.7}$$

$$\delta\theta_{\mathrm{x1}}(x_1,t) = \bar{\Phi}(x_1)\ \delta\bar{a}_{\theta\mathrm{x1,e}}(t) \tag{D.8}$$

It is used that,

$$\bar{\Phi}(x_1)\ \delta\bar{a}_{\theta\mathrm{x1,e}}(t) = \delta\bar{a}^{\mathrm{T}}_{\theta\mathrm{x1,e}}(t)\ \bar{\Phi}^{\mathrm{T}}(x_1) \tag{D.9}$$

The shape functions are introduced into equation D.6,

$$\begin{aligned}\Big[\bar{\Phi}^{\mathrm{T}}(x_1)\ T_{\mathrm{x1}}\Big]_0^{L_\mathrm{e}} &= \int_0^{L_\mathrm{e}} \frac{\partial\bar{\Phi}^{\mathrm{T}}(x_1)}{\partial x_1}\ G\ J\ \frac{\partial\bar{\Phi}(x_1)}{\partial x_1}\ \mathrm{d}x_1\ \bar{a}_{\theta\mathrm{x1,e}}(t) \\ &+ \int_0^{L_\mathrm{e}} \bar{\Phi}^{\mathrm{T}}(x_1)\ \rho\ J\ \bar{\Phi}(x_1)\ \mathrm{d}x_1\ \frac{\partial^2\bar{a}_{\theta\mathrm{x1,e}}(t)}{\partial x_1^2}\end{aligned} \tag{D.10}$$

The stiffness integral is evaluated,

$$\int_0^{L_\mathrm{e}} \frac{\partial\bar{\Phi}^{\mathrm{T}}(x_1)}{\partial x_1}\ G\ J\ \frac{\partial\bar{\Phi}(x_1)}{\partial x_1}\ \mathrm{d}x_1 = \frac{1}{L_\mathrm{e}} \begin{bmatrix} G\ J & -G\ J \\ -G\ J & G\ J \end{bmatrix} \tag{D.11}$$

The mass integral is evaluated,

$$\int_0^{L_\mathrm{e}} \bar{\Phi}^{\mathrm{T}}(x_1)\ \rho\ J\ \bar{\Phi}(x_1)\ \mathrm{d}x_1\ = \frac{L_\mathrm{e}}{6} \begin{bmatrix} 2\ J\ \rho & J\ \rho \\ J\ \rho & 2\ J\ \rho \end{bmatrix} \tag{D.12}$$

The body force integral is evaluated,

$$\Big[\bar{\Phi}^{\mathrm{T}}(x_1)\ T_{\mathrm{x1}}\Big]_0^{L_\mathrm{e}} = \begin{Bmatrix} -T_{\mathrm{x1,Internal,e1}} \\ T_{\mathrm{x1,Internal,e1}} \end{Bmatrix} = \begin{Bmatrix} T_{\mathrm{x1,e1}} \\ T_{\mathrm{x1,e1}} \end{Bmatrix} \tag{D.13}$$

E Soil response results

E.1 Results for soil profile 1

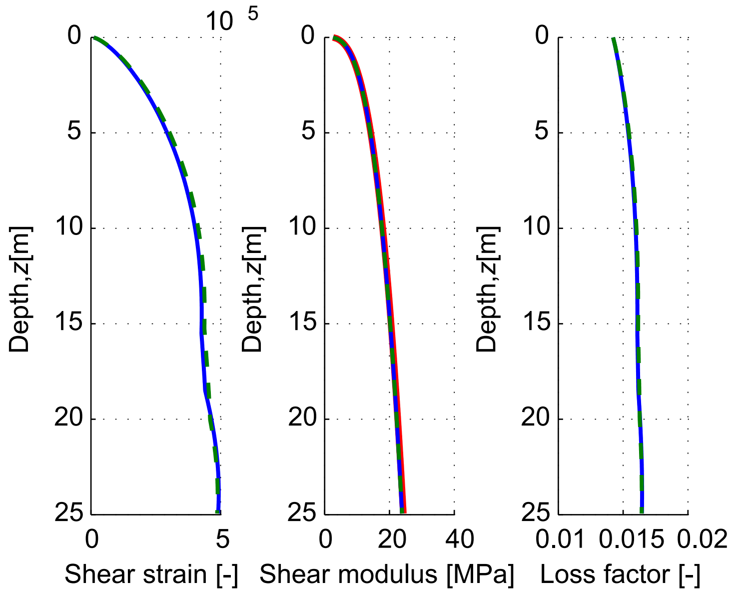

Figure E.1.

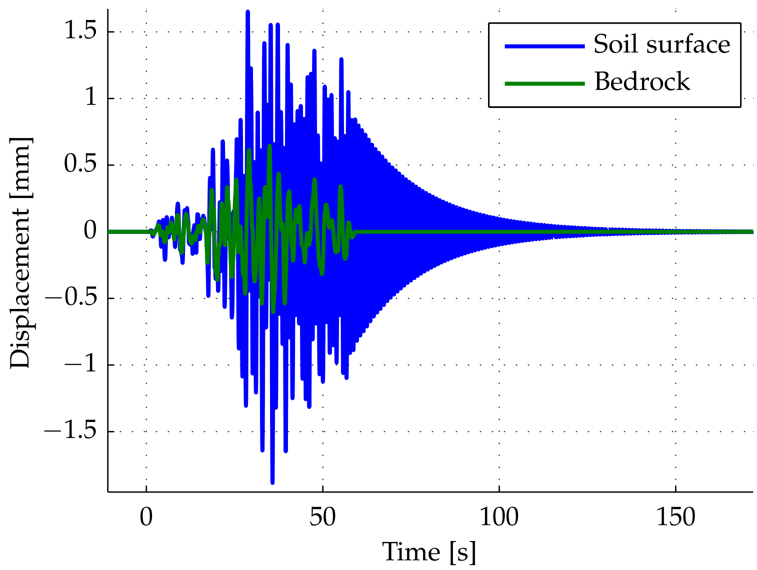

Figure E.2.

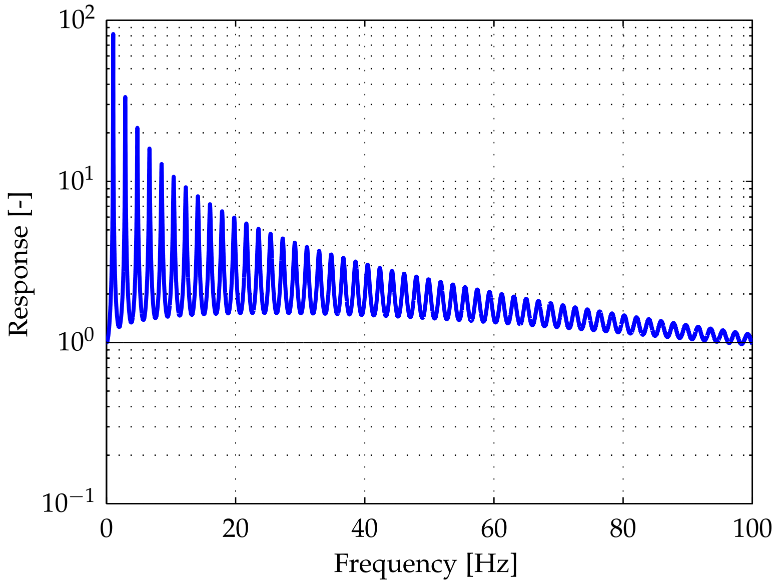

Figure E.3.

E.2 Results for soil profile 2

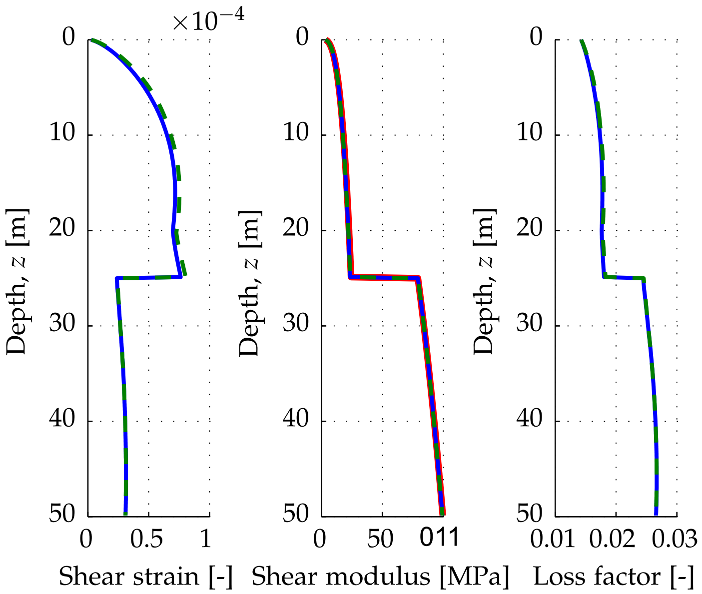

Figure E.4.

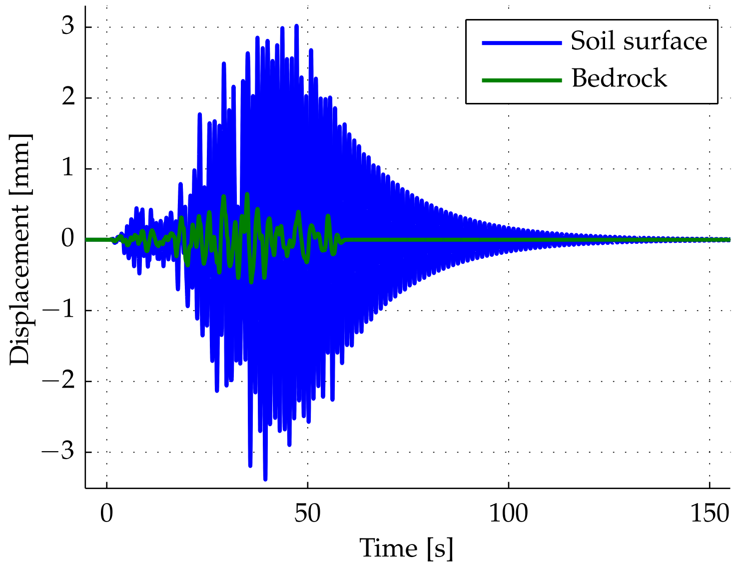

Figure E.5.

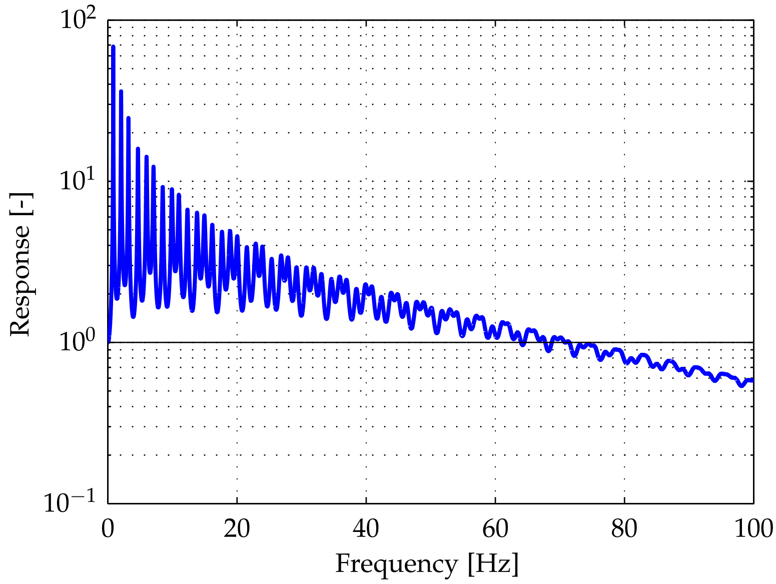

Figure E.6.

F Material Properties for The Bridge Elements

Confer Jensen [2008] the characteristic tangent modulus of elasticity is determined as,

$$E_{\text{concrete}} = 51000 \, \frac{f_c}{f_c + 13} \tag{F.1}$$

where E is the characteristic tangent modulus of elasticity in MPa and f_c is the characteristic compression strength of concrete, which is taken to 35 MPa.

The tangent shear modulus is determined as,

$$G = \frac{E}{2\,(1+\nu)} \tag{F.2}$$

Poisson's ratio for concrete is taken to 0.2, which is a typically used value. The density of concrete is taken to 2500 kg/m^3 due to the fact that prestressed concrete is used and that seismic designed concrete sections generally has a high amount of steel in them.

Confer Bonnerup *et al.* [2009] the modulus of elasticity for steel is taken to 210 GPa, Possion's ratio is taken to 0.3 and the density of steel is taken to 7850 kg/m^3. The tangent shear modulus is determined using equation F.2.

In table F.1 the calculated material properties for both steel and concrete are given.

	Concrete	Steel
Tangent modulus of elasticity, E [MPa]	43550.0	210000.0
Poisson's ratio, ν [-]	0.2	0.3
Tangent shear modulus, G [MPa]	18146.0	80769.0
Density, ρ [kg/m^3]	2500.0	7850.0

Table F.1. Material parameters for the concrete and steel sections.

For the foundations a unit weight of 2400 kg/m^3 is used.

G Dimensions of the Bridge Elements

The dimensions of the bridge steel deck, the concrete columns and the circular concrete foundations are estimated using rough estimates.

The steel section used for the bridge deck is illustrated in figure G.1. The x_2 and x_3 axes refers to the local axes of the bridge deck element.

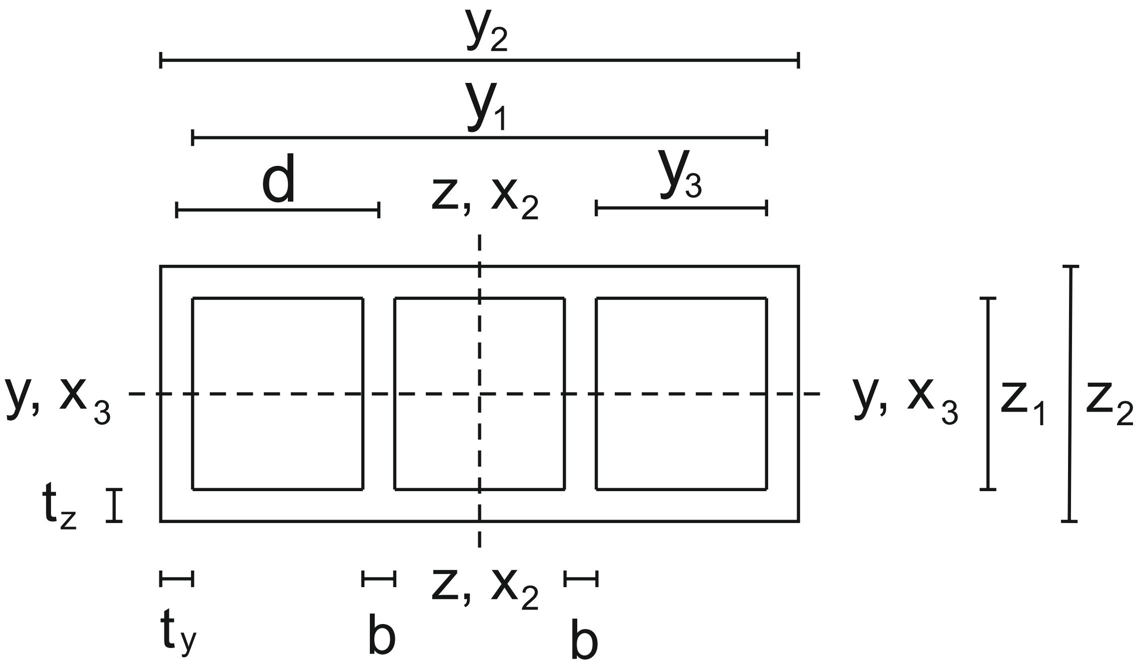

Figure G.1. Cross section of the bridge deck

The second moment of area around the y is first found for the rectangular section,

$$I_{\text{y,rectangular}} = \frac{1}{12} \left(y_2 \; z_2^3 - y_1 \; z_1^3 \right) \tag{G.1}$$

The additional second moment of area from the two girders are found as,

$$I_{\text{y,additional}} = 2 \left(\frac{1}{12} \; b \; z_1^2 \right) \tag{G.2}$$

Thus the total second moment of area around the y-axis is determined as,

$$I_{\text{y,total}} = I_{\text{y,rectangular}} + I_{\text{y,additional}} \tag{G.3}$$

Analogously the second moment of area is found around the z-axis,

$$I_{\text{z,rectangular}} = \frac{1}{12} \left(z_2 \; y_2^3 - z_1 \; y_1^3 \right) \tag{G.4}$$

$$I_{\text{z,additional}} = 2 \left(\frac{1}{12} \; z_1 \; b^3 + z_1 \; b \; \left(\frac{1}{2} \; d \right)^2 \right) \tag{G.5}$$

$$I_{\text{z,total}} = I_{\text{z,rectangular}} + I_{\text{z,additional}} \tag{G.6}$$

In table G.1 the used dimensions are given,

y_2 [m]	20.00
t_y [m]	1.00
y_1 [m]	18.00
y_3 [m]	5.33
d [m]	6.33
z_2 [m]	8.00
t_z [m]	1.00
z_1 [m]	6.00
b [m]	1.00

Table G.1. Dimensions of the steel section.

This gives the resulting moments of area,

$$I_{\text{y,total}} = 565.33 \text{ m}^4 \tag{G.7}$$

$$I_{\text{z,total}} = 2538.67 \text{ m}^4 \tag{G.8}$$

The cross section are is determined as well,

$$A = 64 \text{ m}^2 \tag{G.9}$$

The chosen dimensions are checked calculation the moment capacity of the beam carrying two times its self weight. The moment are found using a simply supported beam of four spans, as the moment does not changes much when the number of spans are increased to 10. Confer Jensen [2009] the maximum moment occurs on top of a support and has the value,

$$M = 0.107 \; l_{\text{span}} \; P \tag{G.10}$$

where l_{span} is the length of the span, which is 200 m, and $|P|$ is the line load in Nm. The line load is determined as,

$$P = 2 \cdot 9.81 \text{ m/s}^2 \cdot 7850 \text{ kg/m}^3 \cdot A = 9.86 \; 10^6 \text{ N/m} \tag{G.11}$$

This gives a moment of $4.22 \; 10^{10}$ Nm. The normal maximum normal stress is determined using Navier's formula,

$$\sigma_{\text{M}} = \frac{M \, \frac{z_2}{2}}{I_{\text{y,total}}} \, 10^{-6} = 298.50 \text{ MPa} \tag{G.12}$$

Using steel S355 the stresses are below the capacity.

The width of the concrete columns are taken as 20 m and the depth are taken as 10 m and the cross section is assumed solid. The diameter of the circular foundation supporting the concrete columns are taken as 25 m and the depth of is taken as 20 m.

H Element Matrices for the 3D FEM Beam Model

The 12 DOF stiffness matrix is given as,

$$
\frac{1}{L_e}\begin{bmatrix}
\frac{A\,E}{L_e} & 0 & 0 & 0 & 0 & 0 & -\frac{A\,E}{L_e} & 0 & 0 & 0 & 0 & 0 \\
0 & \frac{12\,E\,I_{x3}}{L_e^2} & 0 & 0 & 0 & \frac{6\,E\,I_{x3}}{L_e} & 0 & -\frac{12\,E\,I_{x3}}{L_e^2} & 0 & 0 & 0 & \frac{6\,E\,I_{x3}}{L_e} \\
0 & 0 & \frac{12\,E\,I_{x2}}{L_e^2} & 0 & -\frac{6\,E\,I_{x2}}{L_e} & 0 & 0 & 0 & -\frac{12\,E\,I_{x2}}{L_e^2} & 0 & -\frac{6\,E\,I_{x2}}{L_e} & 0 \\
0 & 0 & 0 & G\,K & 0 & 0 & 0 & 0 & 0 & -G\,K & 0 & 0 \\
0 & 0 & -\frac{6\,E\,I_{x2}}{L_e} & 0 & 4\,E\,I_{x2} & 0 & 0 & 0 & \frac{6\,E\,I_{x2}}{L_e} & 0 & 2\,E\,I_{x2} & 0 \\
0 & \frac{6\,E\,I_{x3}}{L_e} & 0 & 0 & 0 & 4\,E\,I_{x3} & 0 & -\frac{6\,E\,I_{x3}}{L_e} & 0 & 0 & 0 & 2\,E\,I_{x3} \\
-\frac{A\,E}{L_e} & 0 & 0 & 0 & 0 & 0 & \frac{A\,E}{L_e} & 0 & 0 & 0 & 0 & 0 \\
0 & -\frac{12\,E\,I_{x3}}{L_e^2} & 0 & 0 & 0 & -\frac{6\,E\,I_{x3}}{L_e} & 0 & \frac{12\,E\,I_{x3}}{L_e^2} & 0 & 0 & 0 & -\frac{6\,E\,I_{x3}}{L_e} \\
0 & 0 & -\frac{12\,E\,I_{x2}}{L_e^2} & 0 & \frac{6\,E\,I_{x2}}{L_e} & 0 & 0 & 0 & \frac{12\,E\,I_{x2}}{L_e^2} & 0 & \frac{6\,E\,I_{x2}}{L_e} & 0 \\
0 & 0 & 0 & -G\,K & 0 & 0 & 0 & 0 & 0 & G\,K & 0 & 0 \\
0 & 0 & -\frac{6\,E\,I_{x2}}{L_e} & 0 & 2\,E\,I_{x2} & 0 & 0 & 0 & \frac{6\,E\,I_{x2}}{L_e} & 0 & 4\,E\,I_{x2} & 0 \\
0 & \frac{6\,E\,I_{x3}}{L_e} & 0 & 0 & 0 & 2\,E\,I_{x3} & 0 & -\frac{6\,E\,I_{x3}}{L_e} & 0 & 0 & 0 & 4\,E\,I_{x3}
\end{bmatrix}
\begin{bmatrix} u_1 \\ v_1 \\ w_1 \\ \theta_{x1,1} \\ \theta_{x2,1} \\ \theta_{x3,1} \\ u_2 \\ v_2 \\ w_2 \\ \theta_{x1,2} \\ \theta_{x2,2} \\ \theta_{x3,2} \end{bmatrix}
\tag{H.1}
$$

The 12 DOF mass matrix,

$$
\rho\,L_e\begin{bmatrix}
\frac{A}{3} & 0 & 0 & 0 & 0 & 0 & \frac{A}{6} & 0 & 0 & 0 & 0 & 0 \\
0 & \frac{13\,A}{35} & 0 & 0 & 0 & \frac{11\,A\,L_e}{210} & 0 & \frac{9\,A}{70} & 0 & 0 & 0 & -\frac{13\,A\,L_e}{420} \\
0 & 0 & \frac{13\,A}{35} & 0 & -\frac{11\,A\,L_e}{210} & 0 & 0 & 0 & \frac{9\,A}{70} & 0 & \frac{13\,A\,L_e}{420} & 0 \\
0 & 0 & 0 & \frac{K}{3} & 0 & 0 & 0 & 0 & 0 & \frac{K}{6} & 0 & 0 \\
0 & 0 & -\frac{11\,A\,L_e}{210} & 0 & \frac{A\,L_e^2}{105} & 0 & 0 & 0 & -\frac{13\,A\,L_e}{420} & 0 & -\frac{A\,L_e^2}{140} & 0 \\
0 & \frac{11\,A\,L_e}{210} & 0 & 0 & 0 & \frac{A\,L_e^2}{105} & 0 & \frac{13\,A\,L_e}{420} & 0 & 0 & 0 & -\frac{A\,L_e^2}{140} \\
\frac{A}{6} & 0 & 0 & 0 & 0 & 0 & \frac{A}{3} & 0 & 0 & 0 & 0 & 0 \\
0 & \frac{9\,A}{70} & 0 & 0 & 0 & \frac{13\,A\,L_e}{420} & 0 & \frac{13\,A}{35} & 0 & 0 & 0 & -\frac{11\,A\,L_e}{210} \\
0 & 0 & \frac{9\,A}{70} & 0 & -\frac{13\,A\,L_e}{420} & 0 & 0 & 0 & \frac{13\,A}{35} & 0 & \frac{11\,A\,L_e}{210} & 0 \\
0 & 0 & 0 & \frac{K}{6} & 0 & 0 & 0 & 0 & 0 & \frac{K}{3} & 0 & 0 \\
0 & 0 & \frac{13\,A\,L_e}{420} & 0 & -\frac{A\,L_e^2}{140} & 0 & 0 & 0 & \frac{11\,A\,L_e}{210} & 0 & \frac{A\,L_e^2}{105} & 0 \\
0 & -\frac{13\,A\,L_e}{420} & 0 & 0 & 0 & -\frac{A\,L_e^2}{140} & 0 & -\frac{11\,A\,L_e}{210} & 0 & 0 & 0 & \frac{A\,L_e^2}{105}
\end{bmatrix}
\begin{bmatrix} u_1 \\ v_1 \\ w_1 \\ \theta_{x1,1} \\ \theta_{x2,1} \\ \theta_{x3,1} \\ u_2 \\ v_2 \\ w_2 \\ \theta_{x1,2} \\ \theta_{x2,2} \\ \theta_{x3,2} \end{bmatrix}
\tag{H.2}
$$

I Torsional Stiffness and Shear Stresses due to Torsion

In the following the torsional second moment of area and the shear stresses due to torsion are determined for the concrete columns as well as the steel section.

Confer Bonnerup *et al.* [2009] the torsional second moment of area of a rectangular section is determined as,

$$K = 0.229\ w\ d^3 \tag{I.1}$$

where w is the width of the cross section, d is the depth and the factor 0.229 is for a w/d ratio of 2. A width of 20 m and a depth of 10 m is used, which gives $K = 4580\ \text{m}^4$.

In order to determine the torsional second moment of area of the steel section following calculation are carried out confer Andersen and Nielsen [2009]. The steel section is illustrated in figure I.1, where it can seen that the torsional center coincides with the enter of gravity of the cross section as it is symmetrical around both the y- and z-axis. The first cell is indexed 1, the mid cell 2 and the right cell 3.

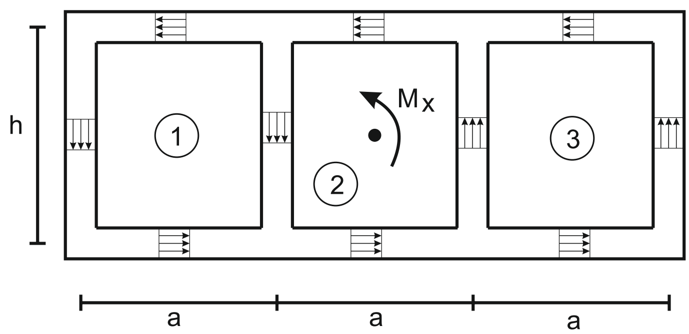

Figure I.1. Cross section of the steel section.

Following formula is used to determine the first moment of area of the respective cells,

$$\sum_k (S_\text{j} - S_\text{k}) \int \frac{d(s_\text{j})}{t(s_\text{j})} = 2\ A_\text{j}\ G\ \frac{\text{d}\theta_\text{x}}{\text{d}x} \tag{I.2}$$

where the index j refers to the to the actual cell, k refers to the neighbor cell, S_j is the first moment of area of the actual cell, S_k is the first moment of area of the neightbor cell, $d(s_\text{j})$ is the length of the wall that is looked at, $t(s_\text{j})$ is the thickness of the wall that is looked at, A_j is the area of the cell that is looked at, G is the shear modulus for steel and $theta_\text{x}$ is the rotation around the x-axis of the section.

Equation I.2 is used for all three cells,

$$\frac{(S_1 - 0)\ a}{t} + \frac{(S_1 - 0)\ h}{t} + \frac{(S_1 - 0)\ a}{t} + \frac{(S_1 - S_2)\ h}{t} = 2\ a\ h\ G\ \frac{\text{d}\theta_\text{x}}{\text{d}x} \tag{I.3}$$

$$\frac{(S_2 - 0)\ a}{t} + \frac{(S_2 - S_1)\ h}{t} + \frac{(S_2 - 0)\ a}{t} + \frac{(S_2 - S_3)\ h}{t} = 2\ a\ h\ G\ \frac{\text{d}\theta_\text{x}}{\text{d}x} \tag{I.4}$$

$$\frac{(S_3 - 0)\ a}{t} + \frac{(S_3 - S_2)\ h}{t} + \frac{(S_3 - 0)\ a}{t} + \frac{(S_3 - 0)\ h}{t} = 2\ a\ h\ G\ \frac{\text{d}\theta_\text{x}}{\text{d}x} \tag{I.5}$$

The three unknown of the three equations is the first moment of area of the three cells S_1, S_2 and S_3. The three equations are solved with respect to the three unknowns, which gives,

$$S_1 = \frac{a\ h\ G\ \dfrac{d\theta_x}{dx}\ (2\ a + 3\ h)}{2\ a^2 + 4\ a\ h + h^2} \tag{I.6}$$

$$S_2 = \frac{2\ a\ h\ G\ \dfrac{d\theta_x}{dx}\ (a + 2\ h)}{2\ a^2 + 4\ a\ h + h^2} \tag{I.7}$$

$$S_3 = \frac{a\ h\ G\ \dfrac{d\theta_x}{dx}\ (2\ a + 3\ h)}{2\ a^2 + 4\ a\ h + h^2} \tag{I.8}$$

The torsional moment can be found as,

$$M_x = 2 \sum_{j=1}^{N} A_j\ S_j = 2\ a\ h\ S_1 + 2\ a\ h\ S_2 + 2\ a\ h\ S_3 \tag{I.9}$$

This can be reformulated as,

$$G\ \frac{d\theta_x}{dx} = \frac{1}{4}\ \frac{M_x\ (2\ a^2 + 4\ a\ h + h^2)}{a^2\ h^2\ t\ (3\ a + 5\ h)} \tag{I.10}$$

Inserting this into equation I.6, I.7 and I.8 the second moment of area of the cells reduce to,

$$S_1 = \frac{1}{4}\ \frac{M_x\ (2\ a + 3\ h)}{a\ h\ (3\ a + 5\ h)} \tag{I.11}$$

$$S_2 = \frac{1}{2}\ \frac{M_x\ (a + 2\ h)}{a\ h\ (3\ a + 5\ h)} \tag{I.12}$$

$$S_3 = \frac{1}{4}\ \frac{M_x\ (2\ a + 3\ h)}{a\ h\ (3\ a + 5\ h)} \tag{I.13}$$

$$\tag{I.14}$$

The torsional second moment of area is found by the formula,

$$K = 2 \sum_{j=1}^{N} A_j\ \frac{S_j}{G\ \dfrac{d\theta_x}{dx}} = \frac{2\ a\ h\ S_1}{G\ \dfrac{d\theta_x}{dx}} + \frac{2\ a\ h\ S_2}{G\ \dfrac{d\theta_x}{dx}} + \frac{2\ a\ h\ S_3}{G\ \dfrac{d\theta_x}{dx}} \tag{I.15}$$

a is determined to 6.67 m, h is 8 m and t is 1 m. This gives a torsional second moment of area of $K = 1864.08\ \text{m}^4$. The absolute value of the shear stresses due to torsion is determined by the formula,

$$\sigma_{xs} = \frac{S_j - S_k}{t(s_j)} \tag{I.16}$$

In figure I.2 the value and direction of the shear stresses due to torsion is given. The shear stresses will be used later, when the stresses in the bridge deck are investigated.

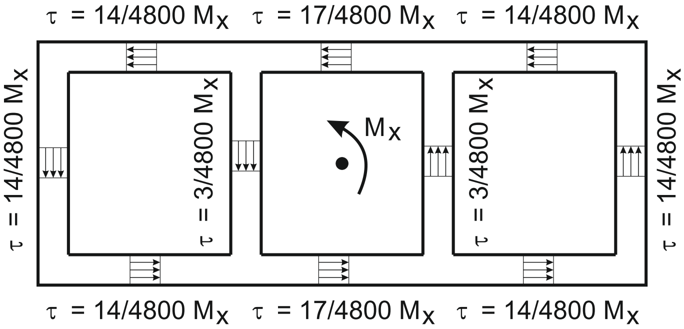

Figure I.2. Shear stresses due to torsion in the steel section.

J Cross Section Properties for the Steel Section

In order to determine the shear stresses and normal stresses in the 10 points illustrated in Figure J.1 the first and second moment of area are determined.

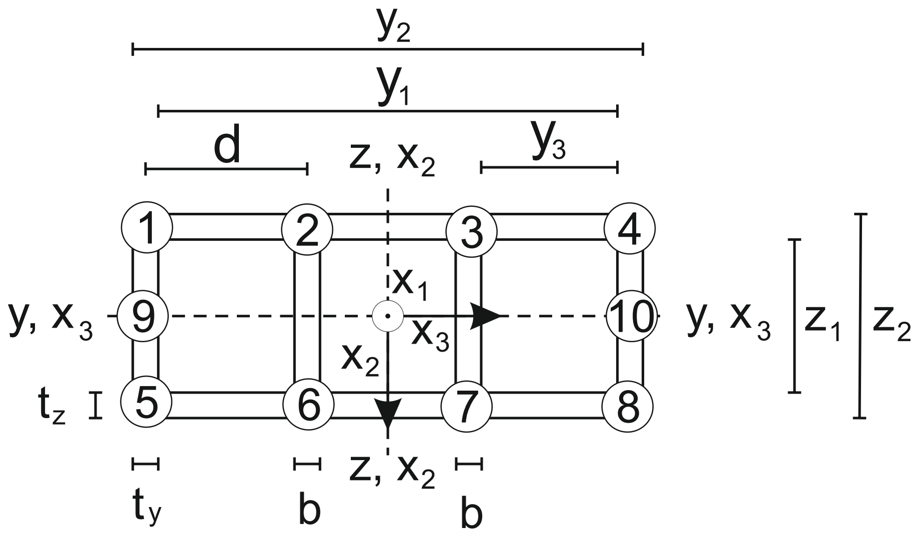

Figure J.1. Cross section of the bridge deck and the ten chosen critical points.

The first moment of area for points 9 and 10 in the middle of the cross section is determined around both axes,

$$S_{\mathrm{x3,mid}} = \left(\frac{z_2}{2} - \frac{t_z}{2}\right)\ (y_1 - 2\,b)\ t_z + 4\ \left(\frac{z_2}{2}\right)\ \left(t_y\ \frac{z_2}{2}\right) \tag{J.1}$$

$$S_{\mathrm{x2,mid}} = \left(\frac{y_2}{2} - \frac{t_y}{2}\right)\ (z_2\ t_y) + 2\ \left(\frac{y_2}{2} - t_y - \frac{y_3}{2}\right)\ (y_3\ t_z) \tag{J.2}$$

$$+ \left(\frac{y_2}{2} - t_y - y_3 - \frac{b}{2}\right)\ (z_2\ b) + 2\ \left(\frac{y_3}{4}\right)\ \left(t_z\ \frac{y_3}{2}\right) \tag{J.3}$$

The first moment of are for points 1 to 8 in the top and bottom flange of the cross section is determined around the two axes,

$$S_{\mathrm{x3,top}} = \left(\frac{z_2}{2} - \frac{t_z}{4}\right)\ \left(\frac{y_2}{2}\ \frac{t_z}{2}\right) \tag{J.4}$$

$$S_{\mathrm{x2,top}} = \left(\frac{y_2}{2} - \frac{t_y}{4}\right)\ \left(\frac{z_2}{2}\ \frac{t_y}{2}\right) \tag{J.5}$$

The dimensions determined in Appendix G is used in the resulting first moment of area is,

$$S_{\mathrm{x3,mid}} = 120\ \mathrm{m}^3 \tag{J.6}$$

$$S_{\mathrm{x2,mid}} = 176\ \mathrm{m}^3 \tag{J.7}$$

$$S_{\mathrm{x3,top}} = 37.5\ \mathrm{m}^3 \tag{J.8}$$

$$S_{\mathrm{x2,top}} = 39\ \mathrm{m}^3 \tag{J.9}$$

(J.10)